Differential roles of α-, β- and γ-actin isoforms in regulation of cytoskeletal dynamics and stability during axon elongation and collateral branch formation in motoneurons

Rolle der α-, β- und γ-Aktin Isoformen bei Regulation von Dynamik und Stabilität des Zytoskeletts während des Axonwachstums und beim Ausbilden von axonalen Verzweigungen in Motoneuronen

Doctoral thesis for a doctoral degree

at the Institute for Clinical Neurobiology,

University Hospital Würzburg

and Graduate School of Life Sciences, Julius-Maximilians-Universität Würzburg

Section: Neuroscience

Submitted by

Mehri Moradi

from Karaj, Iran

Würzburg, February 2017

Submitted on:

Members of the Promotion Committee:

Chairperson: Prof. Dr. Manfred Gessler

Primary Supervisor: Prof. Dr. Michael Sendtner

Supervisor (Second): Prof. Dr. Erich Buchner

Supervisor (Third): Prof. Dr. Utz Fischer

Date of Public defense:

Date of receipt of Certificates:

For Ahmad, Mom and Dad

Table of contents

1. Summary 4
2. Zusammenfassung 6
3. Introduction 8
   3.1 Actin isoforms 8
   3.2 Actin cytoskeleton in neuronal development and plasticity 8
   3.3 Role of mRNA transport and local translation in neuronal development and maintenance 10
      3.3.1 Synaptic plasticity 11
      3.3.2 Axon guidance 12
      3.3.3 Axon elongation 12
      3.3.4 Synaptogenesis and branching 13
      3.3.5 Axon maintenance and regeneration 14
   3.4 Regulation of axonal mRNA transport by cis-elements and transacting factors 16
      3.4.1 SMN; an essential protein for RNP particle assembly 18
      3.4.2 Impaired RNA biogenesis and trafficking in motoneuron diseases 19
   3.5 Aim of the present study 22
4. Materials and Methods 23
   4.1 Materials 23
      4.1.1 Animals 23
      4.1.2 Cell Lines 23
         4.1.2.1 HEK^{293T} cell line 23
         4.1.2.2 NSC-34 cell line 23
         4.1.2.3 Hela cell line 23
      4.1.3 Chemicals, reagents and buffers 24
   4.2 Methods 43
      4.2.1 HEK^{293T} and NSC-34 culture 43
      4.2.2 Cortical neuron culture 43
      4.2.3 Enrichment of embryonic mouse motoneurons and virus transduction 44
      4.2.4 Compartmentalized motoneuron culture 45
      4.2.5 Transient plasmid transfection using lipofectamine^{TM} 2000 reagent 46
      4.2.6 Lentivirus production 46
      4.2.7 Virus titration 46
      4.2.8 DNA isolation 47
      4.2.9 Axonal RNA preparation and cDNA synthesis 50
      4.2.10 cDNA purification 51
      4.2.11 Laser capture microdissection 51

4.2.12 Quantitative qRT-PCR 52
4.2.13 Cloning and creating calibration curves and qRT-PCR absolute quantification 54
4.2.14 Cloning shRNA oligonucleotides targeting 3'UTRs of actin isoforms 57
4.2.15 Cloning LCK-Myr-eGFP-3'UTR report for γ-actin 59
4.2.16 Cloning HA-tag-expression plasmids of actin isoforms and rescue construct for β-actin 63
4.2.17 Protein extraction and quantification 64
4.2.18 G- to F-actin separation 65
4.2.19 Western blotting 65
4.2.20 Fluorescence Recovery After Photobleaching (FRAP) 65
4.2.21 Live cell imaging and data quantification 66
4.2.22 High resolution *in situ* hybridization 67
4.2.23 Immunofluorescence 68
4.2.24 Live cell extraction 69
4.2.25 Survival assay of embryonic primary motoneurons 69
4.2.26 Analysis of neurite growth 70
4.2.27 Image acquisition and processing 70
5. Results 71
5.1 α-, β- and γ-actin isoforms are expressed in mouse motoneurons in embryonic stages and adult 71
5.2 mRNAs of α-, β- and γ-actin isoforms are translocated into axons in motoneurons 73
5.3 Expression and axonal mRNA localization of α-, β- and γ-actin isoforms in primary mouse cortical neurons 79
5.4 α-, β- and γ-actin proteins are differentially distributed in motoneurons 82
5.5 α-, β- and γ-actin transcripts are differentially translated in axonal growth cones and in translational hot spots within axonal branch points. 88
5.6 Actin isoforms accomplish specific functions in motor axon growth; α-actin is required for axonal collateral branch formation and β-actin is required for axonal elongation and growth cone differentiation. 92
5.7 Actin dynamics is differentially regulated by α-, β- and γ-actin isoforms at axonal filopodia and axonal growth cone filopodia 103
5.8 Depletion of one actin isoform induces a compensatory response which leads to upregulation of other two isoforms 107
5.9 Smn is involved in regulation of axonal mRNA trafficking and translation of actin isoforms in motoneurons 114
6. Discussions 117
6.1 Protein and mRNAs for α-, β- and γ-actin isoforms are differentially distributed in axons of cultured motoneurons 117
6.2 α-, β- and γ-actin exert specific and overlapping functions in motoneurons 119
6.3 Compensatory response triggered by α-, β- or γ-actin ablation 125
6.4 Mechanisms of the compensatory response 127

6.5 Mislocalization of α-, β- and γ-actin mRNAs in neurodegenerative diseases 128
7. References 131
8. Appendix 143
8.1 List of figures 143
8.2 List of tables 145
8.3 List of abbreviations 146
9. Affidavit 150
10. Acknowledgments 151
11. Curriculum Vitae 153

1. Summary

In highly polarized cells like neurons, cytoskeleton dynamics play a crucial role in establishing neuronal connections during development and are required for adult plasticity. Actin turnover is particularly important for neurite growth, axon path finding, branching and synaptogenesis. Motoneurons establish several thousand branches that innervate neuromuscular synapses (NMJs). Axonal branching and terminal arborization are fundamental events during the establishment of synapses in motor endplates. Branching process is triggered by the assembly of actin filaments along the axon shaft giving rise to filopodia formation. The unique contribution of the three actin isoforms, α-, β- and γ-actin, in filopodia stability and dynamics during this process is not well characterized. Here, we performed high resolution *in situ* hybridization and qRT-PCR and showed that in primary mouse motoneurons α-, β- and γ-actin isoforms are expressed and their transcripts are translocated into axons. Using FRAP experiments, we showed that transcripts for α-, β- and γ-actin become locally translated in axonal growth cones and translation hot spots of the axonal branch points. Using live cell imaging, we showed that shRNA depletion of α-actin reduces dynamics of axonal filopodia which correlates with reduced number of collateral branches and impairs axon elongation. Depletion of β-actin correlates with reduced dynamics of growth cone filopoida, disturbs axon elongation and impairs presynaptic differentiation. Also, depletion of γ-actin impairs axonal growth and decreases axonal filopodia dynamics. These findings implicate that actin isoforms accomplish unique functions during development of motor axons. Depletions of β- and γ-actin lead to compensatory upregulation of other two isoforms. Consistent with this, total actin levels remain unaltered and F-actin polymerization capacity is preserved. After the knockdown of either α- or γ-actin, the levels of β-actin increase in the G-actin pool indicating that polymerization and stability of β-actin filaments depend on α- or γ-actin. This study provides evidence both for unique and overlapping

function of actin isoforms in motoneuron growth and differentiation. In the soma of developing motoneurons, actin isoforms act redundantly and thus could compensate for each other's loss. In the axon, α-, β- and γ-actin accomplish specific functions, i.e. β-actin regulates axon elongation and plasticity and α- and γ-actin regulate axonal branching.

Furthermore, we show that both axonal transport and local translation of α-, β- and γ-actin isoforms are impaired in Smn knockout motoneurons, indicating a role for Smn protein in RNA granule assembly and local translation of these actin isoforms in primary mouse motoneurons.

2. Zusammenfassung

In stark polaren Zellen wie den Neuronen ist die Etablierung neuronaler Netzwerke ein entscheidender Faktor bei der Entwicklung des zentralen Nervensystems und spielt für die adulte Plastizität eine wesentliche Rolle. Besonders die Aktindynamik ist wichtig für das Neuritenwachstum, die axonale Wegfindung und Verzweigung, sowie die Synaptogenese. Motoneurone bilden mehrere tausend terminale Verzweigungen aus, um neuromuskuläre Endplatten (NMJ) zu innervieren. Die axonale Verzweigung ist ein fundamentales Ereignis bei Ausbildung synaptischer Verbindungen zwischen Motoneuron und innerviertem Muskel. Die Axonverzweigung geschieht durch die Polymerisierung von Aktin entlang des Axonschafts, was zur Entstehung von Filopodien und Lamellopodien führt. Allerdings ist die genaue Funktion der drei Aktin-Isoformen (α-, β- and γ-Actin), im Zusammenhang mit der Regulation der Filopodienstabilität und deren Dynamik, noch weitestgehend unbekannt.

Somit konnten wir in dieser Arbeit mit Hilfe hoch sensitiver in situ Hybridisierungs- und qRT PCR Techniken zeigen, dass in primären Mausmotoneuronen alle drei Aktinisoformen (α-, β- und γ) exprimiert, und deren Transkripte entlang des axonalen Kompartiments transportiert werden. Unsere FRAP Daten weisen darauf hin, dass α-, β- und γ-Aktin sowohl im Wachstumskegel als auch an sogenannten „Translation Hot Spots“ innerhalb axonaler Verzweigungspunkte lokal synthetisiert werden. Anhand von „Live Cell Imaging“ Experimenten konnten wir dann zeigen, dass ein α-Aktin Knockdown die Dynamik axonaler Filopodien stark reduziert, und als Folge, die Anzahl von axonalen Verzweigungen und die Axonlänge verringert ist. Hingegen geht ein β-Aktin Knockdown mit reduzierter Filopodiendynamik im Wachstumskegel und betroffener Differenzierung präsynaptischer Strukturen einher. Veränderungen des axonalen Wachstum und der Filopodiendynamik sind ebenfalls bei einem γ-Aktin Knockdown zu beobachten. Diese Daten weisen darauf hin, dass die drei Aktinisoformen unterschiedliche Funktionen bei der Entwicklung von Motoraxonen

haben. Darüber hinaus zeigen unsere Daten, dass die Herunterregulation einer Aktinisoform durch eine erhöhte Expression der beiden anderen Isoformen kompensiert wird. Dieser Kompensationsmechanismus erlaubt es, die gesamte Aktinmenge und somit die F-Aktin-Polymerisation in der Zelle aufrechtzuerhalten. Sehr interessant dabei ist die Beobachtung, dass nach einem α- oder γ-Actin Knockdown das G/F-Verhältnis verändert ist, so dass die Menge an β-Aktin im G-Aktin Pool steigt und im F-Aktin Pool abnimmt. Daher beruhen Polymerisation und Stabilität von β-Aktin auf den α-, und γ-Aktinisoformen.

Zusammenfassend lässt sich sagen, dass alle drei Aktinisoformen übergreifende Funktionen während Wachstum und Differenzierung von Motoneuronen haben. Im Zellkörper von sich entwickelnden Motoneuronen übernehmen sie ähnliche Aufgaben und können sich somit gegenseitig kompensieren. Im Gegensatz dazu sind die Funktionen im axonalen Kompartiment wesentlich spezifischer. Hier reguliert β-Aktin axonales Wachstum und Plastizität, während α- und γ-Aktin eine entscheidende Rolle bei der Ausbildung axonaler Verzweigungen haben. Unsere Arbeit lässt nun Rückschlüsse über mögliche Funktionen des SMN Proteins beim Aufbau der sogenannten „RNA Granules“ und lokaler Proteinbiosynthese der verschiedenen Aktinisoformen in primären Mausmotoneuronen zu.

3. Introduction

3.1 Actin isoforms

There are six different actin isoforms in higher vertebrates which are encoded by six different genes: α-skeletal, α-cardiac, α-smooth, γ-smooth muscle actin and cytoplasmic β-actin and γ-actin. α-skeletal and α-cardiac isoforms are predominantly expressed in striated muscles, α-smooth and γ-smooth are expressed in smooth muscles and β-actin and γ-actin isoforms are ubiquitously expressed in all cell types. Actin isoforms share about 94% homology in their coding regions and are highly similar in their amino acid sequences. For example, β-actin and γ-actin differ in only four amino acid residues at their N-terminal end. However, these isoforms possess completely different 3'UTRs.

3.2 Actin cytoskeleton in neuronal development and plasticity

The cytoskeleton is involved in many cellular processes such as cell growth, division, migration, cell signaling and intracellular transport. In neurons, the cytoskeleton is composed of actin filaments, microtubules and neurofilaments. Actin dynamics plays an essential role in neurite growth, axon guidance, branching, terminal arborization and establishment of synapses during development and also in maintenance of synapses and plasticity as well as axon regeneration in the adult (Campbell and Holt, 2001; Luo, 2002; Zhang and Benson, 2001).

The first step in axon development is the formation of the axon initiation segment (AIS) which is triggered by neuronal polarization. Mechanisms underlying neuronal polarization involve extracellular cues, intracellular signaling pathways and asymmetric localization of proteins and organelles in the AIS and in somatodendritic compartments (Bradke and Dotti, 1997; Shelly et al., 2007; Shelly et al., 2011). The role of the actin cytoskeleton in the assembly of AIS has been well studied. Super-resolution imaging techniques have shown that actin and βII spectrin form a unique periodic lattice ultrastructure directly underneath the

membrane (Xu et al., 2013). This lattice network starts to assemble in the AIS early during axon development and propagates from the proximal axon to the distal part as neurons further mature (Zhong et al., 2014). This actin-lattice network facilitates incorporation of Na^+-voltage gated channels into the AIS membrane and thus allows establishment of neuronal polarization. Moreover, drug-mediated depolymerization of actin cytoskeleton disrupts asymmetric axonal transport of proteins and causes incorrect localization of dendritic proteins in the axonal compartment (Song et al., 2009). The next step in axonal development is the extension of the newly formed axon which occurs immediately after axon specification. Coordinated reorganization and polymerization of actin and microtubule cytoskeleton enables axonal growth toward the postsynaptic target. Microtubule stabilization which happens as a response to extracellular growth cues drives axonal elongation in the axon shaft and retrograde treadmilling of actin filaments at front part of the growth cone provides a pulling force for growth cone extension (Letourneau et al., 1987; Suter and Miller, 2011). Thus, axon elongation and path finding occur mostly simultaneously. Axonal growth cones possess protrusions (filopodia and lamellipodia) at their tips that are enriched in actin filaments and are therefore highly dynamic. The center of axonal growth cones contains both actin and microtubules (Dent et al., 2011). Attractive guidance cues induce F-actin polymerization in protrusions which allows growth cone turning for a directed axonal extension (Geraldo and Gordon-Weeks, 2009). In contrast, depolymerization of F-actin as response to repulsive cues induces growth cone collapse and prevents axon elongation (Fan et al., 1993). The last step of axon development is formation of axonal collateral branches which allows them to establish several thousand synapses with the postsynaptic target. Thus, branching and synaptogenesis appear to be tightly linked. Axonal branching requires F-actin polymerization which gives rise to filopodia formation (Korobova and Svitkina, 2008) and polymerization of microtubules which in turn stabilizes these nascent filopodia (Gallo, 2011). Formation and stabilization of axonal branches require neuronal activity and synapse formation, respectively (Uesaka et al.,

2007). Mechanism of activity-dependent branching involves RhoA signaling that modulates actin dynamics and reorganization (Ohnami et al., 2008). Stabilization of nascent collateral branches depends on synapse formation and actin remodeling at presynaptic sites allows simultaneous axonal branching and synapse formation *in vivo* (Chia et al., 2014). Clustering of voltage gated Ca^{+2} channels (VGCC) and integration of synaptic vesicles in the presynaptic membrane is a fundamental step during active zone formation. Active zone is composed of scaffold proteins including Rab3-interacting molecules (RIMs), RIM-binding proteins (RIM-BPs), Bassoon and Piccolo/Aczonin, Liprins-α and the UNC-13/Munc-13 proteins and CAST/ELKS/Bruchpilot proteins (Schoch and Gundelfinger, 2006). These so-called "cytomatrix" proteins build a meshwork underneath the active zone membrane and contribute to synaptic vesicles docking, priming, release and turnover as well as recruiting voltage-gated Ca^{2+} channels to the presynaptic membrane. Disruption of F-actin polymerization impairs NAB-1 and Bassoon clustering and results in loss of active zones (Chia et al., 2012; Zhang and Benson, 2001). Therefore, actin cytoskeleton plays a pivotal role in the assembly of cytomatrix proteins into a meshwork at active zones during synaptogenesis.

3.3 Role of mRNA transport and local translation in neuronal development and maintenance

In different cell types, asymmetric subcellular localization and local translation of specific mRNAs allow spatio-temporal regulation of the cellular proteome, particularly in response to extrinsic cues. In *Drosophila* oocytes, diverse maternal transcripts including mRNAs of bicoid, oskar and gurken localize at distinct anterior or posterior regions and contribute to the establishment of dorsal-ventral and anterior-posterior body axes (St Johnston, 2005). In the budding yeast, sorting of different mRNAs to the bud tip determines the mating type of the daughter cell (Paquin and Chartrand, 2008). In *Xenopus*, the mRNAs of Vg1 (a transforming

growth factor β, TGFβ, family member) are sorted to the vegetal pole of oocytes, where they induce formation of the mesoderm (Weeks and Melton, 1987).

Extracellular cues trigger protein synthesis mostly through PI3K-AKT-mTOR (Campbell and Holt, 2001). Binding of protein synthesis inducing cues like netrin1 and BDNF to cell surface receptors leads to autophosphorylation of the kinase receptor that in turn phosphorylates and activates phosphoinositide 3‑kinase (PI3K) (Campbell and Holt, 2001). PI3K/AKT phosphorylates and thereby inactivating the tumor-suppressor tuberous sclerosis complex-1/2 (TSC1/2), which negatively regulates the small Ras-like GTPase RHEB. Activated RHEB associates with mTOR complex-1 and induces its activity. mTOR signaling leads to activation of its downstream target: 70 kDa ribosomal S6 kinase (S6K) and inhibition of 4E-binding protein-1 (4EBP1) and thus promotes translation initiation and elongation (Anjum and Blenis, 2008). Furthermore, ligand-receptor binding induces RSK activity through MAPK signaling pathway which triggers cap-dependent translation via rpS6 (a protein of the 40S ribosomal subunit) and phosphorylation of eukaryotic translation initiation factor-4B (eIF4B) (Shahbazian et al., 2006). Moreover, RSK induces mTOR signaling by phosphorylating and thereby inactivating of TSC2 (Anjum and Blenis, 2008; Hay and Sonenberg, 2004; Piper et al., 2006).

3.3.1 Synaptic plasticity

In neurons, dendritically targeted mRNAs contribute to diverse cellular processes during synaptic plasticity, learning and memory. For instance, upon synaptic activity calcium/calmodulin-dependent protein kinase II α (CaMIIKα) mRNAs become translated directly at dendritic spines and disturbed dendritic trafficking of this transcript associates with decreased LTP and impaired synaptic plasticity, learning and memory (Miller et al., 2002). Similarly, β-actin mRNAs localize to dendrites and become translated upon neurotrophin binding or glutamate receptor activation. In hippocampal neurons, locally translated β-actin

modulates synaptic plasticity by regulating the size and density of the dendritic spines through cytoskeletal remodeling (Eom et al., 2003). Arc/Arg3.1 is another dendritic mRNA that binds to actin filaments and thus regulates synaptic plasticity via cytoskeleton reorganization (Plath et al., 2006). Mice lacking Arc/Arg3.1 exhibit defects in synaptic transmission and long-term memory (Messaoudi et al., 2007).

3.3.2 Axon guidance

Axonal mRNA transport is involved in axon growth, guidance and branching during the development and in synapse maintenance and axon regeneration in the adult. During axonal growth, neurons receive diverse extracellular guidance cues helping them to reach their postsynaptic targets. Several studies have reported that growth cones which were separated from cell bodies could respond to guidance cues both *in vivo* and *in vitro* indicating that axons contain independent translational machinery (Harris et al., 1987; Ming et al., 2002).

Xenopus laevis retinal growth cones turn toward attractive cues such as netrin1 and brain-derived neurotrophic factor (BDNF) and away from repulsive cues such as sema3a and slit1 (Campbell and Holt, 2001). These attractive cues trigger mTOR signaling pathway and thereby inducing asymmetric local synthesis of β-actin mRNA at the growth cone. Thus, actin polymerization and cytoskeletal reorganization on the side near the attractive cue mediates attractive growth cone response (Campbell and Holt, 2001). Inhibition of β-actin local translation abolishes the attractive response of the growth cone toward netrin1 (Leung et al., 2006). On the other hand, repulsive cues induce local translation of actin depolymerizing proteins, RhoA and cofilin, which in turn disassemble the cytoskeleton and result in growth cone collapse (Piper et al., 2006; Wu et al., 2005).

3.3.3 Axon elongation

Local translation is also required for axon elongation. Numerous transcripts involved in the regulation of cytoskeletal dynamics have been reported to be locally translated in the axon

and axonal growth cone. In spinal motoneurons, β-actin mRNA is sorted to the axonal growth cone and becomes locally translated as a response to BDNF signaling (Rathod et al., 2012). Also in sensory and cerebrocortical neurons, β-actin mRNA is trafficked to axons and becomes synthetized there locally (Bassell et al., 1998; Zheng et al., 2001). Depletion of axonal β-actin mRNA from motoneurons or sensory neurons decreases axonal outgrowth (Donnelly et al., 2011; Glinka et al., 2010). NGF and netrin1-stimulated axonal growth requires axonal synthesis of a cytoskeleton regulator, proteinase-activated receptor 3 (PAR3), and axonal ablation of this mRNA inhibits NGF-induced axon elongation (Hengst et al., 2009). β-thymosin binds to actin monomers and prevents their incorporation into F-actin filaments. Preventing axonal translation of β-thymosin promotes axon elongation in cultured neurons indicating that local translation of cytoskeletal regulators plays an essential role in axon elongation (van Kesteren et al., 2006).

3.3.4 Synaptogenesis and branching

Developing axons stop growing once they reach their synaptic targets and start to form synapse upon receiving target-derived cues. Formation of presynaptic structures and maintenance of synaptic plasticity require local protein synthesis. In *Aplysia's* sensory neurons, Staufen, EF1α and Sensorin mRNAs localize equally to axonal branches that make contact to either a specific target motoneuron or a non-specific target. Nevertheless, the axonal translation rate of these mRNAs is elevated only in those branches which contact the specific target motoneuron (Kim and Martin, 2015). Axon branching and terminal arborization allow establishment of synapses to diverse post synaptic targets. Axon branching initiates with polymerization of actin filaments along the axon shaft at so-called "actin patches" that serve as nucleators for filopodia or lamellipodia formation (Ketschek and Gallo, 2010; Mingorance-Le Meur and O'Connor, 2009). Subsequent microtubule invasion and polymerization is then required for maturation of nascent protrusion into branches (Fig.

3.3.4.1) (Dent and Kalil, 2001; Gallo, 2011; Kalil and Dent, 2014). Different studies have shown that intra-axonal protein synthesis is required for axon sprouting *in vivo* (Buckmaster and Wen, 2011; McWhorter et al., 2003; Qiu et al., 2009). Moreover, in cultured sensory neurons, diverse cytoskeletal proteins including β-actin, subunits of Arp2/3 complex, WAVE1, and the complex stabilizer cortactin are locally translated at branch points as a response to NGF (Spillane et al., 2012; Spillane et al., 2013). Furthermore, siRNA depletion of β-actin affects formation of axonal collateral branches in sensory neurons (Donnelly et al., 2013). Synaptic activity is required for axon branching, as recently shown in *C. elegans*, and actin reorganization at presynaptic sites allows simultaneous axonal branching and synapse formation, thus providing a mechanism for synapse-directed sprouting (Chia et al., 2014).

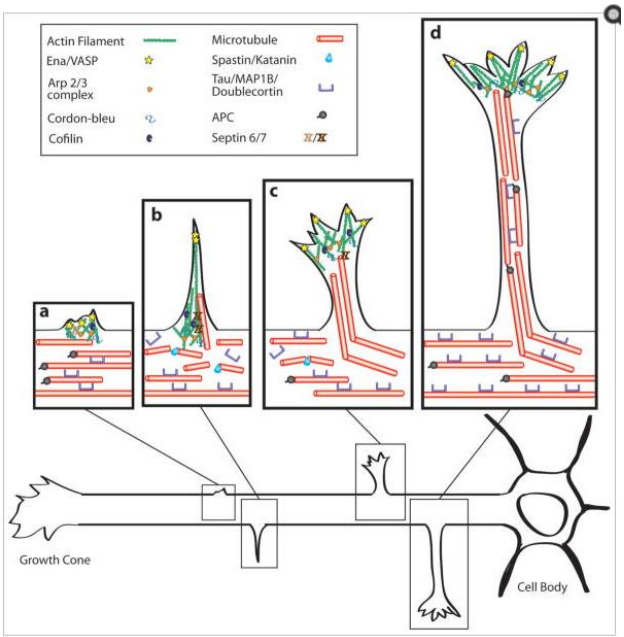

Figure 3.3.4.1 Formation of collateral branches. Actin polymerization in patches gives rise to filopodia or lamellipodia emerging from the axon shaft and requires actin nucleation (ARP2/3), actin branching (ARP2/3) and actin elongation (Ena/VASP) factors. Microtubules stabilize newly formed protrusions, modified from: (Kalil and Dent, 2014).

3.3.5 Axon maintenance and regeneration

Axonal mRNA localization and local translation occur also in mature axons during axon maintenance and especially nerve regeneration after injury. Severed axons are capable of axon

regeneration and blocking protein synthesis inhibits the nerve regeneration capacity *in vitro* (Gumy et al., 2010; Verma et al., 2005). In fact, mature axons contain less mRNA and intra-axonal protein synthesis than developing axons. However; recent studies have shown that the levels of axonally localized mRNAs and protein synthesis machinery increase after nerve lesion (Verma et al., 2005). Formation of an axonal growth cone which is the first step during axon regeneration requires synthesis of new cytoskeletal proteins and transcription factors involved in growth signaling cascades. mRNAs of different transcription regulators including signal transducer and activator of transcription 3 (STAT3) and CEBP-1 (CAAT/enhancer binding protein1) become translated in the axons as a response to nerve injury (Ben-Yaakov et al., 2012; Yan et al., 2009). Similarly, nerve lesion leads to increased axonal trafficking and translation of multiple cytoskeletal proteins including β-actin, neurofilament light chain, β-tubulin, peripherin, vimentin, γ-tropomyosin 3 and cofilin-1, and many non-structural proteins such as resident ER proteins, anti-oxidant and metabolic proteins and heat shock proteins (Willis et al., 2005; Zheng et al., 2001). Overexpression of a transgenic GFP construct which contains 3'UTR of β-actin decreases the mRNA levels of endogenous β-actin in axons and thus affects nerve regeneration *in vivo* (Donnelly et al., 2011). On the other hand, exercises after nerve injury increase the regeneration potential in propriospinal neurons, which interestingly correlates with increased levels of β-actin, GAP-43 and cpg15 mRNAs in the lesioned axons (Sachdeva et al., 2016). Axonal translation of other proteins with transcriptional activity such as cAMP-responsive element (CRE)-binding protein (CREB) is important for axon maintenance and survival. In sensory neurons, retrograde transport of axonally synthetized CREB into the nucleus triggers the expression of diverse genes that promote cell survival (Cox et al., 2008). Also intra-axonal translation of nuclear-transcribed mRNAs encoding mitochondrial proteins, such as cytochrome oxidase subunit 17, propionyl-CoA carboxylase, dihydrolipoamide dehydrogenase, and coenzyme Q subunit 7, contributes to mitochondria function in the axon and thus supports cell survival (Gioio et al., 2001).

3.4 Regulation of axonal mRNA transport by cis-elements and transacting factors

Along with RNA binding proteins, sorted mRNAs form a large mRNP complex, a so-called "RNA granule" (Kiebler and Bassell, 2006). RNA binding proteins (also referred to as transacting factors) play a role in diverse aspects of RNA biogenesis such as splicing, editing, transport, stability, and translation. To transport mRNAs, RNA binding proteins often interact with sequences within untranslated regions (UTRs) of target mRNAs, termed as cis-elements (Bassell and Kelic, 2004). For instance, a 54-nucleotide element within β-actin 3'UTR, termed as "Zipcode", is responsible for trafficking of β-actin mRNA into axons in neurons (Zhang et al., 2001a). Similarly, 3'UTR drives axonal transport of GAP-43 and neural membrane protein-35 mRNAs in sensory neurons, and dendritic transport of CaMKIIα mRNA in hippocampal neurons (Merianda et al., 2013b; Perrone-Bizzozero and Bolognani, 2002; Rook et al., 2000). Interestingly, in hippocampal neurons, 3'UTR of cpg15 mRNA is required for its axonal transport, whereas in sensory neurons, its 5'UTR is responsible for its axonal localization (Merianda et al., 2013a).

The assembly of RNA granules often initiates in the nucleus and continues in the cytoplasm following RNPs nuclear export. RNA granules become transported into distal processes via kinesin, dynein, and myosin motor proteins along the microtubules (Fig. 3.4.1) (Martin and Ephrussi, 2009). During transport process, RNA binding proteins regulate microtubule docking, RNA stability, and translational repression (Adeli, 2011; Shiina et al., 2005), and at the destination they regulate mRNA localization, decay, and translation in response to stimuli (Takei et al., 2001). Other components of RNA granules are RNA helicases, translational factors, scaffold proteins, decay enzymes and miRNAs (Ainger et al., 1993; Anderson and Kedersha, 2006). Zipcode binding protein 1 (ZBP1) is a component of RNA granules that associates with the zipcode domain within the 3'UTR of β-actin mRNA (Welshhans and Bassell, 2011). FMRP is another important RNP involved in both dendritic and axonal transport. FMRP plays a role in translation suppression by recruiting the eIF4E-binding

protein CYFIP1 (Napoli et al., 2008). Loss of function of FMRP causes fragile X syndrome. In *Drosophila*, depletion of this protein causes abnormalities in neuromuscular junction (NMJ) maturation (Zhang et al., 2001b) and pre-synaptic structures (Pan et al., 2008; Tessier and Broadie, 2008), and disturbs Sema3A-mediated growth cone collapse in mouse hippocampal neurons (Li et al., 2009). TAR DNA-binding protein 43 (TDP-43) is a member of the heterogeneous nuclear ribonucleoproteins (hnRNP) involved in transcription repression, splicing, and translation. Mutations in this protein cause a motoneuron disease called Amyotrophic lateral sclerosis (ALS) (Mackenzie et al., 2010). In axons, TDP-43 co-localizes with other RNPs, like FMRP, IMP1, SMN and HuD, and regulates mRNA transport of target genes involved in axon growth (Fallini et al., 2012a).

Other importnat trans-acting elements present in RNA granules are microRNAs, which supress translation of target mRNAs (Schratt et al., 2006). For instance, miR-338 can repress the translation of a subsequet mRNAs, such as COX4I1 (Aschrafi et al., 2008) and ATP5G1 ATP synthase, H+ transporting, mitochondrial F0 complex, and the components of mitochondrial complexes IV and V (Hillefors et al., 2007).

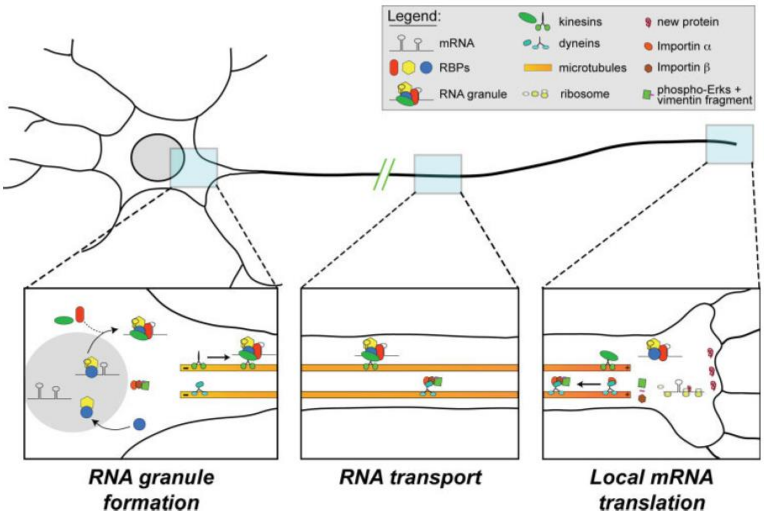

Figure 3.4.1 RNA granule formation for axonal transport. Sorted mRNAs form a complex with RNA binding proteins, a so-called "RNA granules", and become transported along microtubules, modified from: (Wang et al., 2007).

3.4.1 SMN, an essential protein for RNP particle assembly

Survival of Motor Neuron (SMN) is a 38 kD protein that is ubiquitously expressed in all cell types. SMN is encoded by *SMN1* gene located on human chromosome 5q13 (Lefebvre et al., 1995). Smn protein is found in both nucleus and cytoplasm. In the nucleus, Smn is required for the assembly of spliceosomal small nuclear ribonucleoprotein particles (snRNPs), that are involved in splicing and pre-mRNA maturation (Liu and Dreyfuss, 1996). These SnRNPs are composed of an U snRNA (U1, U2, U4, U5, U11 or U12) and a heptameric ring of Sm proteins (Raker et al., 1999). The assembly of Sm proteins into snRNP complex requires the so-called SMN complex, that contains Gemins proteins 2-8, SMN, unr interacting protein (unrip), and ATP (Fig. 3.4.1) (Meister et al., 2001; Ogawa et al., 2009).

In addition to its canonical role in the snRNP biogenesis, Smn facilitates the formation of cytoplasmic RNP particles implicated in axonal mRNA translocation and local translation. Smn has also been shown to interact with hnRNP Q/R, which can bind to the 3'UTR of β-actin mRNA, and it has been questioned whether Smn could also interact with other well-known RNA binding proteins implicated in β-actin mRNA transport such as: ZBP1, HuD, and KSRP (Fallini et al., 2012b; Rossoll et al., 2002). Smn is also required for the axonal transport of candidate plasticity-related gene 15 (cpg15), p21 (cip1/waf1), and polyA mRNAs, as SMN deficiency results in mislocalization of these mRNAs (Akten et al., 2011; Fallini et al., 2011; Hubers et al., 2011).

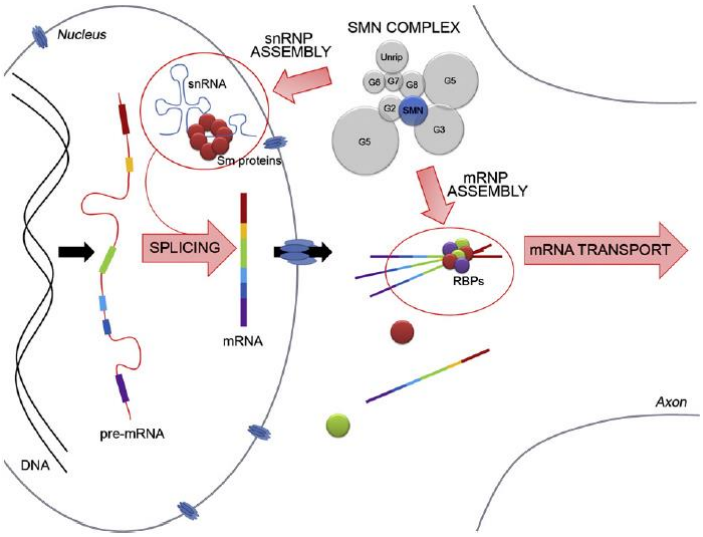

Figure 3.4.1.1 Role of SMN in splicing and mRNP assembly. SMN forms a so-called "SMN complex" together with Sm proteins, Gemins, and Unrips. This complex is involved in splicing of pre-mRNAs, but also facilitates the assembly of sorted mRNAs into RNA granules for axonal transport, modified from: (Fallini et al., 2012b).

3.4.2 Impaired RNA biogenesis and trafficking in motoneuron diseases

Homozygous deletions or mutations in the human *SMN1* gene cause an autosomal recessive neuromuscular disease, called spinal muscular atrophy (SMA). These mutations result in selective degeneration of spinal motoneurons and associate with muscle denervation, weakness, paralysis, and finally death as a result of respiratory dysfunction (Crawford and Pardo, 1996). Many mouse models have been generated to study the pathogenesis of the SMA. Since in mouse there is only one *Smn* copy, knockout of this copy causes embryonic lethality. However, in human there is a second copy of this gene, *SMN2*, which produces only 10% functional protein due to a substitution of C by T, causing skipping of the exon 7 during splicing (Cartegni et al., 2002; Monani et al., 1999). Hence, human *SMN2* gene is introduced into mouse lacking *Smn* (*Smn*$^{-/-}$; *hSMN2tg*) (Hsieh-Li et al., 2000; Monani et al., 2000). These animals develop severe muscle atrophy and die, due to motoneuron dysfunction, within few days after birth. Motoneurons undergo degeneration and exhibit reduced synaptic transmission at NMJs (Winkler et al., 2005). Furthermore, depletion of *Smn* in zebrafish and

cultured motoneurons have been shown to impair axon guidance and elongation (Jablonka et al., 2004; McWhorter et al., 2003).

In vitro studies with primary cultured motoneurons isolated from a severe SMA mouse model have shown that Smn-deficient motoneurons grow shorter axons and smaller growth cones (Rossoll et al., 2003). Interestingly, these observations correlate with reduced β-actin mRNA and protein in the distal axon, indicating that SMN is required for the assembly of ribonucleoptotein particles involved in axonal transport and local translation of β-actin mRNA. Moreover, mouse motoneurons lacking Smn exhibit impaired clustering of voltage-gated Ca^{+2} channels in axon terminals, which correlates with reduced spontaneous excitability. Treatment with cAMP leads to an increase in Smn and β-actin levels, and thus, attenuates observed morphological and functional deficits in motoneuron presynapses (Jablonka et al., 2007). Likewise, suppression of PTEN increases the survival of Smn-deficient motoneurons and improves NMJ innervation and motor functions in SMA mice (Little et al., 2015).

β-actin mRNAs and proteins are highly abundant in the growth cone of developing motoneurons where the local translation of this protein contributes to rapid cytoskeletal rearrangements required for axon pathfinding and presynaptic differentiation (Yao et al., 2006). Thus, impaired axonal mRNA trafficking and local translation upon Smn-deficiency might contribute to the pathogenesis of the SMA.

Amyotrophic lateral sclerosis (ALS) is another common motoneuron disease, which is characterized by progressive degeneration of upper (in the cerebral cortex) and lower motoneurons (in brain stem and the spinal cord), paralysis, and respiratory failure. 90% of all ALS cases are sporadically and only 10% are familial (fALS) (Andersen and Al-Chalabi, 2011). Mutations in more than 30 different genes have been identified as the cause of neuronal death in familial ALS (Renton et al., 2014). These mutations disturb diverse cellular functions, such as protein degradation, mitochondrial function, energy consumption, but also

axonal transport (Tapia, 2014). The second most common genetic cause of fALS is mutations in *SOD1* gene. The mechanism by which mutant *SOD1* gene causes neuronal death, involves oxidative stress, mitochondrial dysfunction, protein aggregation, and glutamate excitotoxicity (Beal, 2000; Robberecht, 2000; Sasaki et al., 2000). Also, mutations in *hnRNP* family members, *TDP-43* and *FUS* genes, have been linked to fALS (Honda et al., 2013). Mutated TDP-43 and FUS form aggregates with SMN (Groen et al., 2013) and are components of stress granules containing sorted mRNAs in ALS patients (Volkening et al., 2009). Hexanucleotide repeat expansions in *C9orf72* gene account for fALS and FTLD (Renton et al., 2011). Corresponding transcripts associate with RNA aggregates within nuclear foci (DeJesus-Hernandez et al., 2011), which undergo RAN translation and form toxic aggregates (Zhang et al., 2014). Thus, disturbed RNA metabolism could contribute to neurodegeneration in both SMA and ALS patients.

3.5 Aim of the present study

Axon arborization and synaptogenesis are two fundamental steps during the development of neuronal circuitry. *In vivo* and *in vitro* studies have shown that the actin cytoskeleton plays a crucial role during these two processes. The dynamics of actin polymerization and stability depend on the three different actin isoforms; α-, β- and γ-actin. The expression of actin isoforms is tissue specific and highly regulated, indicating that these different isoforms might exert specific cellular functions. Interestingly, in neuronal cells, the transcripts and proteins for these isoforms are differentially distributed in the soma and axon. In sensory neurons, only mRNAs for β-actin are sorted into axons (Willis et al., 2011) and it has been shown that the impaired local translation of this isoform disturbs axonal branching in these neurons (Donnelly et al., 2013). Also in motoneurons, β-actin is translated locally in the axonal growth cone which suggests a role for this isoform in axon elongation and guidance in these cells (Rathod et al., 2012; Rossoll et al., 2003). Nevertheless, β-actin motoneuron-specific knockout mice are viable and show no morphological or behavioral defects (Cheever et al., 2011), suggesting a compensatory response for the lack of β-actin in these neurons. Thus, it seems that the expression of actin isoforms is differentially regulated in motoneurons. Unraveling the mechanism of such a compensatory response mediated by α- and γ-actin isoforms would be of major interest.

Furthermore, a key question one would need to answer refers to the local translation of these different actin isoforms and how this could contribute to actin dynamics and rearrangements during motor axon growth and maturation.

The aim of the present study was to investigate the mechanism of axonal trafficking and local translation of α-, β- and γ-actin mRNAs, and to address the differential role of these three isoforms in regulating actin dynamics during axonal elongation, branching, and formation of presynapses in embryonic mouse motoneurons.

4. Materials and Methods

4.1 Materials

4.1.1 Animals

Laboratory animals used in this study were bred in the animal facility of the Institute of Clinical Neurobiology, University Hospital of Würzburg. They were maintained at 20–22°C and 55–65% humidity with a 12 hours light/dark cycle. Animals were provided with food and water in excess amounts. CD-1 mice were maintained as an outbred line obtained from Charles River animal facility and used as wildtype control. SMA type I transgenic mice were generated using C57BL/6 genetic background as previously described (Schrank et al., 1997). Human *SMN2* gene was introduced into the null $Smn^{-/-}$ background to rescue the lethality and this line, $Smn^{+/-}$; *SMN2tgtg*, was used for studying the role of Smn protein in axonal mRNA transport and local translation of the three actin isoforms (Monani et al., 2000).

4.1.2 Cell Lines

4.1.2.1 HEK^{293T} cell line

HEK^{293T} cells were used to generate lentiviral particles and to check generated expression constructs.

4.1.2.2 NSC-34 cell line

NSC-43 cell line was used to check generated knockdown constructs before lentiviral production.

4.1.2.3 Hela cell line

Hela cell line was used to determine virus titer.

4.1.3 Chemicals, reagents and buffers

30% Acrylamide bis acrylamide	Applichem
Acetic acid	Merck
Agarose	Applichem
Ammonium persulfate	Sigma
Ampicillin sodium salt	Sigma
Anisomycin	Sigma
Aqua Poly/Mount	Polysciences
ATP	Sigma
B-27 supplement	GIBCO-Invitrogen
Betaine monohydrate	Sigma
BDNF	Institute of clinical neurobiology
Bromophenol blue	Merck
Bovine serum albumin	Applichem
Boric acid	Applichem
BSA	New England Biolabs
Chelex	BioRad
Chloroform	Applichem
CNTF	Institute of clinical neurobiology
Cycloheximide	Sigma
Diethyl pyrocarbonate (DEPC)	Sigma
Di-Sodium hydrogen phosphate	Merck
DMEM	GIBCO-Invitrogen
DMSO	Sigma
DNA decontamination reagent	Sigma

dNTPs	Fermentas
Donkey serum	Liniaris
DTT	Invitrogen
Dulbecco`s PBS	PAA Laboratories
EDTA	Merck
EGTA	Sigma
Ethanol	Sigma
Ethidium bromide	Merck
Formaldehyde Ampules, Methanol-free	Thermo Scientific
GeneRuler DNA Ladder	Thermo Scientific
Glutamax	GIBCO-Invitrogen
Glucose	Sigma
Glycerol	Sigma
Glycine	Merck
Glycogen RNA grade	Fermentas
Goat serum	Liniaris
HBSS	GIBCO-Invitrogen
HEPES	Sigma
Phusion™ High-Fidelity DNA polymerase	ThermoFisher
Horse serum	Liniaris
Isopropanol	Sigma
Kresylviolett (Acetat)	Merck
Laminin	Invitrogen
Laminin 221/211	Millipore
LB broth base	Sigma

Lipofectamine 2000	ThermoFisher
L-Lysine mono hydrochloride	Sigma
Magnesium chloride	Sigma
Magnesium sulfate	Sigma
Mercaptoethanol	Merck
Methanol	Sigma
Micro-90® concentrated cleaning solution	Sigma
Milk powder	Applichem
Neurobasal medium	GIBCO
Non-essential amino acids	Invitrogen
NP-40	Roche
OptiMEM medium	Invitrogen
Optimum cutting temperature compound	Tissue-Tek Sakura
Page ruler pre stained protein ladder	Fermentas
PBS (RNase free)	Affymetrix
P/S	Invitrogen
PIPES	Sigma
Poly D-L-Ornithine	GIBCO
Potassium chloride	Merck
Protease Inhibitor Cocktail Tablets	Roche
Protein A agarose	New England Biolabs
Proteinase K	Roche
Random Primer N6	Roche
RNase away reagent	Ambion
RNasin® Plus RNase Inhibitor	Promega

Sarcosyl powder	Sigma
Saponin	Sigma
Select Agar	Invitrogen
Sodium bicarbonate	Merck
Sodium chloride	Merck
Sodium di-hydrogen phosphate	Carl Roth
Sodium dihydrogen phosphate	Carl Roth
Sodium (meta) periodate	Sigma
Sucrose	Sigma
10 × Taq buffer	5 Prime
Taq DNA polymerase	5 Prime
TEMED	Merck
Terralin	Schuelke
Tris Base	Roth
Triton-X 100	Sigma
Trypsin	Worthington
Trypsin inhibitor	Sigma
Tween 20	Sigma
Water Molecular biology grade	Applichem

Solutions for DNA extraction and genotyping

Lysis buffer for quick and dirty DNA extraction	2.5 ml 10% sarcosyl solution
	1 ml 5 M NaCl
	2.5 g Chelex (= 5%)
	Add bidistilled water to 50 ml

Lysis buffer for chloroform DNA extraction	10 mM Tris-HCl pH 7.5
	100 mM EDTA pH 8.0
	150 mM NaCl
	0.5% SDS
5 M betaine solution	20.28 g betaine monohydrate,
	add 30 ml bidistilled water
6 × loading buffer	30% glycerin solution in TAE
	0.15% bromophenol blue
	0.15% xylene cyanol
	Add 1 × TAE to 50 ml
50 × TAE buffer	484 g Tris-base
	114.2 ml glacid acetic acid
	200 ml 0.5 M EDTA pH 8
	add bidistilled water to 2 L

Solutions for RNA extraction, qRT-PCR and LMD

DEPC water	add 1 ml diethyl pyrocarbonate to 1 L
	bidistilled water
Lysis buffer for RNA extraction and direct	10 mM Tris-HCL pH 8
cDNA synthesis (100 µl reaction volume)	2 mM dNTPs
	1 mM random hexamer N6
	1 × first strand buffer
	10 µl DTT (10 mM)
	5 µl NP-40 (0.5%)
	20 µg glycogen

	10 U RNasin® Plus RNase Inhibitor
	add RNase free water to 100 µl
Cresyl violet solution	2 g Cresyl violet
	add 200 ml ethanol
EB-BSA	4.5 ml 10 mM Tris-HCL pH 8
	0.5 ml 100 × BSA

Solutions for FRAP

ACSF buffer	127 mM NaCl
	3.0 mM KCl
	1.25 mM NaH_2PO_4H20
	23.0 mM $NaHCO_3$
	25.0 mM glucose (add freshly)

Solutions for motoneuron and cortical neuron cultures

P^{75} panning	dilute anti-p^{75} antibody (MLR2) 1:10000 in 10 mM Tris buffer pH 9.5
Borate buffer	add 0.15 M boric acid to bidistilled water, adjust pH to 8.35 and sterile autoclave
Depolarization solution	30 mM KCl
	0.8% NaCl
	2 mM $CaCl_2$
	add distilled water and sterile autoclave

1% trypsine	2 g trypsine
	200 ml HBSS
	5 ml 1 M HEPES pH 7.3
1% trypsine inhibitor	100 mg trypsine inhibitor
	9.75 ml HBSS
	0.25 ml 1M HEPES p H 7.3
Laminin	dilute laminin in HBSS to obtain 2.5 μg/ml final concentration
100 × PORN solution	500 mg PORN
	dissolve in 10 ml borate buffer for 0.5 mg/ml final concentration
1 M HEPES buffer pH	23.83 g HEPES
7.4	add 100 ml distilled water and autoclave
dissection medium	HBSS
	1 × Na-pyruvat
	0.1% glucose
	10 mM HEPES

Solutions for live cell extraction

Cytoskeleton buffer (CB)	10 mM MES pH 6.1
	150 mM NaCl
	5 mM EGTA
	5 mM glucose
	5 mM $MgCl_2$

Solutions for immunocytochemistry and *in situ* hybridization

0.2 M phosphate buffer pH 7.4	35.6 g $Na_2HPO_4 \times 2H_2O$
	5.42 g $NaH_2PO_4 \times 1H_2O$
Lysine-phosphate buffer	3.66 g L-lysine
	100 ml water
	add 0.1 M Na_2HPO_4 until pH is 7.4
	add 50 ml 0.2 M phosphate buffer
	fill up to 200 ml with distilled water
16% PFA pH 7.4	16 g paraformaldehyde
	dissolve in 50 ml water
	add few drops of NaOH
	dissolve at 60°C
	add 41 ml of 0.2 M Na_2HPO4
	add 9 ml of 0.2 M NaH_2PO4
4% PLP pH 7.4 (10 ml)	7.5 ml lysine phosphate buffer
	2.5 ml 16% PFA
	0.135 g glucose
	0.021 g sodium (meta) periodate
10 × PBS pH 7.4 (1 L)	80 g NaCl
	2.0 g KCl
	14.4 g Na_2HPO4
	2.4 g KH_2PO4
	add distilled water to 1 L and autoclave
Saponin solution (10 mg/ml stock)	100 mg saponin
	10 ml PBS

Block solution	10 % horse or donkey serum 2% 1× BSA 5% sucrose in PBS 0.2 mg/ml saponin 0.3% Triton-X 100

Primary antibodies used for immunofluorescence

Antibody	Host	Working dilution	Company
monoclonal anti-α-actin	mouse	1:500	ThermoFisher, MA5-12542
monoclonal anti-β-actin	mouse	1:1000	GeneTex, GTX26276
monoclonal anti-γ-actin	mouse	1:1000	Santa Cruz, sc-65634
Alexa Fluor® 546 phalloidin	-	1:50	Invitrogen, A22283
polyclonal anti-Tau	rabbit	1:1000	Sigma, T6402
monoclonal anti-α-Tubulin	mouse	1:1000	Sigma, T5168
monoclonal anti-Map2	mouse	1:1000	Sigma, M1406
polyclonal anti-pan-actin	rabbit	1:200	Cytoskeleton, D18C11
monoclonal anti-Gapdh	mouse	1:000	Calbiochem, CB1001
polyclonal anti-vitamin D binding protein	rabbit	5 µg/ml	Thermoscientific, PA5-19802
monoclonal anti-Digoxigenin	mouse	1:500	AbCham, ab420
monoclonal anti-HA	rat	1:1000	Roche, 11867423001

Table 4.1.1 List of primary antibodies used for immunofluorescence

Secondary antibodies used for immunofluorescence

Antibody	Host	Working dilution	Company
Dylight™ 405 anti-rabbit IgG (H+L)	goat	1:250	JIR, 111334
Alexa Fluor® 488 anti-rabbit IgG (H+L)	goat	1:500	Invitrogen, A11008
Cy3 anti-rabbit IgG (H+L)	donkey	1:500	JIR, 711-165-152
DyLight™ 649 anti-rabbit IgG (H+L)	goat	1:500	JIR, 711-495-152
Alexa Fluor® 488 anti-mouse IgG (H+L)	goat	1:500	Invitrogen, A11029
Cy3 anti-mouse IgG (H+L)	goat	1:500	JIR, 115-165-146
Cy5 anti-mouse IgG (H+L)	goat	1:500	JIR, 115-175-146
Alexa Fluor® 488 anti-mouse IgM	goat	1:500	ThermoFisher, A-21042
Alexa Fluor® 488 anti-mouse IgG1	goat	1:500	ThermoFisher, A21121
DyLight™ 550 anti-mouse IgM	goat	1:500	ThermoFisher, SA5-10151
Cy3 anti-rat IgG (H+L)	donkey	1:500	JIR, 712-165-150

Table 4.1.2 List of secondary antibodies used for immunofluorescence

Solutions for G-actin to F-actin separation

Actin stabilization buffer	0.1 M PIPES pH 6.9
	30% glycerol (vol/vol)
	5% DMSO (vol/vol)
	1 mM $MgSO_4$
	1 mM EGTA

	1% Triton X-100 (vol/vol)
	2 mM ATP
	complete protease inhibitor and phosphatase inhibitor

Buffers for western blot analysis

RIPA buffer	1 M Tris-HCl pH 7.6
	150 mM NaCl
	1% NP-40
	0.5% Sodium deoxycholate
	1 × protease inhibitor
10 × TBS pH 7.4	0.2 M Tris-Base
	1.5 M NaCl
1 × TBST pH 7.4 (1 L)	100 ml 10 × TBS
	0.5% Tween 20
	add distilled water to 1 L
10 × SDS running buffer	30.3 g Tris-base
	144 g glycine
	10 g SDS
5 × Laemmli buffer	4% SDS
	125 mM Tris-HCl pH 6.8
	10% mercaptoethanol
	20% glycerol
	0.004% bromophenol blue
Transfer buffer (100 ml)	5 ml 10 × SDS running buffer
	20 ml methanol (20%)
	75 ml millipore water

Blocking buffer	5 g milk powder
	100 ml 1× TBST
Stripping buffer	1 M Tris-HCL pH 6.7
	10% SDS
	100 mM mercaptoethanol

Stacking gel 4%

Reagents	Volume
30% acrylamide bis-acrylamide	850 µl
1 M Tris-HCl pH 6.8	1.25 ml
10% SDS	50 µl
10% Ammonium persulfate	50 µl
TEMED	5 µl
Millipore water	3.4 ml

Separating gel

	Gel %		
Reagents	8%	10%	12%
30% Acrylamide bis-acrylamide	2 ml	2.5 ml	3 ml
1.5 M Tris-HCl pH 8.8	1.87 ml	1.87 ml	1.87 ml
10% SDS	75 µl	75 µl	75 µl
10% Ammonium persulfate	75 µl	75 µl	75 µl
TEMED	5 µl	5 µl	5 µl
Millipore water	3.47 ml	3.47 ml	2.47 ml

Primary antibodies used for western blot analysis

Antibody	Host	Working dilution	Company
monoclonal anti-α-actin	mouse	1:500	ThermoFisher, MA5-12542
monoclonal anti-β-actin	mouse	1:4000	GeneTex, GTX26276
monoclonal anti-γ-actin	mouse	1:1000	Santa Cruz, sc-65634
monoclonal anti-Smn	mouse	1:4000	BD Biosciences, 610646
monoclonal anti-pan actin	mouse	1:3000	Millipore, MAB1501R
monoclonal anti-pan actin	mouse	1:5000	EnCor, MCA-5J11
polyclonal anti-Calnexin	goat	1:5000	Acris, AB0037-200
polyclonal anti-Calnexin	rabbit	1:5000	Enzolifesciences, ADI-SPA-860
monoclonal anti-Gapdh	mouse	1:5000	Calbiochem, CB1001
monoclonal anti-HA	rat	1:5000	Roche, 11867423001

Table 4.1.3 List of primary antibodies used for Western blot

Secondary antibodies used for western blot analysis

Antibody	Host	Working dilution	Company
Peroxidase AffiniPure anti-mouse IgG	goat	1:10000	JIR, 115-035-003
Peroxidase AffiniPure anti-goat IgG	donkey	1:10000	JIR, 705-545-147

Peroxidase AffiniPure anti-rat IgG (H+L)	goat	1:10000	JIR, 112-035-003
Peroxidase AffiniPure anti-rabbit IgG (H+L)	goat	1:10000	JIR, 111-035-003

Table 4.1.4 List of secondary antibodies used for Western blot

Cell culture media

Cell culture	Complete medium
For motoneurons	NB with 1 × Glutamax
	2% horse serum
	1 × B27 supplement
	5 ng/ml BDNF and CNTF
For cortical neurons	NB with 1 × Glutamax
	1 × B27 supplement
	0.5% P/S
For HEK^{293T} and NSC-34	DMEM with 1× Glutamax
	10% FBS
	1 × non-essential amino acids
	1 × P/S

Cloning media

LB-Agar (1 L)	15 g select Agar
	20 g LB
	1 ml ampicillin (10 µg/ml end concentration)
	add distilled water and sterile autoclave

Primers for genotyping

Name	Sequence
Smn-wt/ko-for	5'-CTG GAA TTC AAT ATG CTA GAC TGG CCT G-3'
Smn-wt-rev	5'-AAT CAA TCT ATC ACC TGT TTC AAG GGA GTT G-3'
Smn-ko-rev	5'-GAT GTG CTG CAA GGC GAT TAA GTT G-3'
SMN2tg-for	5'-CGG AAG TCG TCA CTC TTA AG-3'
SMN2tg-rev	5'-GAA GAA GGG TGC TGA GAG CG-3'

Table 4.1.5 List of used primers for genotyping

Primers for qRT-PCR

Name	Sequence
α-actin-for	5'-TAG ACA CCA TGT GCG ACG AAG A-3'
α-actin-rev	5'-ACC TAC CAT GAC ACC CTG GTG A-3'
β-actin-for	5'-GAT GAC CCA GAT CAT GTT T-3'
β-actin-rev	5'-CGT GAG GGA GAG CAT AG-3'
γ-actin-for	5'-ATC GCC GCA CTC GTC AT-3'
γ-actin-rev	5'- GCC GTG TTC GAT AGG GTA -3'
Gapdh-for	5'- AAC TCC CAC TCT TCC ACC TTC - 3'
Gapdh-rev	5'-GGT CCA GGG TTT CTT ACT CCT T-3'
Histone H1f0-for	5'-CCC AAG TAT TCA GAC ATG AT-3'
Histone H1f0-rev	5'-CGC TTG ATG GAC AAC T-3'
18s rRNA-for	5'-CGC GGT TCT ATT TTG TTG GT-3'
18s rRNA-rev	5'-AGT CGG CAT CGT TTA TGG TC-3'
α-actin-HA-for	5'-GAT TAC GCT GGG ATC CGA ATT CA-3'
α-actin-HA-rev	5'-CGG AAG CAT AGA GGG ACA GC-3'

β-actin-HA-for	5’-CCC ATA CGA TGT TCC AGA TTA CGC-3’
β-actin-HA-rev	5’-CAC GGT TGG CCT TAG GGT TCA-3’
γ-actin-HA-for	5’-GAT TAC GCT GGG ATC CGA ATT CAA-3’
γ-actin-HA-rev	5’-GAC AAT GCC GTG TTC GAT AGG GT-3’

Table 4.1.6 List of used primers for qRT-PCR

Oligos for shRNA cloning

Name	Sequence
ShRNA-α-actin 1	5’-CAG GAC GAC AAT CGA CAA T-3’
ShRNA-α-actin 2	5’-CAA TCG ACA ATC GTG CTG T-3’
ShRNA-β-actin 1	5’-GCA CAC CTT ACC TTA CAC A-3’
ShRNA-β-actin 2	5’-GTG CAC ACC TTA CCT TAC A-3’
ShRNA-γ-actin 1	5’-GCA CGC TGT AGA TGA GAA A-3’
ShRNA-γ-actin 2	5’-GCA CGA TGA AGA TTA AGA T-3
ShRNA-γ-actin 3	5’-CTA GCA CGA TGA AGA TTA A-3

Table 4.1.7 List of used oligos for shRNA cloning

Primers for HA-tag expression cloning

Name	Sequence
α-actin-HA-for	5’-TTT TTT GAA TTC AAT GCG ACG AAG ACG AGA CCA CC-3’
α-actin-HA-rev	5’-TTT TTT GAA TTC TTG GAG CAA AAC AGA ATG GCT G-3’
β-actin-HA-for	5’-TTT TTT GAA TTC AAG ATG ACG ATA TCG CTG CGC T-3’
β-actin-HA-rev	5’-TTT TTT GAA TTC GTT TGT GTA AGG TAA GGT GTG C-3’
γ-actin-HA-for	5’-TTT TTT GAA TTC AAG AAG AAG AAA TCG CCG CAC TC-3’
γ-actin-HA-rev	5’-TTT TTT GAA TTC CAG TTA CTG CAG CAC TTT TA-3’

Table 4.1.8 List of used primers for HA-tag expression cloning

Primers for Myr-GFP-3'UTR expression cloning

Name	Sequence
α-actin-3'UTR-for	5'-TGC TAG CTA AGC GCA CTC GCG TCT GCG TT-3'
α-actin-3'UTR-rev	5'-ATG AAT TCT TGG AGC AAA ACA GAA TG GCT GG-3'
β-actin-3'UTR-for	5'-TGC TAG CTA AGC GGA CTG TTA CTG AGC TGC GTT-3'
β-actin-3'UTR-rev	5'-ATG AAT TCG TTT GTG TAA GGT AAG GTG TGC-3'
γ-actin-3'UTR-for	5'-TTC TAG ATA AAT GGA CTG AGC AGG TGC CAG-3'
γ-actin-3'UTR-rev	5'-ATG AAT TCT TCA GTT ACT GCA GCA CTT TTA T-3'

Table 4.1.9 List of used primers for Myr-GFP-3'UTR expression cloning

Primers for β-actin rescue cloning

Name	Sequence
β-actin-for	5'-GTA GGA TCC GCC ACC ATG GAT GAC GAT ATC GCT GCG CTG-3'
β-actin-rev	5'-TAC GGA TCC ACT TTT ATT GGT CTC AAG TCA GTG T-3'

Table 4.1.10 List of used primers for β-actin rescue cloning

List of plasmids

Vector	Insert	Vector Source
pCR®4-TOPO® TA 4.0 kb	qRT-PCR amplicon of α-actin	Invitrogen
	qRT-PCR amplicon of β-actin	
	qRT-PCR amplicon of γ-actin	
pCMV R8.91	Lentiviral packaging helper plasmids	(Dull et al., 1998; Zufferey et al., 1998)
pMD.G VSVG		
pRSV-REV		
pMDLg/pRRE		
	shRNA targeting 3'UTR of α-actin	

pSIH1-H1-Puro shRNA	shRNA targeting 3'UTR of β-actin	System Biosciences
	shRNA targeting 3'UTR of γ-actin	
	shRNA targeting 3'UTR of β-actin and rescue β-actin	
FU-Valentine ubiquitin promoter	HA-tag α-actin (ORF+3'UTR)	Institute of Clinical Neurobiology, provided by Robert Blum
	HA-tag β-actin (ORF+3'UTR)	
	HA-tag γ-actin (ORF+3'UTR)	
FU-Valentine ubiquitin promoter	LCK-Myr-eGFP+3'UTR of α-actin	cloned by Reena Rathod (Rathod et al., 2012)
	LCK-Myr-eGFP+3'UTR of β-actin	
	LCK-Myr-eGFP+3'UTR of γ-actin	
pCDH1-MSC-EF1 ubiquitin promoter	rescue β-actin (ORF+3'UTR)	Institute of Clinical Neurobiology

Table 4.1.11 List of used plasmids for cloning

Commercial Kits

Kits	Company
BCA Protein Assay Kit	Pierce
ECL Western Blotting Detection kit	GE Healthcare
LightCycler® FastStart DNA Master SYBR Green I	Roche
Luminaris Color HiGreen qPCR Master Mix	ThermoFisher
NucleoBond® Xtra Midi/Maxi plasmid purification kit	Macherey-Nagel
Plasmid mini-prep kit	Macherey-Nagel
QIAX II gel extraction kit	Qiagen
RNA extraction kit	Qiagen
Superscript III First strand synthesis	Roche
TOPO® TA cloning kit	Invitrogen

ViewRNA ISH Cell Assay	Affymetrix-eBioscience

Softwares

- ApE plasmid editor
- Adobe Illustrator CS5
- Adobe Photoshop 7.0
- Endnote X7
- ImageJ, Fiji
- GraphPad Prism 6.0
- Leica LAS-AF lite
- Microsoft Office 2010, Excel, Word, Power Point
- Nikon ND software
- Oligo 6 primer design
- OriginLab Viewer

4.2 Methods

4.2.1 HEK^{293T} and NSC-34 culture

After reaching 90% confluency, cells were passaged 3 times/week to maintain desired density. Medium was removed and cells were washed shortly 1 × with pre-warmed trypsin/EDTA to remove cell debris. 2 ml of trypsin/EDTA solution was added and incubated at RT (for HEK^{293T} cell line) or at 37°C (for NSC-34 cell line) for 2 min. Trypsinization was stopped by adding 5 ml fresh pre-warmed full DMEM medium and cells were collected into a 15 ml Falcon tube. After 5 min centrifugation at 400 g, supernatant was aspired and pellet was resuspended in 5 ml fresh DMEM medium. 10 µl of diluted cells was used to determine cell number using a hemacytometer (Neubauer chamber). 5×10^4 cells/cm^2 were seeded in a T-75 cm^2 flask in 25 ml DMEM medium supplied with 10% FCS, 10% DMSO, 1% MEM non-essential amino acids (100 × stock), 6 mM L-glutamine and 1% P/S and maintained in a humidified incubator at 37°C with 5% CO2 supply.

4.2.2 Cortical neuron culture

For cortical neuron culture cortices were dissected from E17 CD1 wild type mouse embryos and collected in 500 µl HBSS. 0.5% trypsin (Worthington) was added and incubated for 20 min in a water bath at 37°C. Trypsinized cells were washed 3 × with dissection medium and 0.25% DNase (Sigma) was added. Cells were then incubated for 5 min at RT and then washed 2 × with dissection medium. 0.5% trypsin inhibitor (Sigma) was added and triturated using a Pasteur pipette. Cell suspension was transferred into a new 15 ml Falcon tube and the remaining cells were triturated once again. Cells were collected by 3 min centrifugation at 400 g. Medium was removed and pellet was resuspended in 5 ml fresh NB medium. One million cells were plated in microfluidic chambers and 20000 cells on poly-l-lysine coated glass coverslips. Cortical neurons were maintained in NB medium supplied with 1 × B27, 0.5% P/S

and 1% Glutamax in a humid CO_2 incubator. Medium was replaced every 3 days. This technique was applied by my colleague Michaela Keßler.

4.2.3 Enrichment of embryonic mouse motoneurons and virus transduction

The isolation and enrichment of primary mouse motoneurons was performed as previously described (Wiese et al., 2010) and motoneurons were enriched by panning using a p^{75NTR} antibody (Wiese et al., 1999).

Motoneurons were seeded on glass coverslips for IF experiments. Coverslips were sterilized by flaming in 70% ethanol and air dried or by 30 min UV sterilization and placed into 4- or 12-well dishes. Wells were coated with PORN solution at a final concentration of 0.5 mg/ml by overnight incubation at 4°C. On the next day, coverslips were washed 3 × with sterile HBSS, laminin solution was added at 2.5 µg/ml final concentration and incubated at RT for at least 1 h. For cell viability assay as well as protein and RNA extraction, cells were plated directly on PORN/laminin pre-coated plastic surface in 12- or 24-well dishes. For transgenic mouse lines, 24-well plates were used for panning and for wt CD1 mouse line, a 10 cm dish was used. P^{75NTR} antibody was diluted in 10 ml Tris buffer and added into panning plates. After 1 h incubation at RT, panning plates/dishes were washed 2 × with HBSS and 1 × with NB and covered with 10 ml and 500 µl of NB for 10 cm dishes and 24-well plates, respectively.

Mice were sacrificed by cervical dislocation and lumbar spinal cords were dissected from E 13.5 mouse embryos. After removing meninges and dorsal root ganglia, each spinal cord was transferred into a 1.5 ml tube containing 90 µl sterile HBSS and kept on ice. Under a cell culture laminar flow, 1% trypsine solution was added to spinal cord tissues and incubated in a water bath (37°C) for 15 min. Trypsinization was stopped by adding 1% trypsine inhibitor to tubes and triturated by pipetting up and down. Suspensions of single motoneurons were transferred into panning dishes (pre-coated with p^{75NTR} antibody) and incubated at RT for 45

min. Panning plates/wells were then washed 3 × with NB medium. After removal of nonadherent cells, attached p^{75NTR}-expressing neurons were dissociated from panning plates by adding 2 ml (for 10 cm dishes) and 500 µl (for 24-well plates) depolarization buffer and incubated for 10 sec. To neutralize depolarization process, 5 ml (for 10 cm dishes) and 500 µl (for 24-well plates) complete NB medium was added to panning plates. Cells were collected in NB medium and transferred into a clean 15 ml Falcon tube. Cell suspension was centrifuged at 400 g for 4 min. Medium was aspired and pellet was resuspended in 200 µl medium. Cells were counted using a hemacytometer (Neubauer chamber) and desired number of cells was transferred into 1.5 ml tubes for virus transduction. Lentiviruses were added directly to the motoneuron suspension (in a total volume of max 50 µl) and incubated for 10-15 min at RT. Laminin was aspired and motoneurons were immediately plated onto glass coverslips or into wells. Cells were maintained in complete NB medium supplied with 5 ng/ml BDNF and CNTF for 5-7 DIVs in a humid CO_2 incubator at 37°C. Medium was replaced 24 h after plating and then every other day.

4.2.4 Compartmentalized motoneuron culture

Compartmentalized microfluidic chambers were used as described previously (Saal et al., 2014). Microfluidic chambers (Xona Microfluidics, SND 150) were washed for 30 min in an ultrasonic bath using 2% Micro-90® concentrated cleaning solution. Chambers were rinsed first in water for 10 min and then in 70% ethanol for 30 min and dried overnight under a laminar flow. Sterile chambers were placed on 10 cm dishes which were pre-coated with PORN and incubated overnight. Next day, PORN was washed 3 × with HBSS and laminin was added to both main channels and microchannels. Laminin was removed and isolated motoneurons were directly plated into one side serving as the somatodendritic compartment. During 7 days culturing, axons grew through the microgrooves to the other compartment (the axonal compartment) as a response to a BDNF gradient which was applied at 20 ng/ml only to

the axonal compartment. CNTF and BDNF were applied to both compartments at 5 ng/ml concentrations. This technique was applied by my colleague Lena Saal.

4.2.5 Transient plasmid transfection using lipofectamine™ 2000 reagent

HEK^{293T} or NSC-34 cells were seeded in T-75 flasks. After cells reached 90% confluency, they were trypsinized, counted and 10^6 cells were seeded in 6-well plates in full DMEM medium without P/S and placed in the incubator. In parallel, 6 µl lipofectamine™ 2000 and DNA plasmid (0.5 µg for expression plasmid and 1.5 µg for shRNA plasmid) were separately added into two 1.5 ml tubes containing each 200 µl Opti-MEM medium and incubated for 10 min at RT under the laminar flow. Next, contents of both tubes were mixed and incubated for another 20 min at RT. DNA lipid complex was added to freshly seeded cells and placed in the incubator for 6 h. Medium was then completely removed and full DMEM medium containing P/S was added. Cells were harvested 36 h after transfection.

4.2.6 Lentivirus production

Lentiviral particles were packaged in HEK^{293T} cells with pCMV-VSVG and pCMVΔR8.91 helper plasmids as described previously (Rehberg et al., 2008). Cells were transfected with Lipofectamine 2000 (Invitrogen) in OptiMEM medium with 10% fetal calf serum for 12–14 h and viral supernatants were harvested 72 h after transfection by ultracentrifugation. This technique was applied by my colleagues Elke Spirk and Hildegard Troll.

4.2.7 Virus titration

To estimate the amounts of infectious viral particles, virus titer was determined. Hela cells were seeded into a 24-well plate (1000 cells/well) and grown in an incubator for 2 days. For a serial dilution of virus, 12 × 1.5 ml tubes were prepared. 50 µl full medium (DMEM + 10% FBS and 1% P/S) was added into the first tube and each 25 µl into the remaining 11 tubes. In the first tube, 2 µl of the virus pellet was added and resuspended by pipetting up and down. 25 µl of the suspension was transferred into the second tube, mixed and again 25 µl was pipetted

into the third tube and likewise a 10-fold serial dilution was created giving a dilution of 10^{-11} in the last tube. The tube contents were added onto seeded cells and incubated overnight. Next day, medium was replaced and cells were fixed 48 h after transduction. The number of infectious particles was determined from the last dilution in which still GFP/HA positive signal was detected.

4.2.8 DNA isolation

For genotyping, DNA was obtained from tails of adult mice or from heads of embryos. DNA was extracted using two different methods:

a) Fast method

¼ of head/tail biopsies were transferred into 2 ml tubes containing 500 µl lysis buffer and 1 mg/ml proteinase K and incubated at 60°C under shaking (750 rpm) for 3 h in a thermomixer. To inactivate proteinase K, samples were boiled at 99°C for 5 min and centrifuged immediately at 18000 g for 5 min. Supernatants were transferred into a 1.5 ml tube and DNA concentration was measured using Nanodrop spectrophotometer. 300 ng DNA was used as a template for the PCR reaction.

b) Chloroform method

Head/tail biopsies were lysed in 500 µl lysis buffer containing 1 mg/ml proteinase K and incubated at 60°C, 750 rpm in a thermomixer overnight. 430 µl 5 % SDS and 170 µL 3 M NaCl were added into tubes and vortexed for 15 sec. Next, 750 µl chloroform was added and vortexed for 30 sec until a white suspension was formed. Suspensions were centrifuged at 4°C, 400 g for 5 min. Upper phase was transferred into a clean 1.5 ml tube and DNA was precipitated by adding 700 µl isopropanol. To pellet DNA, samples were centrifuged at 4°C, 18000 g for 5 min and supernatants were removed. Pellets were washed with 70% ethanol and centrifuged for 2 min at 4°C, 18000 g. Ethanol was removed and the pellet was air dried for

10 min at RT. DNA was reconstructed and dissolved in 100 µl elution buffer (10 mM Tris-HCl pH 8) by 15 min incubation at 65°C in a thermomixer under shaking.

PCR and DNA electrophoresis for genotyping

PCR was performed to determine the genotypes of *Smn* ko mouse line using DNA isolated from tail or heads. 2% agarose gels were made in 1 × TAE buffer. 8 µl 6 × DNA loading dye was pipetted onto samples and mixed. 15 µl samples were loaded on an agarose gel and run at 120 mV for 40 min.

PCR reaction for *Smn* wt (PCR amplicon 879 bp)

Components	50 µl reaction	Final concentration
DNA	1	300-600 ng
5 prime Taq polymerase	0.3	1.3 units
10 × 5-prime Taq polymerase buffer	5	1 ×
dNTPs (10 mM)	1	200 µM
Betain (5 M)	10	1 M
Smn-wt/ko-for primer (10 mM)	1.5	300 µM
Smn-wt-rev primer (10 mM)	1.5	300 µM
water	29.7	

PCR reaction for *Smn* knockout (PCR amplicon 600 bp)

Components	50 µl reaction	Final concentration
DNA	1	300-600 ng
5 prime Taq polymerase	0.3	1.3 units
10 × 5-prime Taq polymerase buffer	5	1 ×
dNTPs (10 mM)	1	0.2 mM
Betain (5 M)	10	1 M
Smn-wt/ko-for primer (10 mM)	1.5	0.3 mM

Smn-ko-rev primer (10 mM)	1.5	0.3 mM
water	29.7	

PCR reaction for *SMN2tg* (PCR amplicon 200 bp)

Components	50 µl reaction	Final concentration
DNA	1	300-600 ng
5 prime Taq polymerase	0.3	1.3 units
10 × 5-prime Taq polymerase buffer	5	1 ×
dNTPs (10 mM)	1	0.2 mM
SMN2-for primer (10 mM)	1.5	0.3 mM
SMN2-rev primer (10 mM)	1.5	0.3 mM
water	39.7	

PCR program for *Smn* wt and *Smn* knockout

Step	Temperature (°C)	Duration	Number of cycles
Initial denaturation	94	3 min	1
Denaturation Annealing Extension	94 57 72	30 sec 30 sec 1.5 min	30
Final extension	72	5 min	1
Hold	15	∞	

Table 4.2.1 PCR program for Smn wt and Smn knockout

PCR program for *SMN2tg*

Step	Temperature (°C)	Duration	Number of cycles
Initial denaturation	94	3 min	1
Denaturation Annealing	94	30 sec	

Extension	56 72	30 sec 30 sec	30
Final extension	72	5 min	1
Hold	15	∞	

Table 4.2.2 PCR program for *SMN2tg*

4.2.9 Axonal RNA preparation and cDNA synthesis

We used a direct cDNA synthesis protocol for motoneuron cultures in order to avoid RNA loss during RNA preparation steps (Durand et al., 2006). In this method, cells are harvested directly in a lysis buffer which contains reverse transcriptase components (RT buffer), so that RNA extraction and reverse transcription can happen at the same time. For compartmentalized microfluidic chambers, total RNA was first extracted from the axonal compartment and then from the somatodendritic compartment. RT buffer was prepared using random primers. Motoneurons were washed 2 × with RNase free PBS and lysed directly in 100 µl RT buffer and transferred into RNase free 0.5 ml PCR tubes. Lysates were denatured at 70°C for 2 min and immediately incubated on ice for 1 min. The tube contents were collected by a brief centrifugation and incubated for 4 min at 37°C for random hexamers binding. 1 µl Superscript III Reverse Transcriptase was added and incubated at 38°C for 2 h. RT reaction was continued for 8 h at 39°C.

For HEK^{293T} or NSC-34 cells, total RNA was extracted using RNA extraction kit (Qiagen) following the manufacturer's instructions and quantified in Nanodrop spectrophotometer. 50-200 ng total RNA was applied to cDNA synthesis using random primers and superscript III reverse transcriptase kit (Invitrogen). cDNA was diluted 1:10 in EB-BSA buffer and applied to qRT-PCR.

4.2.10 cDNA purification

We purified cDNA using the QIAEX II purification kit (Qiagen). This step is required for complete removal of the RT buffer components, as these components could inhibit the subsequent qRT-PCR reaction. cDNA samples were pipetted into 1.5 ml tubes containing 700 µl solubilization buffer and 5 µl DNA-binding matrix (suspension buffer) and incubated at 25°C for 15 min, at 1300 rpm in a thermomixer. Samples were spun down for 2 min and supernatants were removed. 100 µl ice cold wash buffer was added to pellets, briefly vortexed and spun down for 1 min. This wash step was repeated and the pellet was dried at 37°C for 13 min. To eluate cDNA, 20 µl EB-BSA was added to pellets and incubated at 50°C for 3 min. Samples were centrifuged for 1 min and supernatants were transferred into 0.5 ml tubes containing 2 µl EB-BSA. To increase cDNA yield, elution step was repeated using same amounts of EB-BSA buffer. All centrifugation steps were performed at 18000 g at RT.

4.2.11 Laser capture microdissection

For Laser Capture Microdissection (LMD), lumbar spinal cords of E18 embryos or 12 week old mice were dissected and embedded in optimum cutting temperature compound (Tissue-Tek). These were then dipped in isopentane and immediately frozen in liquid nitrogen. Using a Leica cryostat, 15 µm cross-sections were prepared from spinal cords and transferred to 0.9 µm POL membranes. Tissue sections were first fixed in ice cold 70% ethanol for 2 min and then stained in 4°C cresyl violet solution for 1 min. Tissues were rinsed briefly first with 4°C 70% ethanol and then 100% ethanol and air dried for 5 min at RT. Using a Leica DM6000B laser microdissection system, somata of motoneurons were excised from ventral horn of cresyl violet stained spinal cords and collected into the lid of RNase free 0.2 ml PCR tubes. For cell lysis and direct cDNA synthesis, 15 µl RT lysis buffer was pipetted into the lid of tubes, incubated first at 72°C for 2 min and then for one min on ice. Cell lysates were collected in the tubes by a brief centrifugation step at 18000 g. Reverse transcriptase and

subsequent cDNA purification were performed as described in sections 4.2.10 and 4.2.11, respectively.

4.2.12 Quantitative qRT-PCR

qRT-PCR was used to detect mRNAs for actin isoforms in somata and axons of mouse motoneurons. Specific primers were designed for α-, β- and γ-actin using Oligo 6.0 software (MedProbe) (Table 4.6). $MgCl_2$ concentration was optimized for different PCR conditions using 2 and 3 mM end concentrations. Also, primer concentration was optimized using 20, 30 and 40 pmol/µl end concentrations. PCR amplicon of each actin isoform was validated by DNA gel electrophoresis and corresponding products were verified by sequencing. To avoid genomic DNA contamination, we used primers which were either intron spanning or covering an exon-exon junction and further excluded this possibility by analyzing product melting curves and minus RT control assays. 18srRNA and Gapdh were used as positive control for quality control of cDNA samples. Control experiments with primers for Histone H1f0 were carried out to exclude contamination of RNA in the axonal compartments. Data were analyzed by relative or absolute quantification. Relative quantification was performed according to Pfaffl et al. (Pfaffl, 2001) using following equation:

$$\text{Ratio} = (E_{\text{target}})^{\Delta CP \text{ target (control – sample)}} / (E_{\text{ref}})^{\Delta CP \text{ ref (control – sample)}}$$

Gapdh was used as reference gene for data normalization of knockdown samples versus control.

qRT-PCR reactions:

FastStart SYBR Green I master mix

Components	20 µl reaction
cDNA	2
$MgCl_2$	1.6 (2 mM)
FastStart SYBR Green I master mix	2
For-primer (20 pmol/µl)	2
Rev-primer (20 pmol/µl)	2
water	10.4

Luminaris Color HiGreen master mix

Components	20 µl reaction
cDNA	2
Luminaris Color HiGreen master mix	10
For-primer (20 pmol/µl)	2
Rev-primer (20 pmol/µl)	2
water	4

qRT-PCR program using FastStart SYBR Green I master mix

Step	Temperature (°C)	Duration	Number of cycles
Initial denaturation	95	10 min	1
Denaturation	95	0 sec	40-50
Annealing	55-63	5 sec	
Extension	72	8-10 sec	
4^{th} segment	81-85	5 sec	
Melting	95	0 sec	1
	65	15 sec	
	95	0 sec	
cooling	40	∞	

Table 4.2.3 qRT-PCR program using FastStart SYBR Green I master mix

qRT-PCR program using Luminaris Color HiGreen master mix

Step	Temperature (°C)	Duration	Number of cycles
Initial denaturation	95	10 min	1
Denaturation	95	15 sec	
Annealing			

Extension 4th segment	55-63 72 81-85	30 sec 30 sec 5 sec	35-50
Melting	95 65 95	0 sec 15 sec 0 sec	1
cooling	40	∞	

Table 4.2.4 qRT-PCR program using Luminaris Color HiGreen master mix

Annealing and 4th segment temperatures

Target gene	Annealing (°C)	4th segment (°C)	Nr. of amplification cycles
α-actin	63	84	40
β-actin	60	83	40
γ-actin	63	85	40
18sr RNA	57	81	35
Gaphd	59	83	40
Histone H1f0	55	84	35

4.2.13 Cloning and creating calibration curves and qRT-PCR absolute quantification

Absolute copy numbers of α-, β-, γ-actin and Gapdh were determined using external calibration curves. Generation of calibration curves and absolute quantification have been described previously (Durand et al., 2006). Briefly, qRT-PCR amplicons of α-, β- and γ-actin were first amplified by PCR using the same primers applied for qRT-PCR (Table 4.6) and cloned into TOPO®TA vector. These products were then used for generation of calibration curves.

PCR reaction for amplification of α-actin, β-actin and γ-actin qRT-PCR amplicons

Components	50 µl reaction	Final concentration

cDNA	1	50-200 ng
Phusion™ High-Fidelity DNA polymerase	0.5	1.5 units
10 × High-Fidelity GC buffer	5	1 ×
dNTPs (10 mM)	1	0.2 mM
for primer (10 mM)	1	0.3 mM
rev primer (10 mM)	1	0.3 mM
water	40.5	

PCR program for amplification of α-actin, β-actin and γ-actin qRT-PCR products

Step	Temperature (°C)	Duration	Number of cycles
Initial denaturation	95	10 min	1
Denaturation	95	30 sec	35
Annealing	60	30 sec	
Extension	68	30 sec	
Final extension	68	7 min	1
Hold	4	∞	

Table 4.2.5 PCR program for amplification of α-actin, β-actin and γ-actin qRT-PCR products

PCR products were subjected to electrophoresis on 2% agarose gels, corresponding bands were cut from gels and purified using QIAEX II PCR purification kit (Qiagen) following the manufacturer's instructions. In the final extension step of the PCR reaction, Taq polymerase adds 3'-A overhangs to the amplified PCR products. The TOPO® TA vector is linearized with 3'-T overhangs for direct ligation of the PCR product and activated with covalently bound topoisomerase I.

18 ng PCR product, 1 µl salt and 1 µl TOPO® TA vector were added into a 0.5 ml tube and total volume was adjusted to 6 µl with water. Samples were incubated at RT for 10 min. 2 µl of the reaction was used to transform TOP10 chemically competent E. coli cells. Cells were kept on ice for 10 min to thaw, ligation reaction was added and mixed by gently flicking the

tubes and incubated on ice for 30 min. Tubes were inserted into a 42°C water bath for 30 sec for the heat-shock and placed immediately on ice for 10 min. 1 ml LB medium was added to tubes and incubated at 37°C, 750 rpm in a thermomixer for 1 h. Cells were centrifuged at 400 g for 5 min. 90% of supernatant was removed and cells were resuspended in the remaining medium. 100 µl suspension was plated on ampicillin LB-Agar plates and incubated at 37°C overnight in a dried incubator. Next day, 10 colonies were picked and inoculated into 10 ml glass tubes containing 5 ml ampicillin-LB and incubated in a thermomixer at 37°C, 180 rpm overnight. 2 ml overnight cultures were used for plasmid isolation using plasmid mini-prep kit (Qiagen). The correct insertion of PCR amplicons in TOPO® TA vector was examined by restriction enzyme digestion and sequencing as well.

EcoR I restriction digestion:

Reagents	(20 µl) Volume
plasmid	300-50 ng
EcoR I (Fermentas)	0.5 µl
10 × Tango buffer (Fermentas)	2 µl
add water	

The digestion reaction product was incubated at 37°C for 1 h and restriction product size was examined by DNA gel electrophoresis (on 1% agarose gels). For plasmid midi-preparation, positive colonies were inoculated and transferred into 100 ml ampicillin-agar medium and grown overnight at 37°C under constant shaking (180 rpm). Plasmid midi-preparation was performed using NucleoBond® Xtra Midi/Maxi plasmid purification kit (Qiagen).

Next, inserted amplicons were cut out of the vector using EcoR I restriction digestion and ran on a 2% agarose gel. Corresponding bands on the agar gel were cut and purified using gel purification kit and quantified using Nanodrop. Serial dilutions of 2 to 10^6 molecules were made and used as template for the qRT-PCR reaction to generate external calibration curves.

Y-intercept and slopes were read from calibration curves and absolute copy numbers were determined using following formula: copy # = $10^{(\text{cross.point - Y})}$ / slope.

4.2.14 Cloning shRNA oligonucleotides targeting 3'UTRs of actin isoforms

To study differential functions of α-, β- and γ-actin isoforms in motoneuron growth and differentiation *in vitro*, we designed isoform-specific shRNA lentiviral constructs to knockdown these isoforms. For each actin isoform, three independent specific shRNA oligonucleotides were designed using software available on http://sirna.wi.mit.edu (Table 4.7) and cloned into the pSIH-H1 shRNA vector (System Bioscience). The pSIH-H1 vector contains a dual promotor system; CMV promotor drives the expression of GFP which is used for the identification of transduced cells and the H1 promotor drives the expression of the shRNA.

Restriction digest of pSIH-H1 vector

Reagents	(50 µl) Volume
pSIH-H1 vector	3 µg
BamHI (Fermentas)	3 µl
EcoRI (Fermentas)	2 µl
10 × Tango buffer (Fermentas)	10 µl (2 ×)
add water	

The digestion reaction product was incubated at 37°C for 1 h. Restriction products were seperated on a 1% agarose gel and correct bands were cut from the gel and purified using QIAEX II gel purification kit. As negative control, the vector was digested with only one RE as well as without any RE. DNA was measured using Nanodrop. Sense and antisense shRNA oligos were synthetized commercially and annealed as followed:

Annealing of shRNA oligonucleotides

Reagents	(50 µl) Volume
shRNA oligonucleotide sense	1 µl
shRNA oligonucleotide antisense	1 µl
10 × Tango buffer (Fermentas)	5 µl (1 ×)
add water	

The reaction product was heated to 95°C for 5 min and incubated for 1 h at 37°C. Oligonucleotides were placed on ice and diluted 1:10 in water. Diluted oligonucleotides were applied directly to ligation or were stored at -20°C for up to one month.

Ligation

Reagents	(20 µl) Volume
pSIH-H1 vector	25 ng
Annealed diluted oligonucleotides	1 µl
T4 ligase (Fermentas)	2 µl
10 × T4 ligase buffer (Fermentas)	2 µl (1 ×)
add water	

As negative control, a ligation reaction was prepared without annealed oligonucleotides. 10 µl of ligation reaction was used to transform chemically competent TOP10 E. coli cells and incubated on ice for 15 min. For the heat-shock transformation, tubes were inserted into 42°C water bath for 50 sec and placed immediately on ice. After 10 min incubation on ice, 1 ml LB medium was added to cells and cells were then incubated at 37°C for 1 h under constant shaking (750 rpm) in a thermomixer. Bacteria were plated on ampicillin-agar plates as described in section 4.2.14. Grown colonies were inoculated into 5 ml LB medium containing 50 µg/ml ampicillin and incubated at 37°C overnight. Next day, 1 µl of cell suspension was used as template for colony PCR to screen for positive colonies.

Plasmid was extracted from the cell suspension of positive colonies using plasmid mini-preparation kit and DNA was sent to sequencing to examine the correct insertion of shRNA oligonucleotides into the pSIH-H1 vector. For plasmid maxi-preparation, positive colonies were inoculated into 200 ml ampicillin-agar medium and grown at 37°C, 180 rpm overnight. Plasmid maxi-preparation was performed using NucleoBond® Xtra Midi/Maxi plasmid purification kit following manufacture‘s instruction.

4.2.15 Cloning LCK-Myr-eGFP-3’UTR report for γ-actin

Myristoylated and palmitoylated eGFP ($eGFP^{myr}$) reporter construct for β-actin has been already used for studying local translation of this isoform in primary motoneurons (Rathod et al., 2012). We generated $eGFP^{myr}$ reporter constructs for α- and γ-actin to study local translation of these isoforms in axonal branch points or axonal growth cones. 3’ UTRs of α- and γ-actin mRNAs were amplified by PCR using cDNA from cultured motoneurons and inserted into FU-Val $eGFP^{myr}$ expression lentiviral vector (Fig. 6.5.1 A). LCK-Myr-eGFP-3’UTR reporters for α- and β-actin were cloned by my colleague Reena Rathod (Thesis of Reena Jagdishbhai Rathod). LCK-Myr-eGFP-3’UTR reporter for γ-actin was cloned by me. First, PCR amplified 3’UTR of γ-actin was sub-cloned into a pcDNA vector which contained the GFP coding sequence and then GFP + 3’UTR of γ-actin was excised and inserted into FU-Valentine vector.

For PCR amplification of γ-actin 3’UTR, primers with XbaI and EcoRI restriction sites were designed (Table 4.9).

PCR reaction:

Components	50 µl reaction	Final concentration
cDNA from spinal cord	1	50-200 ng
Phusion™ High-Fidelity DNA polymerase	0.5	1.5 units
10 × High-Fidelity GC buffer	5	1 ×

dNTPs (10 mM)	1	0.2 mM
for primer (10 mM)	1	0.3 mM
rev primer (10 mM)	1	0.3 mM
water	40.5	

First a gradient PCR was performed to find the best annealing temperature for the PCR program.

PCR program (product size: 724 bp)

Step	Temperature (°C)	Duration	Number of cycles
Initial denaturation	94	2 min	1
Denaturation Annealing Extension	94 60 68	30 sec 45 sec 1 min	35
Final extension	68	7 min	1
Hold	4	∞	

Table 4.2.6 PCR program for cloning LCK-Myr-eGFP-3'UTR report for γ-actin

PCR products were separated on 2% agarose gels. Bands of 724 bp were cut from gels and purified using QIAEX II gel purification kit and quantified using Nanodrop. Next, the PCR product of γ-actin 3'UTR with XbaI and EcoRI overhangs was inserted into the pcDNA vector. For this step, the pcDNA vector was first digested with XbaI and incubated at 37°C for 1 h.

Digestion of pcDNA vector with XbaI

Reagents	(50 µl) Volume
pcDNA vector	2 µg vector
NheI (Fermentas)	1 µl
10 × Tango buffer (Fermentas)	5 µl (1 ×)

1 µl EcoRI and 6.25 µl 10 × Tango buffer (for 2 × end concentration) were added into the restriction reaction mixture and incubated for another 1 h at 37°C. The restriction reaction was run on a 1% agarose gel, the vector band was cut and purified using gel purification kit. In parallel, the insert (PCR product of γ-actin 3'UTR) was cut using XbaI and EcoRI and incubated in 37°C for 2 h. The restriction reaction was purified using PCR purification kit and quantified using Nanodrop.

Digestion of the insert (γ-actin 3'UTR) with XbaI and EcoRI

Reagents	(50 µl) Volume
Insert (γ-actin 3'UTR)	150 ng
XbaI (Fermentas)	2 µl
EcoRI (Fermentas)	1 µl
10 × Tango buffer (Fermentas)	10 µl (2 ×)
add water	

Next, the resulting insert (γ-actin 3'UTR) and pcDNA vector were ligated and incubated at 37°C for 1 h at RT. A ligation reaction without insert was carried out as negative control.

Ligation

Reagents	(20 µl) Volume
pcDNA vector	25 ng
Insert (PCR product of γ-actin 3'UTR)	19.25 ng
T4 ligase (Fermentas)	2 µl
10 × T4 ligase buffer (Fermentas)	2 µl (1 ×)
add water	

For transformation, 2.5 µl of ligation reaction was added into TOP10 chemically competent E.coli and incubated on ice for 30 min. Heat shock was carried out at 42°C for 90 sec and the bacteria were then again incubated on ice for 2 min. E.coli bacteria were plated on ampicillin-agar plates. Positive colonies were screened using a control digestion with EcoRI and BamHI.

Control digestion of positive colonies

Reagents	(20 µl) Volume
Positive colonies	200 ng
BamHI (Fermentas)	1 µl
EcoRI (Fermentas)	0.5 µl
10 × Tango buffer (Fermentas)	4 µl (2 ×)
add water	

Digestion reaction products were run on a 1% agarose gel and colonies which gave a band of 3 kb (for pcDNA vector) and a band of 1495 bp (for GFP + γ-actin 3'UTR) were verified by sequencing. Plasmids were purified using NucleoBond® Xtra Midi/Maxi plasmid purification kit as described in section 4.2.15. In the final step, GFP + γ-actin 3'UTR was cloned into FU-based lentiviral vector. For this, FU-Val vector was cut with EcoRI and BamHI and incubated at 37°C for 2 h. Restriction reaction products were run on a 1% agarose gel, 1495 bp band of the insert (GFP + γ-actin 3'UTR) and 10 kb band of the FU-Val vector were cut and purified using gel purification kit (Qiagen). For ligation, 25 ng FU-Val vector and 125 ng insert (GFP + γ-actin 3'UTR) were used.

Restriction of FU-Val vector and pcDNA vectors (containing 3'UTR of γ-actin) with EcoRI and BamHI

Reagents	(20 µl) Volume
FU-Valentine/ pcDNA (with 3'UTR of γ-actin)	2 µg
BamHI (Fermentas)	2 µl
EcoRI (Fermentas)	1 µl
10 × Tango buffer (Fermentas)	4 µl (2 ×)
add water	

TOP10 chemically competent E.coli cells were transformed with ligation products and positive colonies were checked by restriction with EcoRI and BamHI and verified by sequencing.

4.2.16 Cloning HA-tag-expression constructs of α-, β- and γ-actin and rescue construct for β-actin

The complete ORF + 3'UTR of α-, β- and γ-actin were cloned into the FU-Val vector. The vector contains a HA-tag at the 5'UTR and the expression of HA-tagged insert is driven by the ubiquitin promotor. Primers were designed to have EcoRI restriction overhangs at both 5' and 3' sites (Table 4.8). ORF + 3'UTR of α-, β- and γ-actin were amplified by PCR. For amplification of β-actin ORF, cDNA from motoneuron cultures was used as template. For PCR amplification of both α-actin and γ-actin ORFs, plasmids were purchased from Harvard's plasmid repository.

PCR program

Step	Temperature (°C)	Duration	Number of cycles
Initial denaturation	98	30 sec	1
Denaturation	98	10 sec	25
Annealing	56 for α-actin, 58 for β-actin and 59 for γ-actin	30 sec	
Extension	72	1 min	
Final extension	72	5 min	1
Hold	4	∞	

Table 4.2.7 PCR program for cloning HA-tag-expression constructs of α-, β- and γ-actin and rescue construct for β-actin

The product size of α-actin cDNA was 1373 bp, for β-actin 1810 bp and for γ-actin 1862 bp. FU-Val vector as well as PCR products of actin isoforms were cut using EcoRI enzyme in 2 × tango buffer. Vector was dephosphorylated by directly adding alkaline phosphatase enzyme

(Fermentas) to the RE reaction and incubated at 37°C for 10 min. Enzyme was inactivated by heating at 65°C for 15 min. 18.5 ng digestion product of α-actin and 25 ng digestion products of β-actin, γ-actin and FU-Val vector were used for ligation. For screening of the grown colonies, plasmids were cut by EcoRI and sent for sequencing. To examine whether inserts are located in the correct 5' to 3' direction, restriction controls were performed using following REs:

Insert	Restriction enzyme	Products size (bp)
α-actin	XhoI and BstXI	10186 and 455
β-actin	BstEII and XhoI	10573 and 555
γ-actin	XhoI and NheI	1268 and 9824

For generation of a shRNA resistant rescue construct for β-actin, the target sequence of the shRNA which is located 3'of the poly A site in the 3'UTR of β-actin mRNA was first deleted by PCR. This region does not contain any binding sequence of known RNA binding proteins. The complete ORF and shRNA deleted 3'UTR of mouse β-actin were then inserted by BamH1 restriction into the pCDH1-MSC-EF1 expression vector containing the ubiquitin promotor. The ubiquitin-β-actin cassette was then excised and inserted into shActβ-1 vector by blunt end ligation. The β-actin rescue construct was generated by me and my colleague Patrick Lüningschrör.

4.2.17 Protein extraction and quantification

For protein extraction from motoneurons, about 300.000 primary motoneurons were plated on 24-well cell culture plates. On DIV5 or 7, cells were washed 2 × with pre-warmed PBS and directly lysed with 2 × Laemmli buffer. Protein lysates were boiled at 99°C for 5 min and centrifuged for 4 min at 4°C. For protein extraction from NSC-34 and HEK^{293T}, cells were washed 2 × with pre-warmed PBS and lysed in 500 µl RIPA buffer. Lysates were transferred into 1.5 ml tubes and incubated on ice for 30 min. Total protein concentration was quantified

using a BCA kit and equal amounts of protein were applied to SDS-gel electrophoresis. 2 × Laemmli buffer was added to samples, boiled at 99°C for 5 min and centrifuged at 4°C. Samples were stored at -80°C.

4.2.18 G- to F-actin separation

For separation of G- and F-actin pools, actin stabilization buffer was added directly onto 24-wells with cultured neurons and incubated at 37°C for 10 min. Protein extracts were collected in 1.5 ml tubes and ultracentrifuged (Beckman TLA 12.2) for 75 min at 37°C and 100.000 g. Supernatants containing G-actin were recovered and pellets containing F-actin were resuspended in RIPA buffer. Protein concentration was determined by BCA kit. This experiment was conducted by my colleague Rajeeve Sivadasan.

4.2.19 Western blotting

20 µg protein extracts were loaded onto 10-12% SDS-PAGE gels and ran at 50 mV for 30 min followed by 2 h at 120 mV. Samples were blotted onto nitrocellulose membranes (GE Healthcare Lifesciences) at 120 mA for 1.5 h. Membranes were blocked in 5% milk solution for 1 h and probed with primary antibodies overnight and secondary antibodies for 1 h at RT. Primary and secondary antibodies were washed 3 × in TBST each time for 15 min and membranes were developed using ECL systems. For stripping, membranes were washed 2 × in TBST each time for 15 min to remove ECL buffer. Membranes were incubated with strip buffer for 30 min at 60°C in a water bath and washed afterwards 4 × in TBST each time for 15 min. Membranes were blocked in 5% milk solution and incubated with primary and secondary antibodies as described above.

4.2.20 Fluorescence Recovery After Photobleaching (FRAP)

Fluorescence recovery after photobleaching was performed as previously described (Rathod et al., 2012). Motoneurons were transduced with α-, β- and γ-actin lentiviral $eGFP^{myr}$-reporters and plated on µ-dishes (Ibidi, Martinsried, Germany). Imaging was performed in

ACSF medium. This was placed for 2 h prior to imaging in a humid incubator in order to adjust the pH and temperature. On DIV5 or 6, medium was removed and cells were washed 2 × with pre-warmed ACSF medium. 3 ml ACSF medium containing 10 ng/µl BDNF and CNTF was added to cells and taken to the microscope. FRAP experiments were performed with an inverted Leica SP5 confocal microscope which was equipped with a 60 × 1.35 NA oil objective. Cells were placed on a heated stage chamber supplied with 5% CO_2. 8-bit images with 512 × 512 pixel resolution were taken for a total duration of 1 h at 30 sec intervals using 19% laser intensity. 100 µm of distal axons was bleached with 80% laser power (Leica 488 nm laser line) at ~3 Hz speed. 8 frames were taken prior to bleaching and 120 frames post bleaching. Fluorescence recovery was analyzed in defined Regions Of Interests (ROIs) in axonal branch points and axonal growth cones. Using Leica LAS lite software (Leica), mean signal intensity of grey values/pixel was measured in ROIs. The average mean intensity of 8 pre-bleach frames was set as F0. The average mean intensity of the first 10 post-bleach frames was subtracted from all post-bleach values to eliminate the remaining signal after bleaching. Background was also subtracted from all intensity values. Post-bleach signal intensities were normalized to F0 for calculation of the % recovery. To exclude diffusion of GFP protein from the proximal axon, motoneurons were incubated with protein synthesis inhibitors; anisomycin (50 ng/µl for 2 h) or cycloheximide (10 µg/ml overnight).

4.2.21 Live cell imaging and data quantification

For analysis of filopodia dynamics in axons and axonal growth cones, motoneurons were transduced with shActα-, shActβ and shActγ lentiviral constructs and plated on µ-dishes (Ibidi). These shRNAs coexpress GFP which allowed us to visualize filopodia dynamics using an epifluorescence microscope with a 470 nm cool LED lamp. On DIV6, medium was replaced with NB full medium without phenol red containing 10 ng/ml BDNF and CNTF. Live cell imaging was performed with an inverted Nikon TE2000 microscope equipped with a

heated stage chamber (TOKAI HIT CO., LTD), a 60 × 1.4 NA objective and an Orca Flash 4.0 V2 camera (Hamamatsu) in the presence of 5% CO_2. GFP was excited with 2-4% light emission intensity. 12-bit images with 1024 × 1024 pixel resolution were acquired. Imaging period was 40 min with 20 sec intervals. Dynamics of axonal filopodia were examined for each single filopodium by analyzing: (i) frequency of filopodia initiation, (ii) filopodia life time, (iii) rate of filopodia dynamic movement (growth/retractions with a minimum length of 1 µm) and (iiii) total absolute changes in length for individual filopodia. For quantification of total change in filopodia length, the length of individual filopodia was measured in all 120 frames and absolute length changes between two subsequent frames were summed up. The velocity of filopodia movement in axonal growth cones was analyzed using ImageJ plugin as previously described (Sivadasan et al., 2016). All images were first staked into a Z-projection image, the central point of the growth cone was selected and inserted into the time lapse movie. A multiple kymograph was created which represented the time (in sec) as x-axis and the filopodia length (in µm) as y-axis. The velocity of filopodia movement was then measured as filopodia length divided by the time for each pick from the Kymograph.

4.2.22 High resolution *in situ* hybridization

High resolution *in situ* hybridization was used for detection of α-, β- and γ-actin mRNAs in axons of motoneurons. This technique was carried out following the manufacturer's instructions from Panomics. Antisense probes detecting mouse α-, β- and γ-actin, Gapdh, 18srRNA and *Ecoli*-DapB transcripts were obtained from Panomics. Only RNase-free solutions or tubes were used. DIV5-7 motoneurons were washed 2 × with pre-warmed PBS and fixed with 4% PLP buffer for 10 min at RT. After 3 × PBS wash, cover slips were transferred into a semi-wet chamber. For permeabilization, a supplied detergent solution was added onto cells and incubated for 4 min at RT. Cells were washed 3 × with PBS and proteinase K was added in order to unmask mRNAs from bound proteins. This was diluted at

1:8000 in PBS and incubated for 4 min. Probes were diluted 1:100 in pre-warmed hybridization buffer and hybridization was carried out at 40°C overnight in a dry incubator. In triplex assays, cells were incubated with a mixture of up to three different probes with different fluorescent tags. Probes were washed 3 × with supplied wash buffer (Panomics) at RT. Preamplifier oligos were diluted 1:25 in amplifier diluent buffer and incubated for 1 h at 40°C. These were washed 3 × with wash buffer at RT. Amplifier oligos were diluted 1:25 in diluent amplifier buffer, incubated for 1 h at 40°C and washed 3 × with wash buffer at RT. Finally, label probes diluted 1:25 in label probe diluent buffer were added and incubated for 1 h at 40°C. After 3 × wash with supplied wash buffer, cells were rinsed 2 × in PBS and proceeded for immunofluorescence.

4.2.23 Immunofluorescence

For immunofluorescence, 5000 motoneurons were plated on glass cover slips and cultured for 5 or 7 days. After 2 × wash with pre-warmed PBS, cells were fixed with 4% PLP buffer for 15 min at RT. With exception of α-, β-, γ-actin and DBP immunostaining, permeabilization was carried out using 0.3% Triton X-100 for 20 min at RT. For immunofluorescence detection of α-actin, 0.1% Triton X-100 was used for 15 min. For immunofluorescence detection of β- and γ-actin, cells were first exposed to ice cold methanol for 5 min at -20°C and then incubated with 0.3 % Triton X-100 for 10 min at RT. For DBP, cells were exposed to ice cold acetone for 5 min at -20°C. Cells were washed 3 × with PBS, blocking solution was added and incubated for 1 h at RT. Primary antibodies were diluted in blocking solution and incubated at 4°C overnight. α-actin antibody was incubated at RT for 3 h. Secondary antibodies were diluted in PBS and incubated for 1 h at RT. Primary and secondary antibodies were washed 3 × 10 min with PBS containing 0.1% Triton X-100. DAPI was added and incubated for 1 min at RT. Cover slips were rinsed in water and mounted using Aqua Poly/Mount (Polysciences, 18606). For F-actin staining, Alexa Fluor® 546 phalloidin

(Invitrogen, A22283) was used. This was diluted 1:50 in PBS and incubated for 1 h at RT after secondary antibody application.

4.2.24 Live cell extraction

"Live cell extraction" was performed to remove G-actin from motoneurons. We used either 0.01% saponin or 0.25% Triton X-100. Both reagents were diluted in a cytoskeleton buffer (CB), as this buffer stabilizes the actin ultrastructure (Auinger and Small, 2008; Lee et al., 2013). Cells were plated on glass cover slips and cultured for 5 days. Medium was removed and cells were rinsed in PBS. For saponin extraction, 0.01% saponin in CB buffer was added onto cells, incubated for 10 sec and washed briefly with PBS. Cells were fixed immediately in 4% PLP. For immunocytochemistry, the permeabilization step was omitted and cells were incubated directly with blocking solution without saponin. For Triton X-100 extraction, 0.25% Triton X-100 and 0.3% glutaraldehyde in CB were added onto cells and incubated for 1 min. Following 3 × PBS wash, cells were post-fixed for 15 min in 2% glutaraldehyde in CB. To remove background caused by glutaraldehyde, a solution of 0.2% glycine in CB was added onto cover slips and incubated for 7 min. Cells were washed with PBS and then subjected to the blocking step.

Vitamin D-binding protein (DBP) (5 µg/ml, Calbiochem, 345802) was used for labeling of G-actin (Lee et al., 2013; Van Baelen et al., 1980).

4.2.25 Survival assay of embryonic primary motoneurons

1000 motoneurons transduced with shActα, shActβ, shActγ and shCtrl were seeded on plastic surface in a 4-well dish and cultured for 7 days. For viability assay, cells were counted 18 h after plating and at day 7. Neurotrophic factors; BDNF and CNTF (5 ng/ml) were added into culture media to provide motoneuron survival. In negative control cultures, BDNF and CNTF were omitted which resulted in decreased survival by 70%.

4.2.26 Analysis of neurite growth

For analysis of soma size, axon length, axonal filopodia length, collateral branches as well as dendrite number and length, motoneurons were transduced with shActα, shActβ, shActγ and shCtrl and plated on laminin 111. DIV7 motoneurons were fixed and immunostained against dendritic (Map2) and axonal markers (Tau, Tubulin and Phalloidin). For analysis of axonal growth cone size, motoneurons were plated on laminin 221 and cultured for 5 days. For axon length analysis, the longest neurite was measured and for collateral branches, neurites with a minimum length of 40 µm along the main axon were counted. Axon length as well as axonal growth cone size analysis with shActβ-2, shActγ-2 and shActγ-3 transduced motoneurons were performed by my colleague Benjamin Dombert.

4.2.27 Image acquisition and processing

For immunofluorescence and *in situ* hybridization, 12-bit single or multiple stack images were acquired with an Olympus Fluoview 1000 confocal system. For axon length and branch measurements, images were acquired with a Keyence BZ-8000K fluorescence microscope.
All images were processed with ImageJ 1.42I software (Schneider et al., 2012).

5. Results

5.1 α-, β- and γ-actin isoforms are expressed in mouse motoneurons during embryonic stages and in the adult

Previous studies have shown that β- and γ-actin isoforms are expressed in all neuronal subtypes (Rubenstein, 1990), but the expression of α-actin isoform has not been yet investigated in neurons. We investigated the expression of actin isoforms in motoneurons in spinal cords of E18 embryos and 12 weeks old adult, using laser capture microdissection (LMD) and qRT-PCR. For absolute quantification of qRT-PCR data, we created external calibration curves for α-, β- and γ-actin, which allowed us to determine absolute mRNA levels of each isoform (Fig. 5.1.1, A-C). We detected mRNAs for all three actin isoforms in microdissected motoneurons in cDNA samples of both E18 and adult mice. We found that α-actin is expressed at relatively low levels, and that β- and γ-actin are expressed at high levels (Fig. 5.1.2, A-C). Comparison of this embryonic stage with the adult stadium revealed that the expression of all three actin isoforms is higher in embryonic stages than in adult. To examine the identity of microdissected motoneurons, we performed qRT-PCR using primers for the motoneuron specific marker, ChAT. We detected ChAT in cDNA of E18 and adult microdissected motoneurons, but not in cDNA samples obtained from cultured cerebellar neurons and heart tissues (Fig. 5.1.2 D).

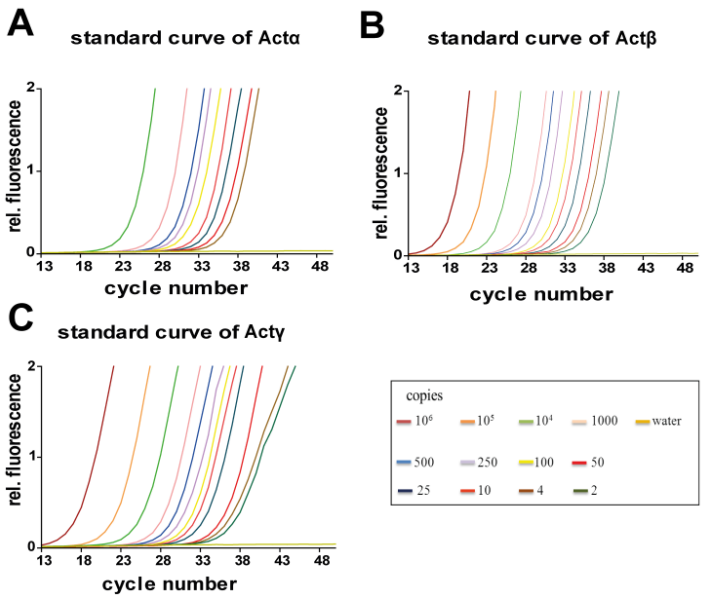

Figure 5.1.1 External calibration curves for α-, β- and γ-actin. (A-C) For absolute quantification of qRT-PCR data, standard curves were generated using 2 to 10^6 start molecules of these transcripts as template for the qRT-PCR reaction.

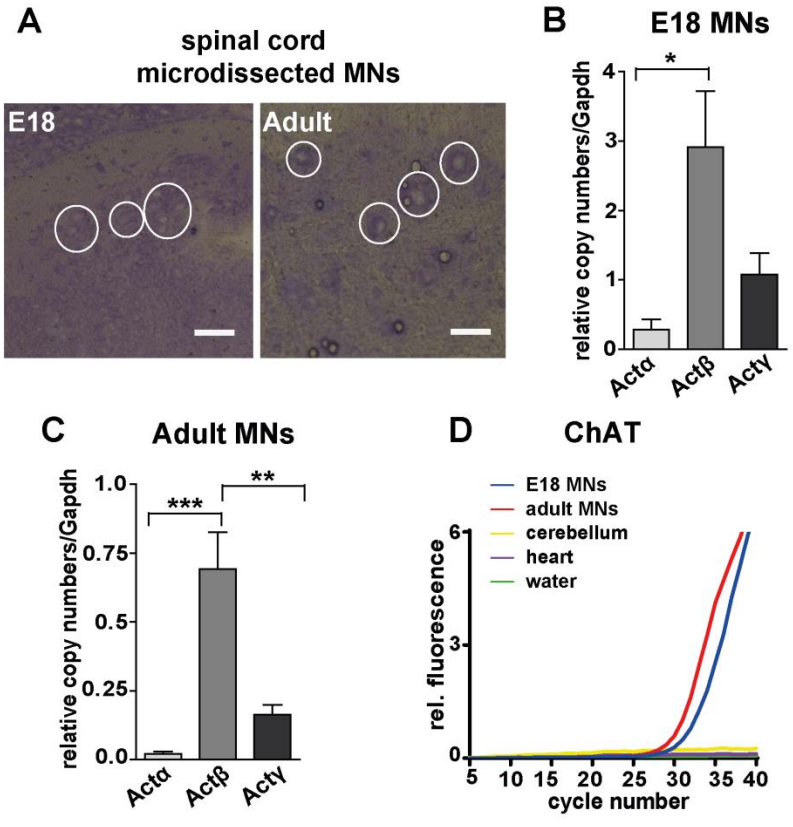

Figure 5.1.2 α-, β- and γ-actin transcripts are expressed in motoneurons *in vivo*. (A) Cresyl violet stains somata of motoneurons (in white circles) in ventral horn of E18 and adult spinal cord sections. Scale bar: 200 µm. (B and C) RNA was extracted from LMD cut motoneurons and absolute copy number of α-, β- and γ-actin and Gapdh transcripts were determined by qRT-PCR. mRNAs of α-, β- and γ-actin are detected in both E18 (n =

3) and adult motoneurons (n = 4) (* $p < 0.05$, ** $p < 0.0016$ and *** $p < 0.0005$). (D) ChAT transcripts are detectable only in RNA samples from microdissected motoneurons, and not in cultured cerebellar neurons or heart tissues. Data are shown as mean ± SEM.

5.2 mRNAs of α-, β- and γ-actin isoforms are translocated into axons in motoneurons

mRNAs for α-, β- and γ-actin are highly similar and share more than 90% homology within their coding regions (Vandekerckhove and Weber, 1978), but differ completely in their 3'UTRs. β-actin mRNA contains a ZIP code domain in the 3'UTR which binds to ZBP1 protein and is necessary for the axonal transport of this mRNA (Kislauskis et al., 1993). However, this ZIP code domain is not preserved in the 3'UTRs of α- and γ-actin indicating that transport and translation of these mRNAs are differentially regulated. In line with this, previous studies have shown that mRNAs for α-, β- and γ-actin localize differently within subcellular compartments in neuronal cells and myoblasts. For instance, transcripts for α-actin have been shown to localize to a perinuclear compartment in muscle cells, while transcripts of β-actin localize predominantly to highly dynamic regions, like lamellae at the cell periphery (Taneja and Singer, 1990). In cultured spinal motoneurons, β-actin mRNAs become sorted into axons and locally translated in the axonal growth cones (Rathod et al., 2012; Rossoll et al., 2003). Also in cortical and sensory neurons, mRNAs for β-actin are transported into axons, unlike mRNAs for γ-actin which remain in the soma (Bassell et al., 1998; Willis et al., 2007; Zhang et al., 2001a). Thus, it seems that, in sensory and cortical neurons β-actin is the only actin isoform that is locally translated in the distal axon. The axonal mRNA transport and local translation of two other isoforms, α- and γ-actin, has not yet been investigated in motoneurons. We investigated the mRNA transport of these isoforms using two sensitive methods: (i) compartmentalized cultures and qRT-PCR (ii) and high resolution in situ hybridization. To obtain mRNA only from axons, motoneurons were grown in microfluidic chambers for 7 days (Fig. 5.2.1 A), total RNA was extracted separately from somatodendritic and axonal compartments and subjected to qRT-PCR. To our surprise, transcripts for all three

actin isoforms were detected in the axonal compartment (Fig. 5.2.1 B). As positive control we used 18srRNA and Gapdh mRNA, which were detectable in both somatodendritic and axonal compartments, and used Histone H1f0 as negative control which was detectable only in the somatodendritic compartment and not in the axonal compartment (Fig. 5.2.1 B).

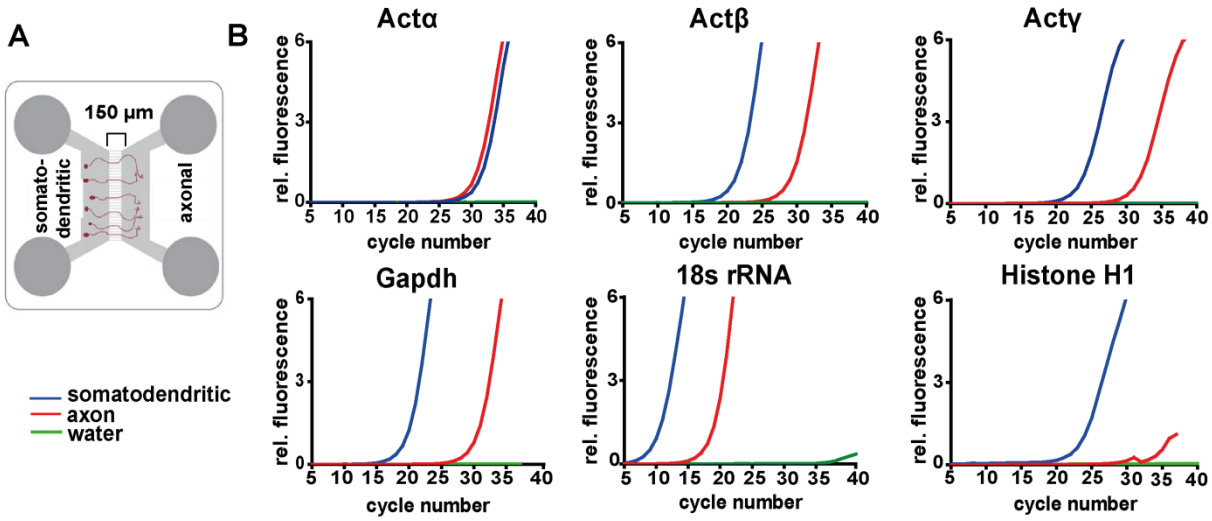

Figure 5.2.1 α-, β- and γ-actin transcripts are transported into axons in motoneurons. (A) Motoneurons were grown in microfluidic chambers. Somatodendritic and axonal RNA fractions were analyzed by qRT-PCR. (B) qRT-PCR amplification curves for α-actin, β-actin, γ-actin, Gapdh mRNAs and 18sRNA. These transcripts are detected in the axonal compartment, whereas Histone H10 mRNAs were not detected in this compartment.

Absolute quantification showed that, both in somatodendritic and axonal compartments, mRNA levels of β-actin were higher than mRNA levels of α- and γ-actin (Fig. 5.2.2, A and B). Nevertheless, mRNA levels of α-actin were higher in the axonal versus somatodendritic compartment, indicating that transcripts for this isoform are highly enriched in the axons of cultured motoneurons (Fig. 5.2.2 C). These data indicate that in cultured motoneurons, in addition to β-actin, transcripts for α- and γ-actin are sorted into axons.

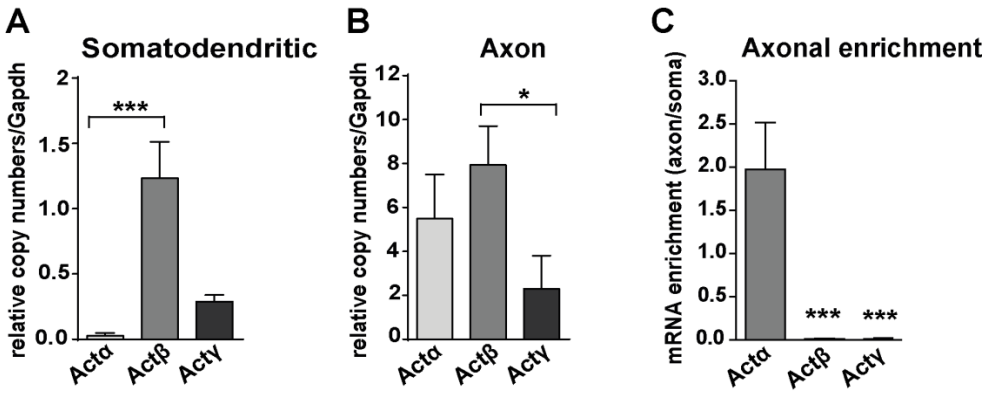

Figure 5.2.2 mRNAs for α-actin are enriched in axons of motoneurons. (A and B) Absolute quantification of qRT-PCR data revealed that β-actin is the most abundant isoform in both somatodendritic (*** $p < 0.0004$) and axonal compartments (* $p < 0.018$ for $n = 6$). (C) Comparing mRNA levels in axon to somatodendritic compartment revealed that α-actin transcripts are highly enriched in the axonal compartment (*** $p < 0.0003$). Statistical analysis: one way ANOVA with Bonferroni posthoc test. Data are shown as mean ± SEM.

Next, we asked whether transcripts for α-, β- and γ-actin localize to different regions within the axons. To address this, we performed high resolution *in situ* hybridization in DIV5 cultured motoneurons. Using specific probes for each isoform, we detected transcripts for α-, β- and γ-actin in the soma, axon and axonal growth cone, which confirms the axonal translocation of these transcripts (Fig. 5.2.3, A-C). In the soma, we detected only low levels of α-actin, but relatively high levels of β-actin and γ-actin (Fig. 5.2.3 D). Interestingly, we detected relatively high enrichment of α-actin transcripts in the axon, which confirms the results obtained from our qRT-PCR assay (Fig. 5.2.3 E). In the axonal growth cone, we observed relatively high levels of β-actin transcripts compared to α- and γ-actin (Fig. 5.2.3 F). These results indicate that transcripts for α-, β- and γ-actin are sorted differentially in motoneurons, with α-actin predominantly in the axon and β-actin in the axonal growth cone.

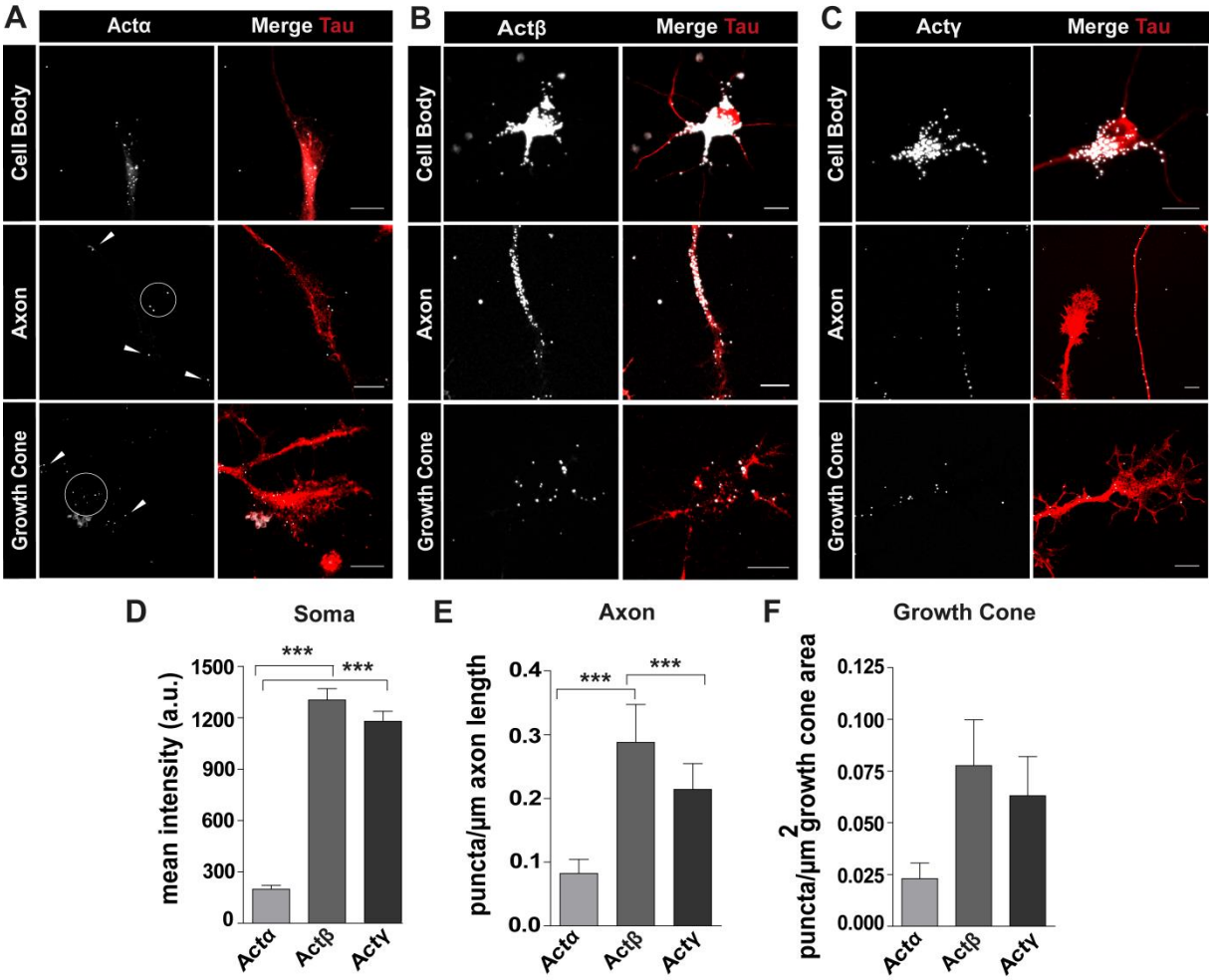

Figure 5.2.3 α-, β- and γ-actin transcripts show different localization in cultured motoneurons. (A) *In situ* hybridization shows localization of α-actin (A), β-actin (B) and γ-actin mRNAs (C) in different subcellular compartments of cultured motoneurons. Tau immunofluorescence marks cell boundaries. (D-F) Quantification of FISH signals in soma (A), axons (B) and axonal growth cones (C). Transcripts for β- and γ-actin are highly abundant in the soma. Transcripts for α-actin are enriched in axons and transcripts for β-actin are abundant in both axons and axonal growth cones (*** $p < 0.0001$ by one way ANOVA with Dunn's posttest for $n = 6$). Data are shown as mean ± SEM. Scale bar: 10 µm.

Afterwards we asked whether α-, β- and γ-actin mRNAs are present in different or the same RNP transport granules. To investigate this, we conducted a triplex assay using specific probes for α-, β- and γ-actin, each having a different fluorescent tag. Triplex assay revealed a unique and specific localization pattern for α-, β- and γ-actin, indicating that these mRNAs are packed into different RNA granules (Fig. 5.2.4 A). Furthermore, this results rules out the

possibility of cross-hybridization between these isoform-specific probes, since the corresponding spots to α-, β- and γ-actin probes did not show any overlap in triplex assays.

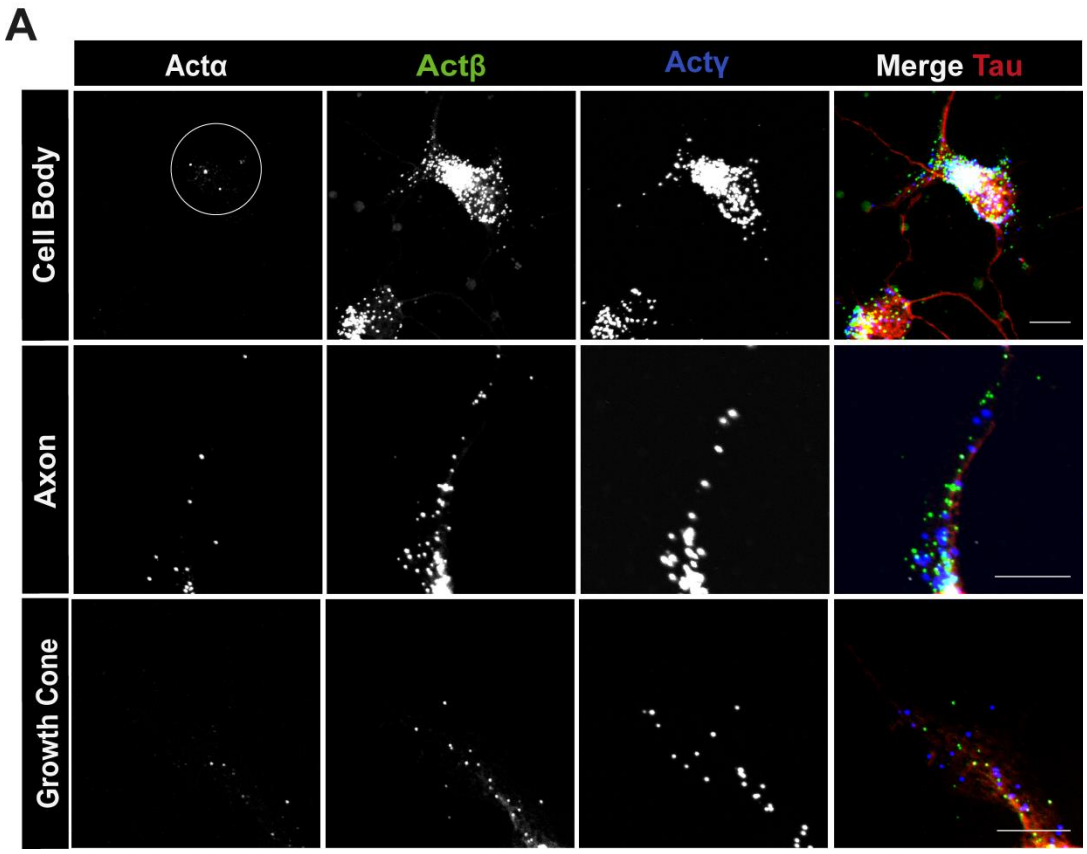

Figure 5.2.4 α-, β- and γ-actin mRNAs are present in different RNA transport granules. (A) Triplex assay using probes for α-, β- and γ-actin shows different localization pattern of these mRNAs in soma, axons and growth cones indicating that these mRNAs are part of different RNP granules. Scale bar: 10 µm.

As positive control, we used probes for Gapdh mRNA and 18srRNA which were both detectable in axons of cultured motoneurons (Fig. 5.2.5, A and B). As negative control, we (i) performed "no-probe" assay, in which we omitted the probe and incubated cell only with pre- and amplifier oligos coupled to different fluorescent dyes, i.e. Alexa488, Cy3 and Cy5, and (ii) used a scramble probe to DapB, which is a bacterial mRNA (Fig. 5.2.5, C and D). The scrambled probe was not detectable in motoneurons and in "no probe" assay the corresponding signals were reduced to undetectable levels. To validate the specificity of probes we knocked down α-, β- and γ-actin using isoform-specific shRNA lentiviral

constructs. In respective shRNA transduced motoneurons, the FISH signal for α-, β- and γ-actin decreased significantly, which verifies the specificity of these probes (Fig. 5.2.6, A-C). Collectively, these results clearly indicate that the mechanisms of axonal mRNA transport for actin isoforms differ in motoneurons compared to sensory and cortical neurons and thus, local translation of α-, and γ-actin could also contribute to motor axon growth and development.

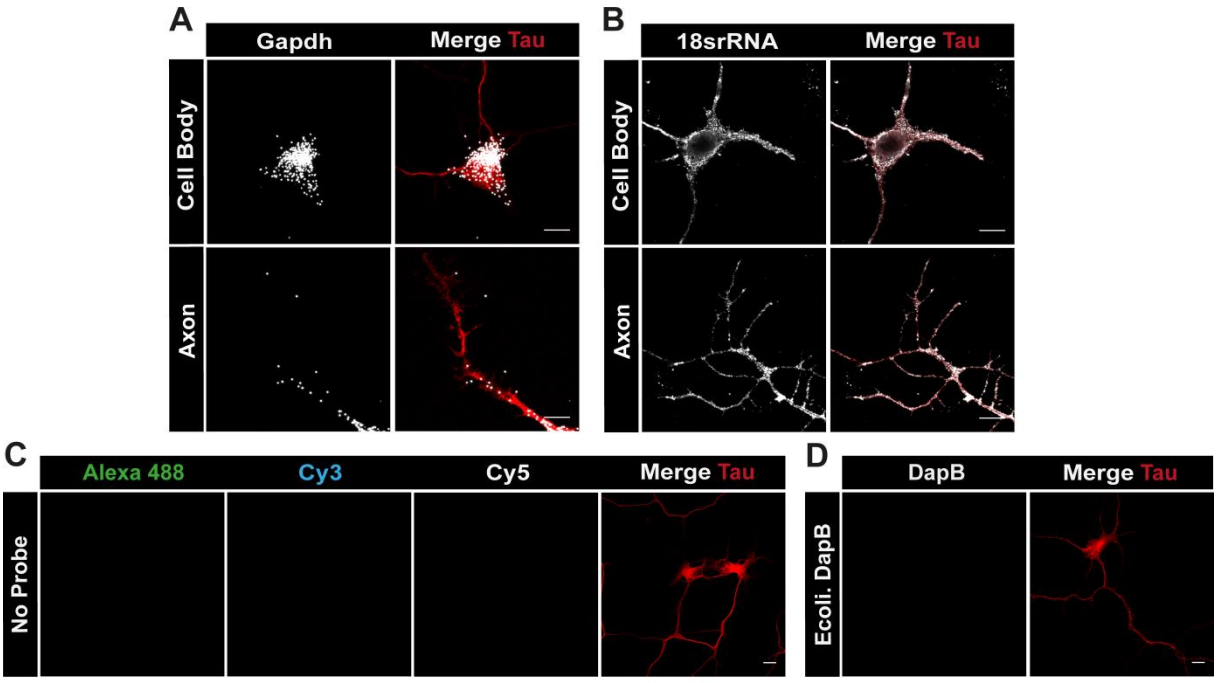

Figure 5.2.5 Gapdh mRNA and 18srRNA, but not DapB are detected in motoneurons. Probes for Gapdh mRNAs (A) and 18srRNA (B) detect these transcripts in soma and axons of motoneurons. (C) In "no-probe" assays no signal is detected in Alexa488, Cy3 and Cy5 channels. (D) Scrambled probes to Ecoli-DapB mRNAs do not give rise to signal in cultured motoneurons. Scale bar: 10 µm.

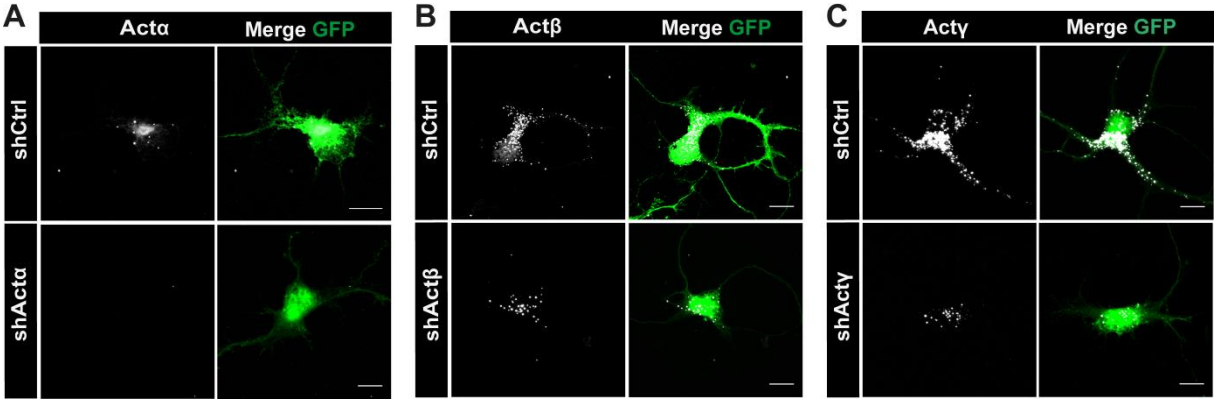

Figure 5.2.6 Signals for α-, β- and γ-actin mRNAs are decreased after shRNA repression of these isoforms. (A-C) ShRNA-mediated depletion of α-actin (A), β-actin (B) and γ-actin (C) results in marked decrease in corresponding signal intensities of these probes. Scale bar: 10 μm.

5.3 Expression and axonal mRNA localization of α-, β- and γ-actin isoforms in primary mouse cortical neurons.

Previous studies with primary cortical neurons have reported that mRNAs for β-actin become transported into axons, whereas mRNAs for γ-actin are restricted in the cell body (Bassell et al., 1998; Willis et al., 2007; Zhang et al., 2001a). There is no report on the expression and mRNA distribution of α-actin in these neurons. To address whether mRNA transport of γ-actin is neuron type specific, we cultured primary mouse cortical neurons for 5-7 days and performed in situ hybridization assays. Interestingly, in addition to β-actin (Fig. 5.3.2 A), we detected mRNAs for γ-actin (Fig. 5.3.3 A) in the axon, but mRNAs for α-actin were undetectable in this compartment (Fig. 5.3.1 A).

Furthermore, we cultured cortical neurons in microfluidic chamber for qRT-PCR analysis (Fig. 5.3.4 A). Absolute quantification showed that in comparison to β-actin, mRNA levels of γ-actin are relatively low in axons and mRNA levels of α-actin are below detection level (Fig. 5.3.4 B). Thus, both *in situ* hybridization and qRT-PCR assays confirm that in cortical neurons the mRNAs for β- and γ-actin but not α-actin localize into axons, but in contrast to motoneurons, α- and γ-actin transcripts are not enriched in the axon in these neurons.

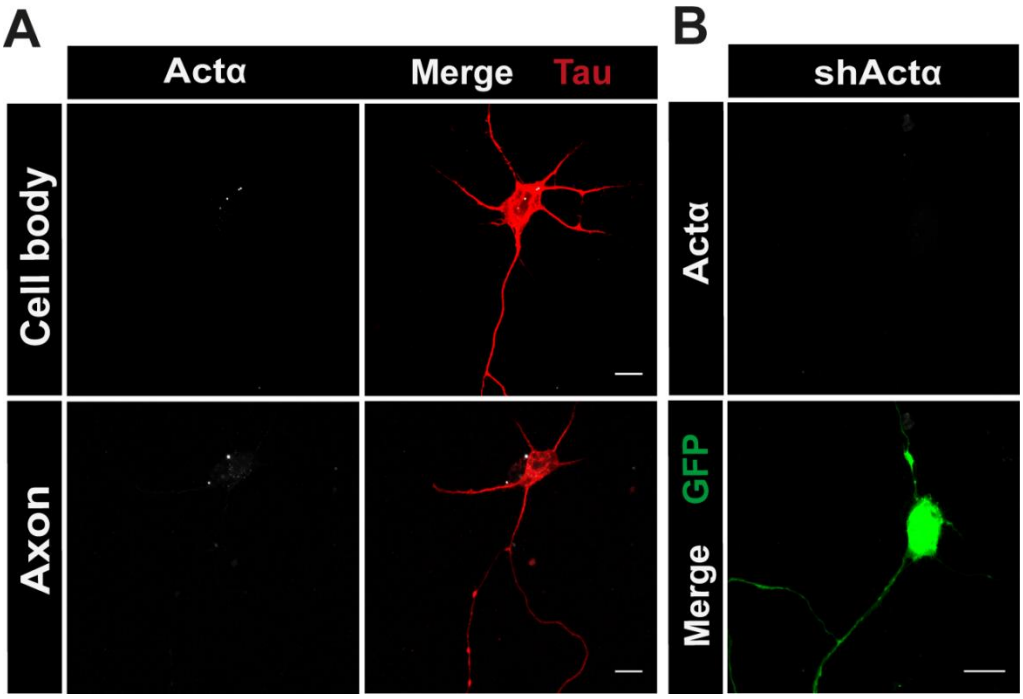

Figure 5.3.1 α-actin isoforms expression in mouse primary cortical neurons. (A) *In situ* hybridization using specific probes shows mRNA localization of α-actin in soma and axons of primary cortical neurons. α-actin is expressed at low levels in the soma and is undetectable in axons. (B) Control experiments with α-actin knocked down cortical neurons show a significant reduction in α-actin signal intensity, confirming the specificity of these probe sets. Scale bar: 10 µm.

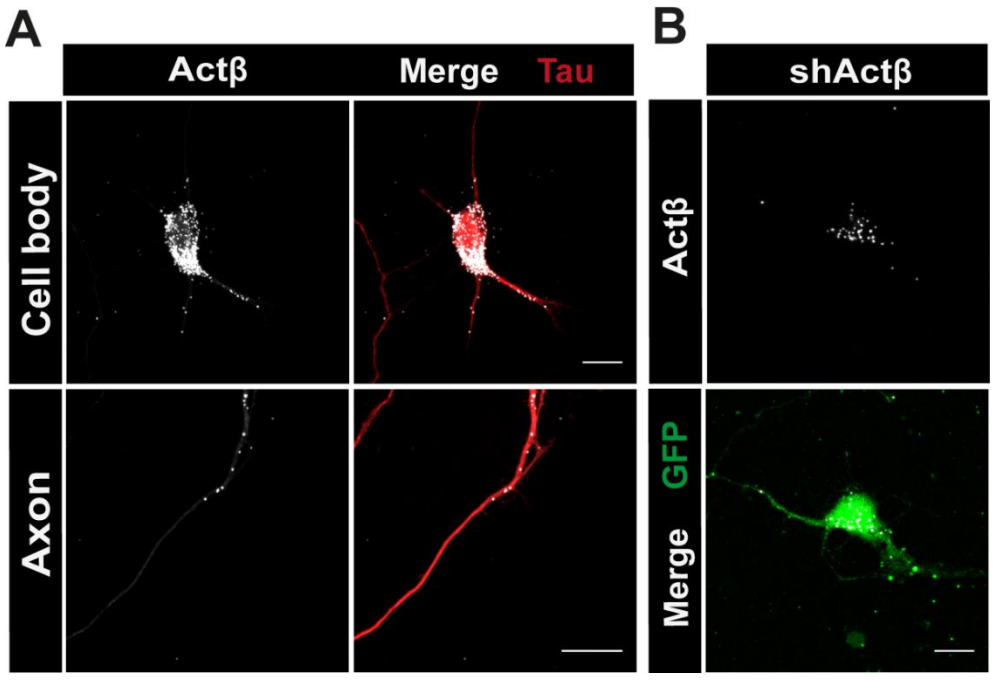

Figure 5.3.2 Localization of β-actin mRNA in mouse primary cortical neurons. (A) *In situ* hybridization using specific probes shows that β-actin mRNAs are present in soma as well as in axons of primary cortical neurons. (B) ShRNA-mediated knockdown of β-actin in cortical neurons results in marked reduction in signal intensity verifying the specificity of probes. Scale bar: 10 µm.

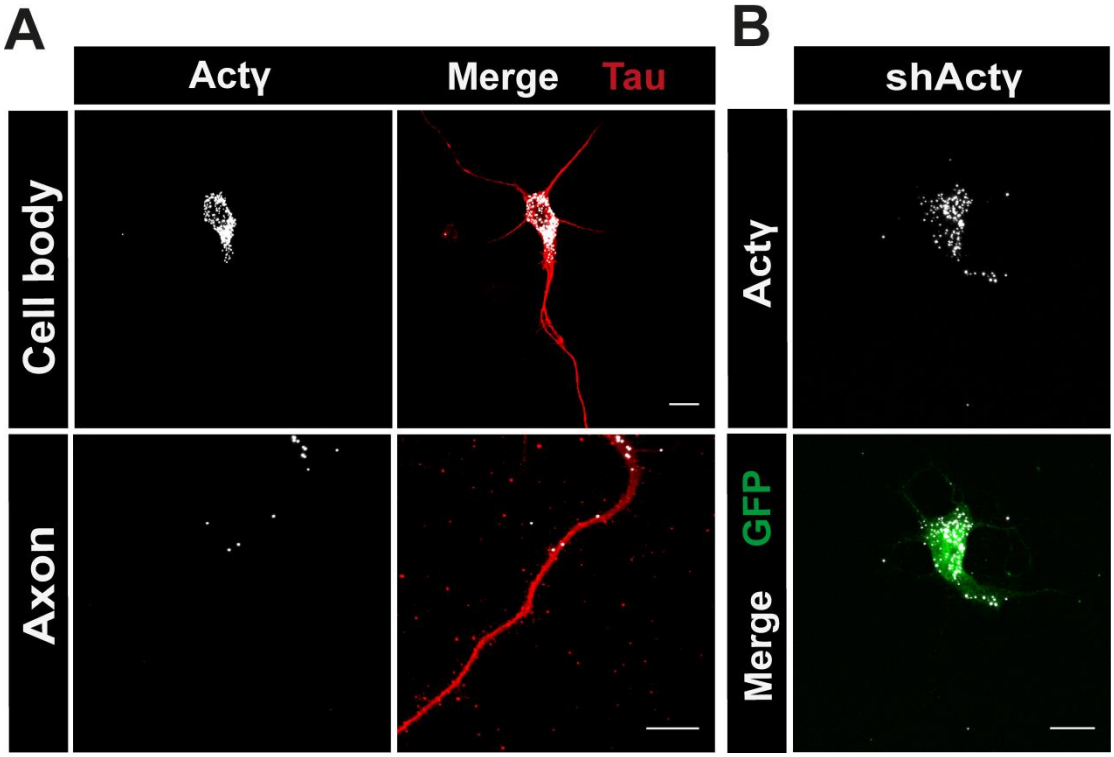

Figure 5.3.3 Localization of γ-actin mRNAs in mouse primary cortical neurons. (A) mRNAs for γ-actin are detected in soma and axons of cortical neurons by *in situ* hybridization using specific probes. (B) ShRNA-mediated knockdown of γ-actin reduces the signal intensity of γ-actin probes in cortical neurons. Scale bar: 10 µm.

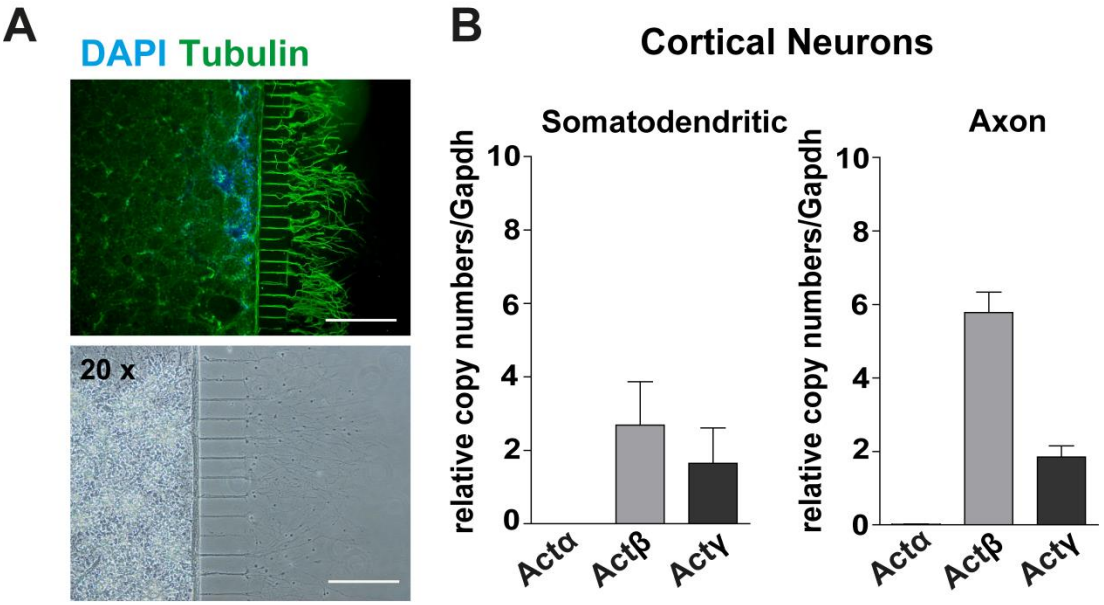

Figure 5.3.4 qRT-PCR detection of α-, β- and γ-actin transcripts in axons of cultured cortical neurons. (A) DAPI and Tau immunostaining of cortical neurons grown in microfluidic chambers. No DAPI signal is detectable in the axonal compartment. Scale bar: 200 µm. (B) qRT-PCR analyses of RNA fractions from

somatodendritic and axonal compartments revealed that mRNAs for β- and γ-actin but not α-actin are detected in the axonal compartment. Data are shown as mean ± SEM.

5.4 α-, β- and γ-actin proteins are differentially distributed in motoneurons

Though actin isoforms differ at only 4 amino acids at their N-terminal end, the spatial expression and subcellular distribution of these proteins is highly regulated. β- and γ-actin are expressed in nearly all cell types, while α-actin is expressed mostly in muscle cells. γ-actin is sorted to costameres (structures between sarcolemma and the z-disk) as well as to z-disks in muscle cells (Papponen et al., 2009; Rybakova et al., 2000), but is uniformly expressed in other cell types (Otey et al., 1986). β-actin predominantly localizes to regions undergoing remodeling; e.g. to the leading lamellae in fibroblasts or endothelial cells (Hoock et al., 1991), and to the axonal growth cone in neurons (Bassell et al., 1998; Micheva et al., 1998).

We investigated the expression and localization of isoactin proteins in developing motoneurons by Western blot as well as immunocytochemical experiments, using isoform-specific antibodies. The specificity of the respective antibodies was validated by Western blot using total lysates obtained from cultured wild type or actin isoform-specific knockdown motoneurons (Fig. 5.4.1, A-C). In knockdown cultures, protein levels of α-actin were reduced by 60%, protein levels of β-actin by 95% and protein levels of γ-actin by 85% thus, confirming the specificity of these antibodies (Fig. 5.4.1 D). The antibody to α-actin binds to both striated muscle α-actin isoforms (skeletal muscle and cardiac muscle α-actins) (Crawford et al., 2002). Since, the used shActα knockdowns only skeletal muscle α-actin, hence the remaining signal on the Western blot shown in Fig. 5.4.1 A must represent cardiac muscle α-actin. In addition, we performed immunocytochemical assays with cultured wild type and shRNA-treated motoneurons using these antibodies, and observed a significant reduction in corresponding immunofluorescence signals in shRNA transduced motoneurons (Fig. 5.4.2, A-C). Furthermore, we transiently transfected HEK^{293T} cells with HA-α-actin, HA-β-actin or

HA-Actγ expression vectors and probed the lysates with α-actin antibody. The α-actin antibody reacted only with the HA-tagged α-actin and not with HA-tagged β- or γ-actin proteins (Fig. 5.4.3 A).

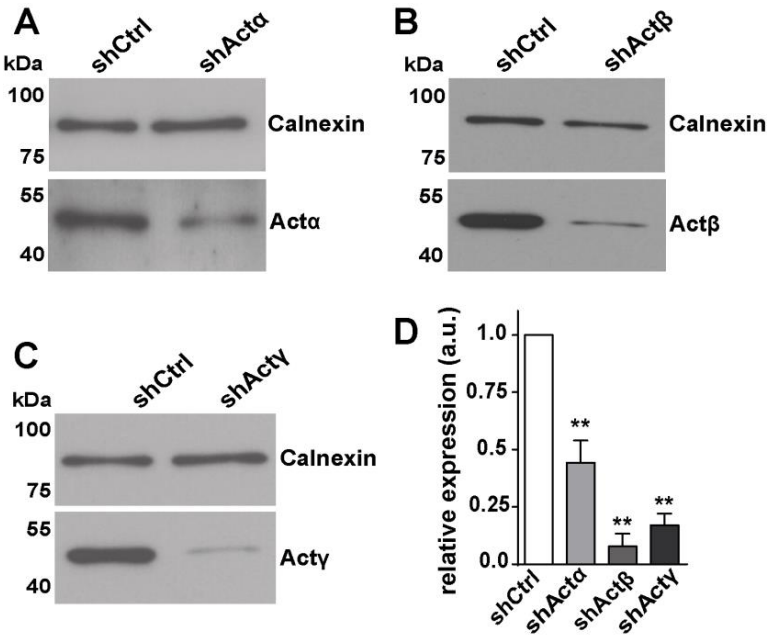

Figure 5.4.1 Validation of actin isoform-specific antibodies by Western blot. (A-C) Lysates of cultured motoneurons transduced with shActα, shActβ, shActγ and shCtrl were analyzed by Western blot using specific antibodies to α-actin (A), β-actin (B) and γ-actin (C). Calnexin was used as loading control. (D) α-actin protein levels are decreased by 60% in lysates of shActα transduced motoneurons (** $p < 0.004$ for $n = 4$), β-actin protein levels are decreased by 95% in lysates of shActβ transduced motoneurons (** $p < 0.002$ for $n = 10$) and γ-actin protein levels are decreased by 85% in lysates of shActγ transduced motoneurons (** $p < 0.005$ for $n = 5$ by one-tailed Mann-Whitney test). Data are shown as mean ± SEM.

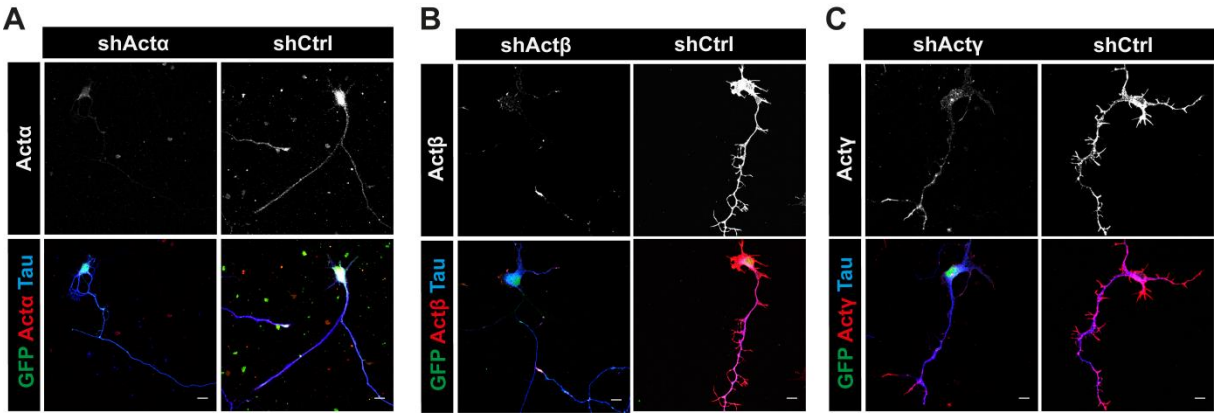

Figure 5.4.2 Validation of actin isoform-specific antibodies by immunocytochemistry experiments. Immunofluorescence reactivity of α- (A), β- (B) and γ-actin (C) antibodies are decreased in α-, β- and γ-actin knockdown motoneurons. Scale bar: 10 µm.

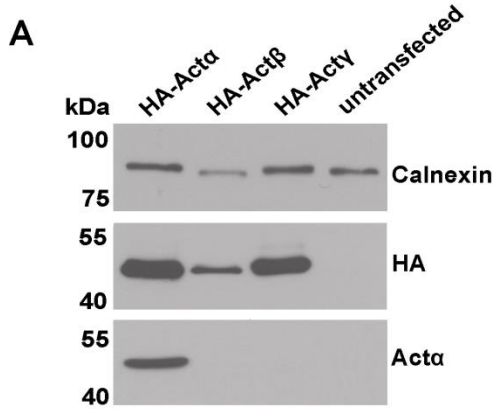

Figure 5.4.3 Specificity of α-actin antibody is validated by Western blot using α-, β- and γ-actin expression plasmids. (A) HA-tagged α-, β- and γ-actin plasmids were expressed in HEK^{293T} cells and lysates were probed with HA and α-actin specific antibodies. HA antibody detects HA-tagged α-, β- or γ-actin, α-actin antibody detects only HA tagged-α-actin. Calnexin was used as loading control.

Immunocytochemical data showed that α-, β- and γ-actin proteins are distributed differentially in motoneurons. α-actin is not abundant in the soma, but interestingly this isoform accumulates at defined regions within the axons which correspond to axonal branch points (Fig. 5.4.4 A). On the contrary, β- and γ-actin proteins are abundant in the soma and dendrites (Fig. 5.4.4, B and C). In the axon, β- and γ-actin localize to highly dynamic regions, in particular to the axonal filopodia. In the axonal growth cone, β-actin is highly abundant in filopodia as well as in the center of the growth cone (Fig. 5.4.4 B), γ-actin is present mostly in the filopodia and α-actin is not enriched in filopodia (Fig. 5.4.4, A and C).

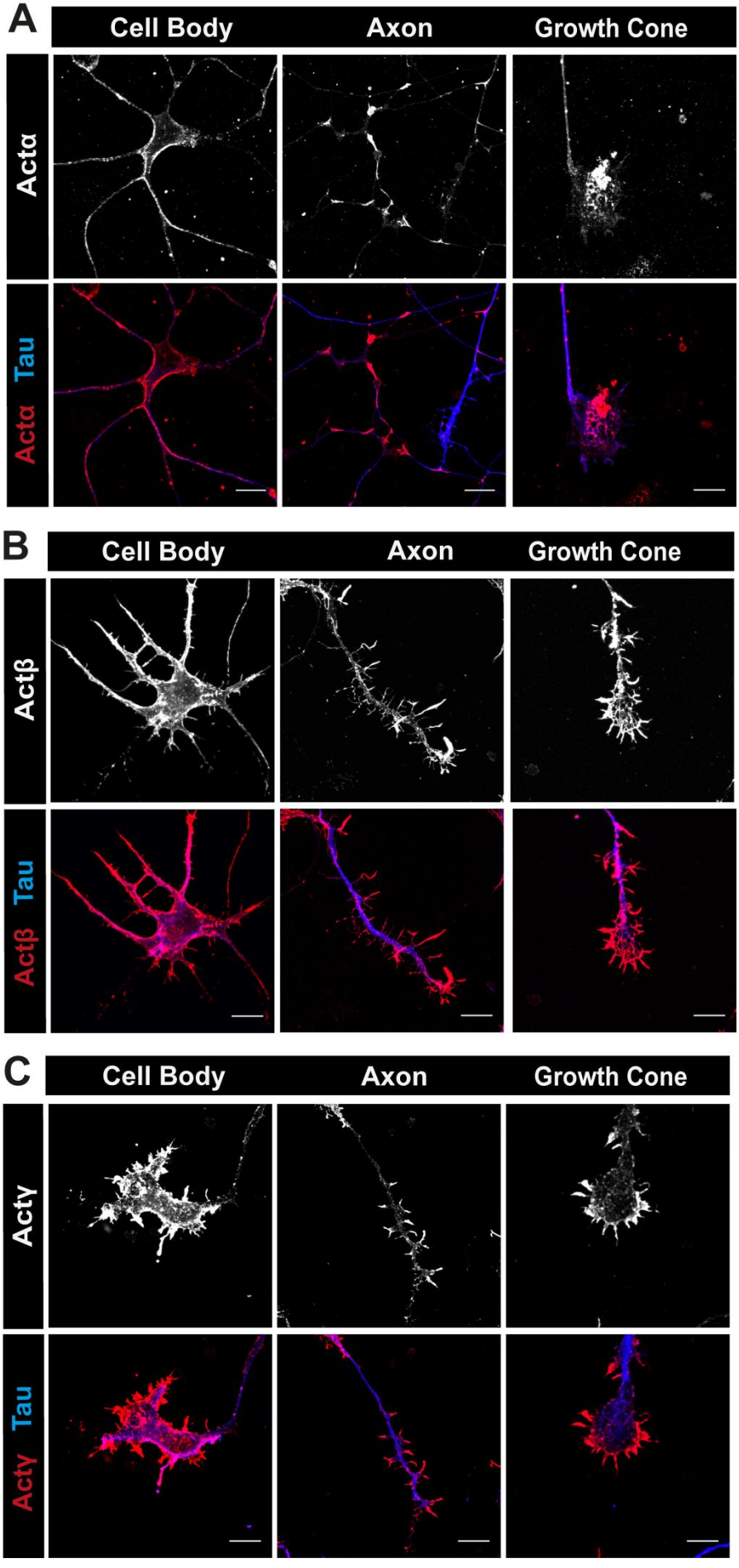
A
Cell Body
Axon
Growth Cone
Actα
Actα Tau
B
Cell Body
Axon
Growth Cone
Actβ
Actβ Tau
C
Cell Body
Axon
Growth Cone
Actγ
Actγ Tau

Figure 5.4.4 Differential localization of isoactin proteins in cultured motoneurons. (A-C) Motoneurons were stained against Tau and α-actin (A), β-actin (B) and γ-actin (C). α-actin proteins localize mostly to axonal branch points and neurites (A). β- (B) and γ-actin proteins (C) localize particularly to axonal filopodia and axonal growth cone filopodia. Scale bar: 5 µm.

The specific spatial localization of α-, β- and γ-actin suggests that these isoforms might contribute differentially to F-actin polymerization in different sub-compartments of motor axons and thus accomplish unique axonal functions. To address this issue, we used detergents, Triton X-100 or saponin, to remove soluble G-actin from motoneurons, fixed them and performed immunocytochemistry using isoform-specific antibodies as well as phalloidin. After the G-actin washout, we observed a co-localization of α-actin with phalloidin mostly in the axon and axonal branch points and only a poor co-localization in the cell body and axonal growth cones (Fig. 5.4.5 A). This finding indicates that α-actin incorporates into filamentous actin especially in these regions. On the contrary, we observed a high co-localization of β-actin and phalloidin particularly in the axonal growth cone and growth cone filopodia, indicating that this isoform incorporates into F-actin in highly dynamic regions (Fig. 5.4.5 B). γ-actin showed a high co-localization with phalloidin in particular in the cell body, but also in specific regions within the axon (Fig. 5.4.5 C). Interestingly, after "live cell extraction" β- and γ-actin disappeared from motile area in dendrites which indicates that these two isoforms are present in a G-actin pool in the cell periphery. To test whether G-actin was efficiently removed from motoneurons, we performed immunofluorescence experiments using vitamin D binding protein which specifically labels the G-actin pools (Lee et al., 2013). After Triton X-100 treatment, the immunoreactivity of the vitamin D binding protein antibody was markedly reduced (Fig. 5.4.6 A). Moreover, we examined the removal of Gapdh as another globular protein, and observed a significant reduction in corresponding signal intensity (Fig. 5.4.6 B).

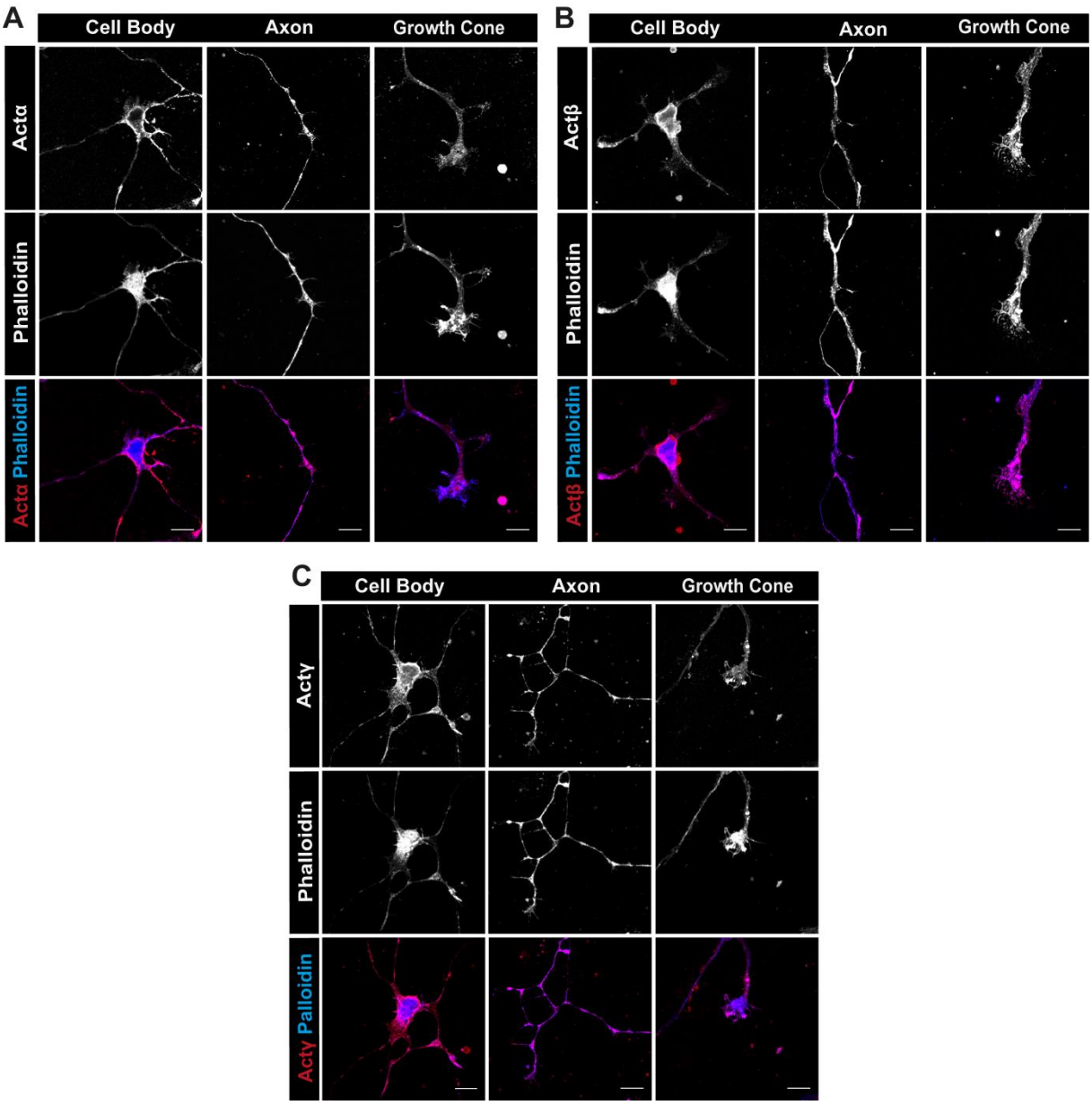

Figure 5.4.5 Actin isoforms incorporate into F-actin in different regions within the axon. (A-C) G-actin was removed from cultured motoneurons, using Triton X-100 or saponin prior to fixation. Cells were immunostained with phalloidin and against α-actin (A), β-actin (B) and γ-actin (C). (A) α-actin co-localizes with phalloidin particularly in axonal branch points. (B) β-actin c-localizes with phalloidin mostly in axonal growth cone filopodia. (C) γ-actin co-localizes with phalloidin in the cell body as well as specific regions within axons. Scale bar: 5 µm.

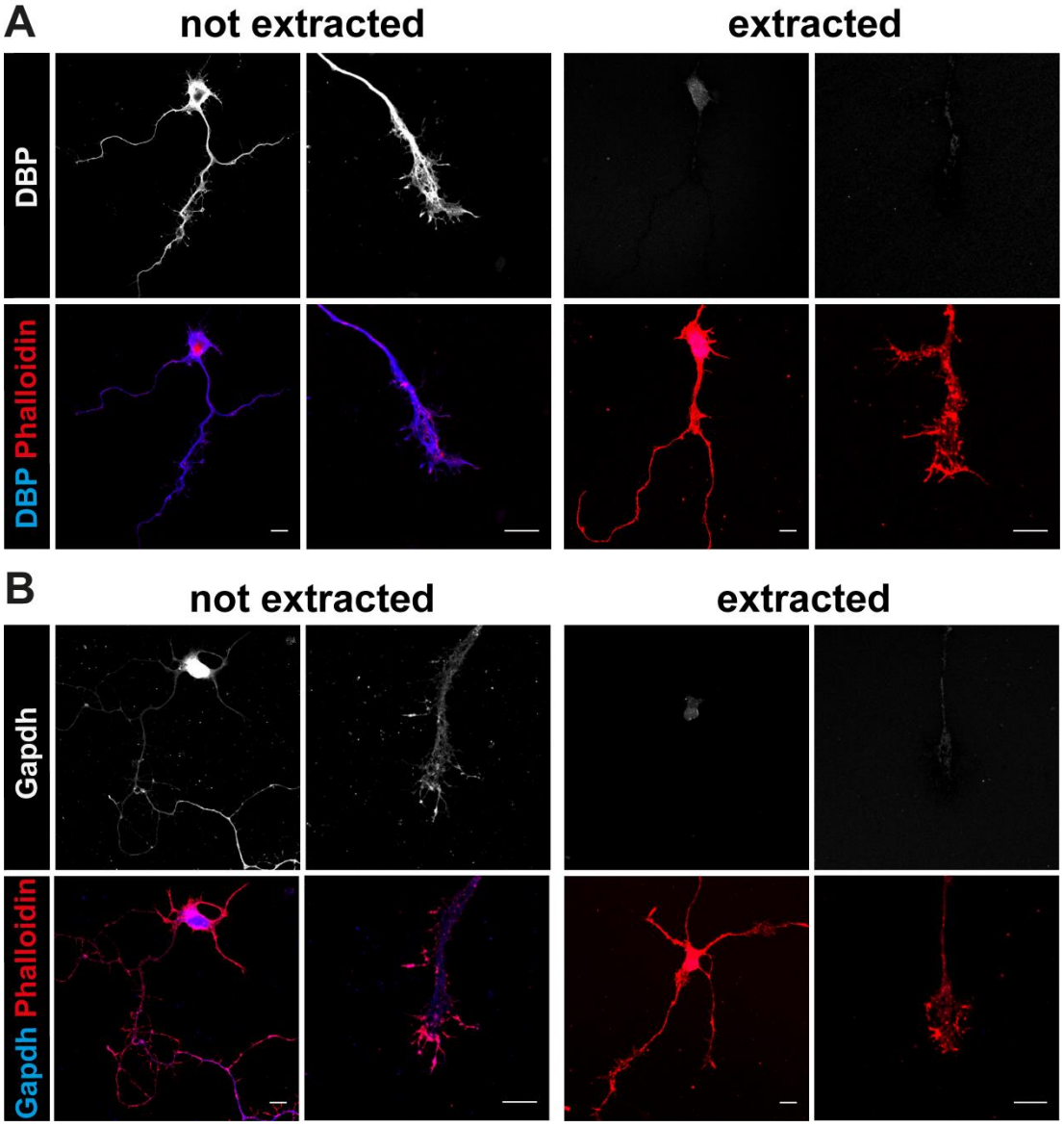

Figure 5.4.6 G-actin and other globular proteins are washed out after Triton X-100 treatment. (A and B) Motoneurons were extracted with Triton-100 and stained with phalloidin and DBP or Gapdh antibodies. Triton X-100 treatment decreases signals corresponding to DBP (A) and Gapdh (B). Scale bar: 10 µm.

5.5 α-, β- and γ-actin transcripts are differentially translated in axonal growth cones and in translational hot spots within axonal branch points.

Axonal localization of α-, β- and γ-actin mRNAs in motoneurons indicates that intra-axonal protein synthesis of these isoforms could play a role in axon growth and differentiation. In sensory neurons, axonally synthesized β-actin contributes to axon branching and nerve regeneration (Micheva et al., 1998; Spillane et al., 2012; Spillane et al., 2013; Zheng et al.,

2001). In *Xenopus* retinal neurons, local translation of β-actin in axonal growth cones is required for axon path finding, as inhibiting its local synthesis abolishes the growth cone turning toward extra cellular guidance cues (Leung et al., 2006). In motoneurons, β-actin becomes locally translated in the axonal growth cone as a response to different laminin isoforms and BDNF as well (Rathod et al., 2012). However, local translation of α- and γ-actin in motoneurons has not been studied yet. mRNA transport and local translation are highly regulated in neuronal cells. Target mRNAs form a complex with RNA binding proteins (RBPs) which recognize specific elements mostly within 5'UTR and/or 3'UTRs of these target mRNAs (Buxbaum et al., 2015). In this context, it has been shown that the ZIP code domain within the 3'UTR of the β-actin mRNA is sufficient for its axonal transport and local translation (Kislauskis et al., 1993). Hence, in order to study local translation of actin isoforms, we generated a $eGFP^{myr}$ lentiviral reporter construct for each actin isoform which contained the corresponding 3'UTRs of α-, β- and γ-actin and performed fluorescence recovery after photobleaching (FRAP) experiments (Fig. 5.5.1 A). Motoneurons were transduced with these lentiviral constructs and cultured for 5 days. 100 µm of the distal axons was bleached and fluorescence recovery was monitored for 1 h post bleach at 30 sec intervals (Fig. 5.4.1 B).

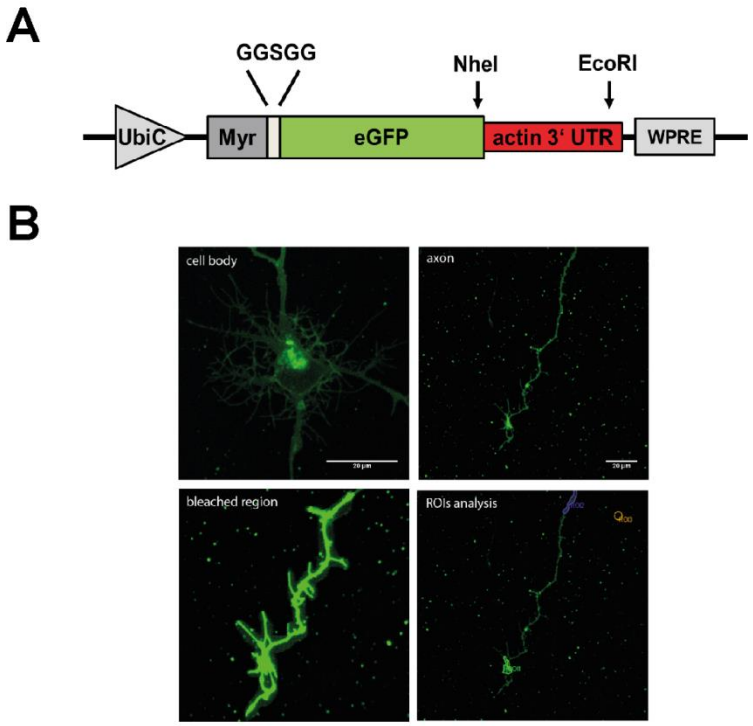

Figure 5.5.1Studying local translation of α-, β- and γ-actin using eGFP^{myr} reporters. (A) Scheme of the lentiviral eGFP^{myr} reporter construct with respective α-, β- and γ-actin 3'UTRs. (B) Transduced motoneurons express eGFP throughout axons at DIV5. Distal axons are bleached and recovery is monitored in defined ROIs.

Quantification of FRAP data showed a 60% recovery for 3'UTR-reporters of α-, β- and γ-actin in axonal growth cones (Fig. 5.5.2, A-D). Thus, transcripts of these different actin isoforms become locally translated with almost the same rate in axonal growth cones. Moreover, these data confirm that the 3'UTRs of α-, β- and γ-actin mRNAs are sufficient to drive their axonal transport in motoneurons. In control experiments, we treated motoneurons with translational blockers: cycloheximide (overnight) and anisomycin (1 h prior to FRAP assay), to rule out the potential diffusion of eGFP^{myr} protein from the proximal axon, and/or its refolding after bleaching. After treatments with either cycloheximide or anisomycin we noticed a significant reduction in florescence recovery of eGFP^{myr} (Fig. 5.5.2, B-D). This shows that the recovery observed for α-, β- and γ-actin reporters are due to their local translation in axonal growth cones, and not to the diffusion of eGFP^{myr} from the proximal axon.

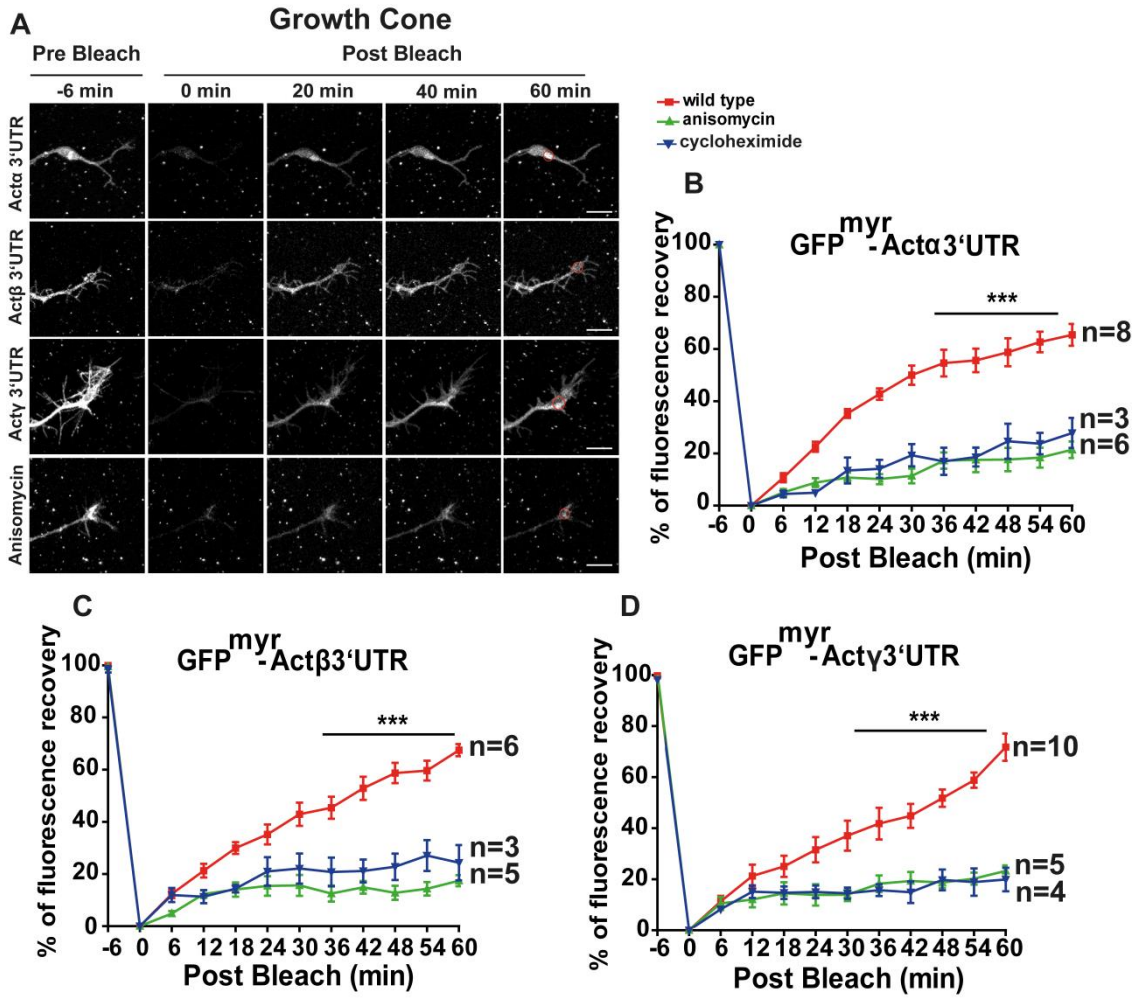

Figure 5.5.2 Reporters of α-, β- and γ-actin are locally translated in axonal growth cones of motoneurons. (A) Representative time lapse images of axonal growth cones of motoneurons transduced with α-, β and γ-actin eGFP^{myr} reporters before and after photo bleaching. (B-D) Graphs show 60% fluorescence recovery for α-actin (B), β-actin (C) and γ-actin (D) eGFP^{myr} reporters. Anisomycin and cycloheximide treatments decrease the observed recovery for α-actin, β- and γ-actin eGFP^{myr} reporters (*** $p < 0.001$). Statistical analysis: Two way ANOVA with Bonferroni posthoc test. Data are shown as mean ± SEM. Scale bar: 10 µm.

Our immunofluorescence experiments showed that α-actin protein predominantly localizes to axonal branch points (Fig. 5.4.4 A). Thus, we asked how the specific distribution of this protein in axonal branches correlates with its local translation in this particular axonal region. Quantification of fluorescence recovery in axonal branch points revealed that reporters for all three actin isoforms become translated in translational hot spots within the axonal branch

points (Fig. 5.5.3 A). Intriguingly, compared to β- and γ-actin reporters, the recovery rate for the α-actin reporter was remarkably higher in axonal branch points during the first 20 min post bleach (Fig. 5.5.3, B and C) which suggests an important role for locally synthetized α-actin in axon branching and arborization.

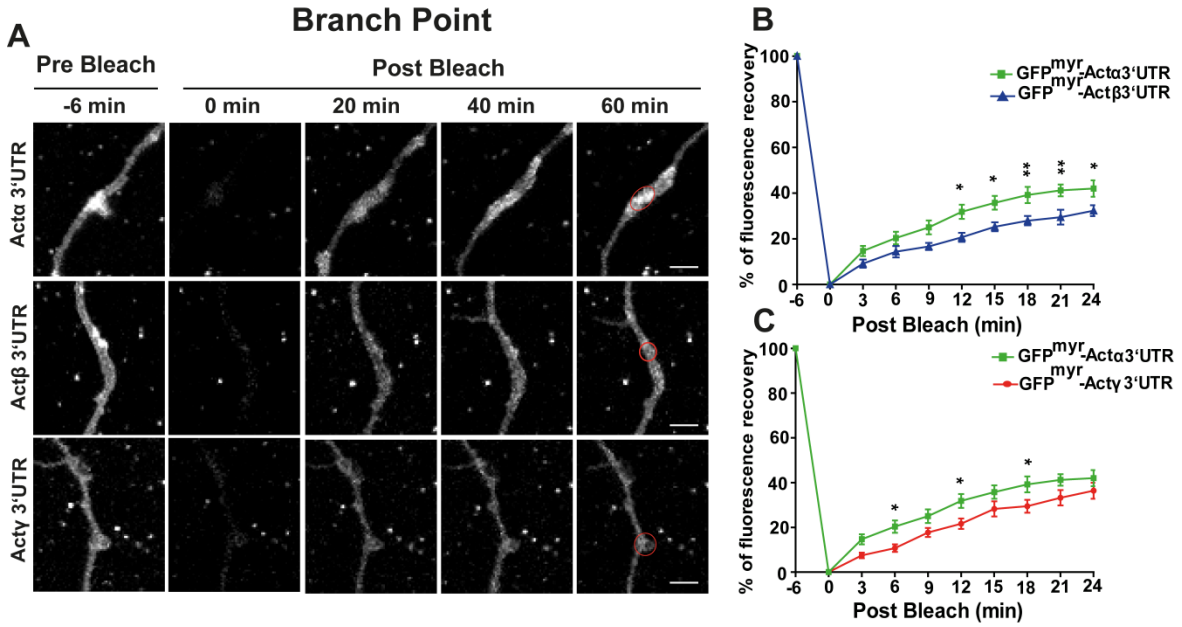

Figure 5.5.3 α-actin reporter shows a faster recovery rate in axonal branch points compared to β- and γ-actin reporters. (A) Representative time lapse images of axonal branch points of motoneurons transduced with α-, β and γ-actin eGFP^{myr} reporters before and after photo bleaching. (B and C) Quantification of FRAP indicated that α-actin eGFP^{myr} reporter becomes translated faster than β-actin (* $p < 0.05$ and ** $p < 0.01$) and γ-actin (* $p < 0.05$) eGFP^{myr} reporters in axonal branch points during the first 20 min post bleach. Statistical analysis: Two way ANOVA with Bonferroni posthoc test. Data are shown as mean ± SEM. Scale bar: 10 µm.

5.6 Actin isoforms accomplish specific functions in motor axon growth: α-actin is required for axonal collateral branch formation and β-actin is required for axonal elongation and growth cone differentiation.

The specific and unique distribution of α-, β- and γ-actin protein and mRNAs in axons of motoneurons refers to their specific cellular functions. Relatively high enrichment of α-actin protein in axonal branch points on the one hand and its high local translation rate in these regions on the other hand suggests that this isoform might play a role in formation of axonal collateral branches. To examine this hypothesis we generated several different lentiviral

shRNA constructs which specifically targeted α-, β- or γ-actin isoforms and depleted these individual mRNAs in primary motoneurons. Application of these knockdown shRNA lentiviruses significantly reduced both mRNA and protein levels of the respective isoforms. The efficiency of shRNA-1 against α-actin was tested both by qRT-PCR and Western blot analyses, which showed a 60% reduction in α-actin protein levels (Fig. 5.3.1 D) and a 90% reduction in its mRNA levels (Fig. 5.6.1 A). Similarly, shRNA-2 against α-actin caused 60% reduction in α-actin mRNA levels (Fig. 5.6.1 A). ShRNA-1 against β-actin resulted in 95% reduction in protein levels (Fig. 5.4.1 D) and 75% reduction in mRNA levels of this isoform (Fig. 5.6.1 B). ShRNA-2 against β-actin caused 90% reduction in its mRNA levels (Fig. 5.6.1 B). ShRNA-1 against γ-actin reduced protein levels of this isoform by 85% (Fig. 5.6.1 D) and mRNA levels by 80% (Fig. 5.6.1 C). mRNA levels of γ-actin were reduced by 85% after application of shRNA-2 and by 70% after application of shRNA-3 (Fig. 5.6.1 C).

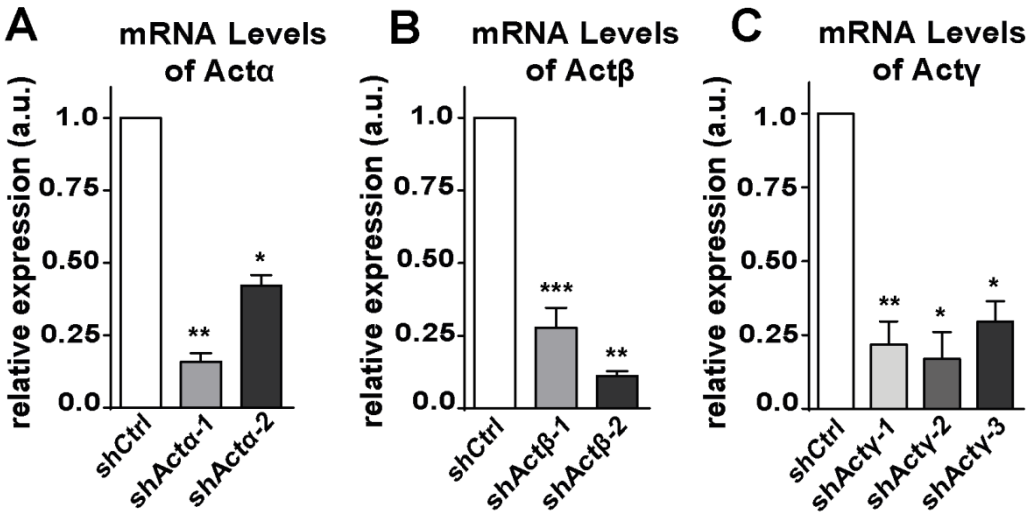

Figure 5.6.1 mRNA levels of α-, β- and γ-actin isoforms are significantly reduced after respective shRNA mediated knockdown of these isoforms. (A) qRT-PCR analysis of cultured motoneurons showed that α-actin mRNA levels are reduced by 85% and 60% after shActα-1and shActα-2 lentiviral transduction, respectively (* $p < 0.01$ and ** $p < 0.0037$, $n = 5$ for shActα-1 and $n = 4$ for shActα-2). (B) Transduction of motoneurons with shActβ-1 leads to 75% reduction in β-actin mRNA levels and with shActβ-2 to 90% reduction (** $p < 0.008$ and *** $p < 0.0006$, $n = 6$ for shActβ-1 and $n = 3$ for shActβ-2). (C) mRNA levels of γ-actin are reduced by 80%,

85% and 70% after application of shActγ-1, shActγ-2 and shActγ-3, respectively (* $p < 0.014$ and ** $p < 0.0013$, n = 5 for shActγ-1, n = 4 for shActγ-2 and n = 3 for shActγ-3). Statistical analysis: one-tailed Mann-Whitney test. Data are shown as mean ± SEM.

We first examined whether knockdown of α-, β- or γ-actin could affect cell viability. For this purpose, we performed survival assays with cultured motoneurons after shRNA-mediated depletion of each isoform. As shown in Fig. 5.6.2, A-C, knockdown of α-, β- and γ-actin alone did not affect cell viability. Then, we analyzed the length and number of dendrites in isoform-specific knockdown motoneurons and found that also these parameters were not affected (Fig. 5.6.3, A-C). However, we found a 20% reduction in cell body size after knockdown of α-actin, while knockdown of β- or γ-actin had no influence on soma growth (Fig. 5.6.3 D).

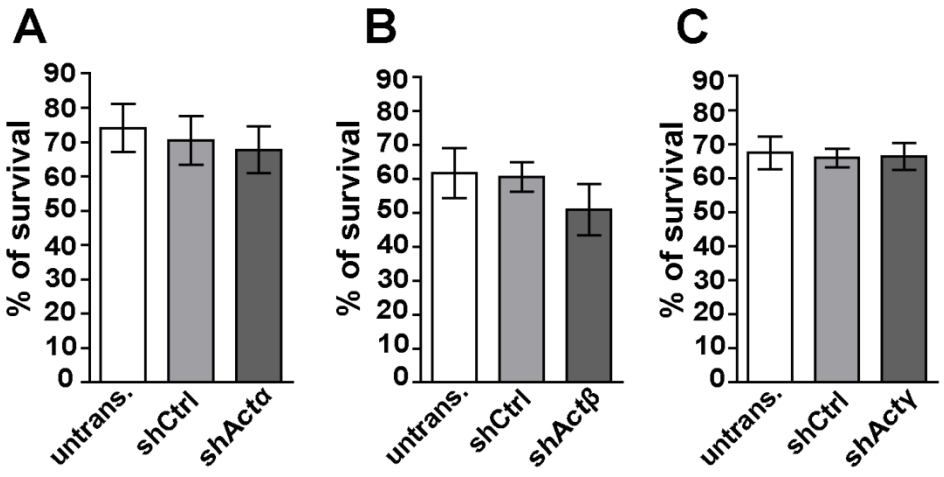

Figure 5.6.2 Depletion of α-, β- or γ-actin does not affect survival of motoneurons. (A-C) Viability of motoneurons is not reduced after knockdown of α-actin (A for n = 6), β-actin (B for n = 5) or γ-actin (C for n = 5). Data are shown as mean ± SEM.

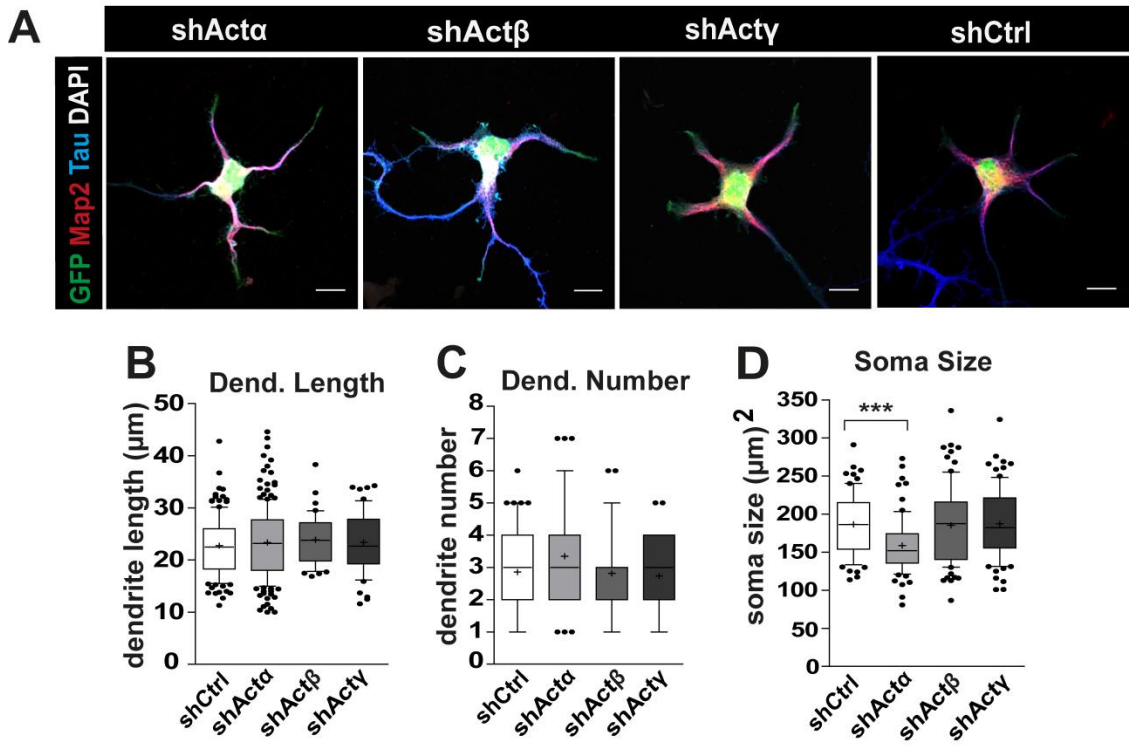

Figure 5.6.3 Depletion of α-, β- or γ-actin isoforms does not affect dendrite growth. ShRNA-mediated knockdown of α-, β- or γ-actin has no influence on dendrite length (B) and number (C) (sample size: B: shActα: n = 190, shActβ: n = 116, shActγ: n = 149, shCtrl: n = 136, C: shActα: n = 58, shActβ: n = 38, shActγ: n = 46, shCtrl: n = 49 for n = 5). (D) α-actin depletion significantly reduces soma size (*** $p < 0.0001$ for n = 5, sample size: shActα: n = 76, shActβ: n = 82, shActγ: n = 83, shCtrl: n = 69). Scale bar: 10 µm.

Analysis of axonal collateral branches showed that upon α-actin knockdown, the number of axons without collateral branches increases and the number of axons with 3 or more branches decreases (Fig. 5.6.4, A and B). This result indicates that α-actin is required for axon arborization in motoneurons. Interestingly, knockdown of β-actin associated with increased number of axonal collateral branches (Fig. 5.6.4 C). In contrast to α- and β-actin, the depletion of γ-actin did not affect collateral branch formation (Fig. 5.6.4 D).

Analysis of axon growth revealed that α-, β- or γ-actin depleted motoneurons grow shorter axons in culture after DIV7. We observed that depletion of β-actin had a more prominent effect on axon elongation, as knockdown of this isoform reduced axon length by 41%,

whereas depletion of α- and γ-actin reduced it by 29% and 19%, respectively (Fig. 5.6.5, A-C).

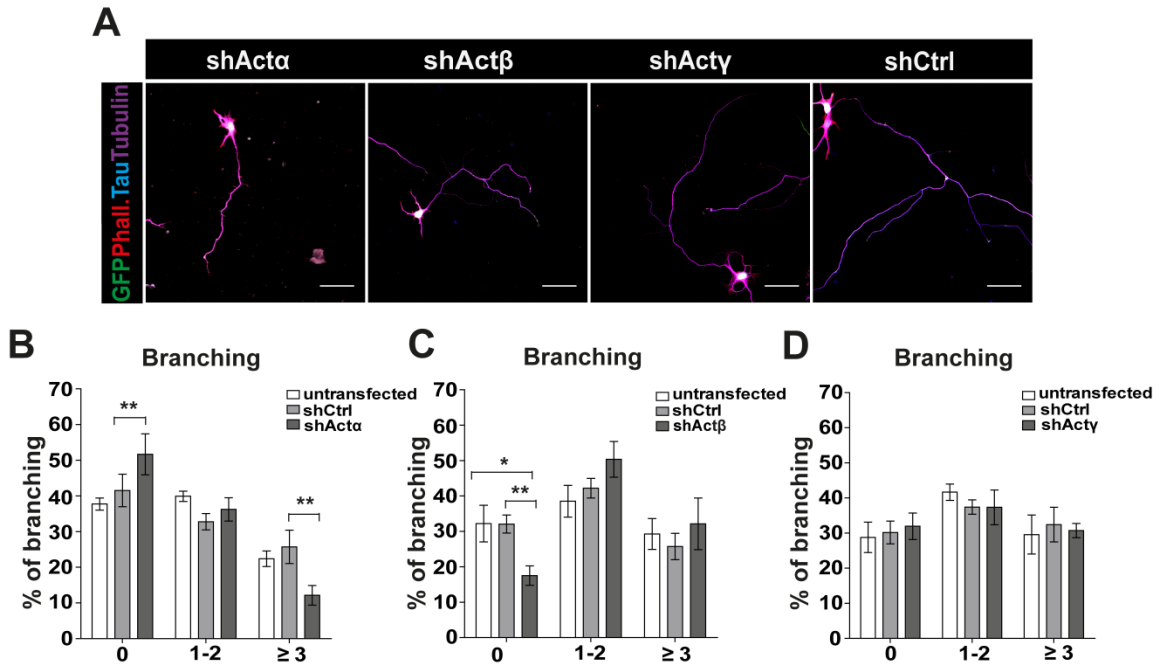

Figure 5.6.4 Depletion of α-actin isoform impairs axonal branching in motoneurons. (A) Motoneurons were transduced with shActα, shActβ, shActγ or shCtrl lentivirus constructs. Axons and mature branches are labeled with phalloidin, Tau and Tubulin. GFP is used to identify transduced cells. (B) After depletion of α-actin, the number of axons without collateral branches increases, and the number of axons with ≥ 3 branches decreases (** $p < 0.01$ for $n = 5$). (B) Axonal branching is enhanced in β-actin knockdown motoneurons (* $p < 0.031$ and ** $p < 0.01$ for $n = 6$). (D) Knockdown of γ-actin does not influence axonal branching ($n = 4$). Data are shown as mean ± SEM. Scale bar: 50 µm.

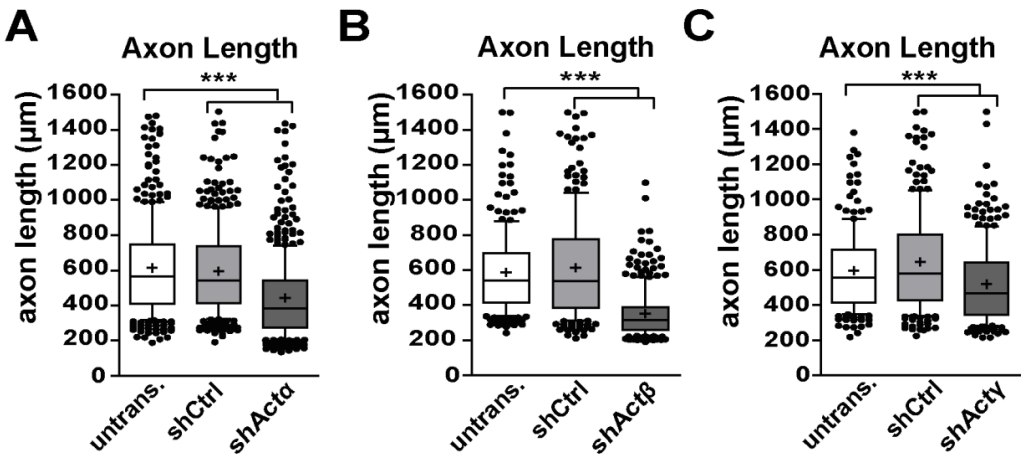

Figure 5.6.5 Depletion of α-, β- or γ-actin impairs axon elongation in cultured motoneurons. (A-C) Cultured motoneurons transduced with shRNA against α-actin (A), β-actin (B) or γ-actin (C) exhibit shorter axons compared to untransduced or shCtrl transduced motoneurons. (A: *** $p < 0.0001$ for n = 5, sample size: shActα: n = 452, shCtrl: n = 380, untransduced: n = 328, B: *** $p < 0.0001$ for n = 5, sample size: shActβ: n = 279, shCtrl: n = 227, untransduced: n = 219, C: *** $p < 0.0001$ for n = 4, sample size: shActγ: n = 252, shCtrl: n = 228, untransduced: n = 180). Statistical analysis: one way ANOVA with Dunn's posttest.

In order to study possible effects of α-, β- and γ-actin knockdown on axonal growth cone maturation, we plated motoneurons on a synapse specific laminin (laminin 221) as a substrate. This matrix protein has been shown to induce formation of presynaptic structures in axonal growth cones of cultured motoneurons (Jablonka et al., 2007; Porter et al., 1995). To visualize axonal growth cone filopodia, we stained DIV5 motoneurons with phalloidin and Tau (Fig. 5.6.6 A). Analysis of axonal growth cones on this laminin isoform revealed that knockdown of β-actin results in 50% reduction in growth cone size which further associates with a significant reduction in number of growth cone filopodia (Fig. 5.6.6, B and C). Interestingly, these effects were unique for β-actin since depletions of the other two isoforms did not impair axonal growth cone morphology (Fig. 5.6.6, B and C). Collectively, these data confirm a specific function for α-actin in axonal arborization and for β-actin in pathfinding and differentiation of growth cones into functional synapses.

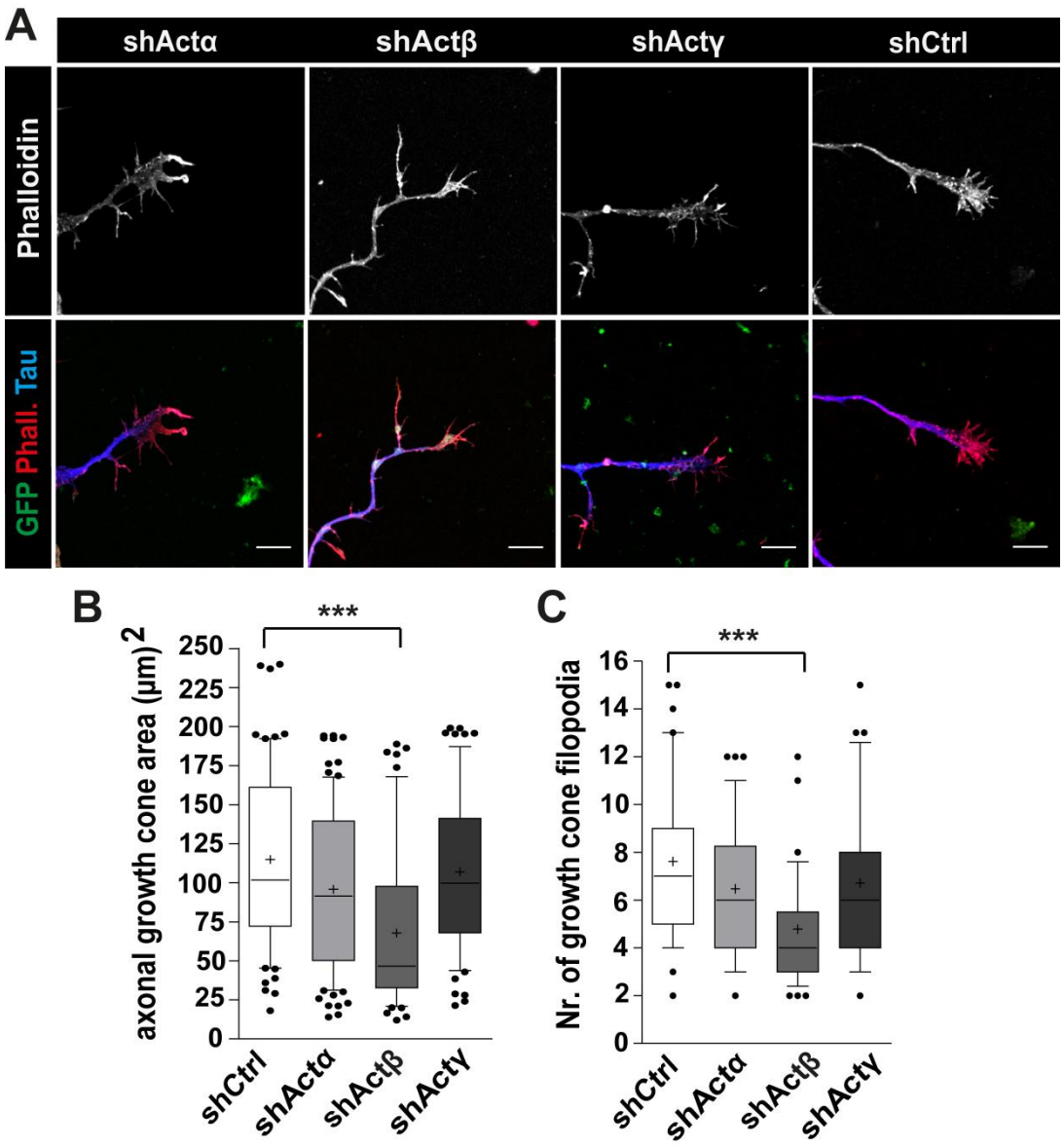

Figure 5.6.6 β-actin knockdown motoneurons show defective growth cones maturation. (A) Motoneurons were plated on laminin 221. Growth cone were labeled by Tau and phalloidin. Scale bar: 10 µm. (B and C) Depletion of β-actin significantly reduces growth cone area (B) and number of growth cone filopodia (C). Depletions of α- or γ-actin isoforms do not impair growth cone morphology (*** $p < 0.0001$ for n = 6, sample size: shActα: n = 96, shActβ: n = 54, shActγ: n = 67, shCtrl: n = 70). Statistical analysis: one way ANOVA with Dunn's posttest.

Though shRNA-mediated knockdown of each actin isoform created distinct and specific phenotypes, these observed defects in axon growth and differentiation might also be due to a possible off-target effect of these shRNAs. To exclude this possibility, we designed multiple

different shRNAs against α-, β- and γ-actin and assessed axon morphology in motoneurons transduced with these shRNAs (Fig. 5.6.2, A-C). Depletion of α-actin by shActα-2 caused defects in axon growth (Fig. 5.6.7 A) and decreased the number of collateral branches confirming the results obtained with shActα-1 (Fig. 5.6.7 B). Transduction of motoneurons with shActβ-2 significantly reduced axon length (Fig. 5.6.8 A) and growth cone size (Fig. 5.6.8 B). Motoneurons transduced with either shActγ-2 or shActγ-3 exhibited deficits in axon elongation (Fig. 5.6.8 C). These additional control experiments clearly indicate that the observed phenotypes are the result of actin isoform-depletion and not due to off-target effects and thus confirm the target specificity of the applied shRNAs. Moreover, we generated a rescue construct for β-actin by introducing a shRNA-resistant version of β-actin into the shActβ-1 construct (Fig. 5.6.9 A). As shown in Fig. 5.6.9 B, the β-actin rescue construct was overexpressed in cultured motoneurons. Western blot quantification showed that β-actin protein levels were restored to 75% after expression of this shRNA resistant construct (Fig. 5.6.10, A and B). Re-expression of this β-actin isoform rescued deficits in axon growth and maturation caused by β-actin knockdown. No significant differences were observed in axon length of cultured motoneurons transduced with this β-actin rescue construct and the control group (Fig. 5.6.11, A and B). Similarly, axonal growth cone size (Fig. 5.6.12, A and B) and number of growth cone filopodia (Fig. 5.6.12, A and C) were not different between β-actin rescue construct transduced and control motoneurons.

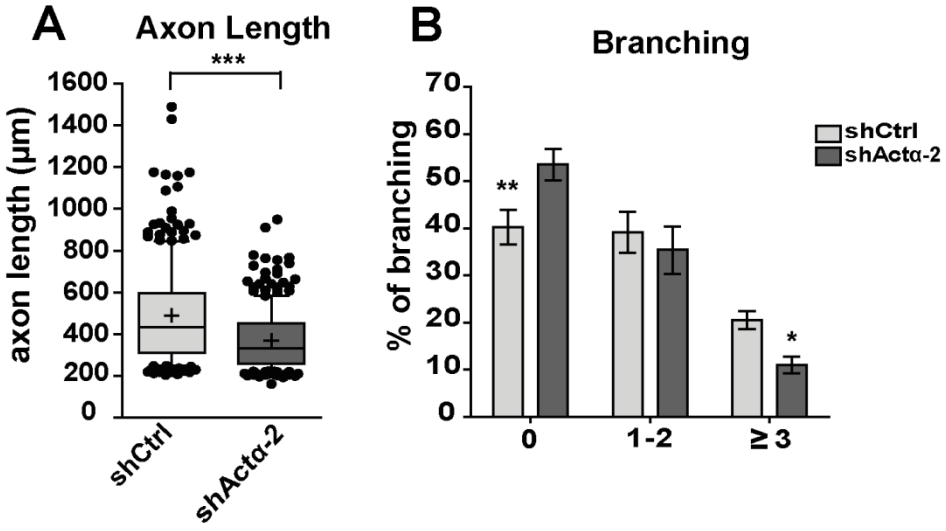

Figure 5.6.7 ShActα-2 lentiviral transduction impairs axonal growth and collateral branch formation in cultured motoneurons. (A and B) Motoneurons were transduced with shActα-2 and cultured for 7 days. (A) Analysis of axon length showed that shActα-2 transduced motoneurons grow shorter axons (*** $p < 0.0001$ for n = 3 independent experiments, sample size: shActα-2: 252, shCtrl: 242, by two-tailed Mann-Whitney test). (B) In shActα-2 transduced motoneurons, the number of axons without collateral branches is increased and the number of axons with ≥ 3 branches is decreased (* $p < 0.05$ and ** $p < 0.01$for n = 3, by two way ANOVA with Bonferroni posthoc test). In B data are shown as mean ± SEM.

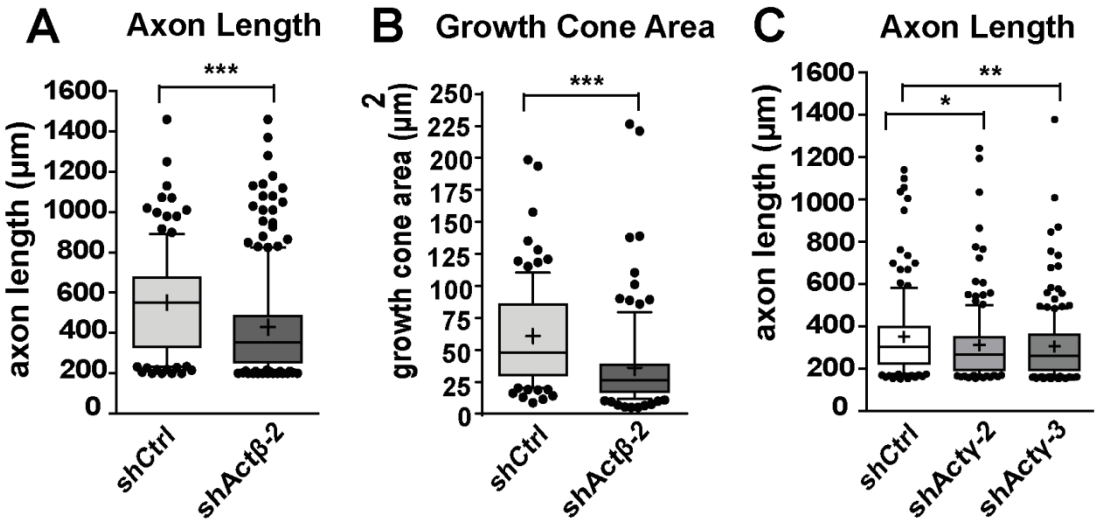

Figure 5.6.8 ShActβ-2, shActγ-2 and shActγ -3 cause similar defects in axon elongation and axonal growth cone differentiation as shActβ-1 and shActγ-1. (A) ShActβ-2 transduction leads to 21% reduction in axon length (*** $p < 0.0001$ for n =3, sample size: shActβ-2: 220, shCtrl: 126). (B) Depletion of β-actin by ShActβ-2 reduces growth cone size by 40% (*** $p < 0.0001$ for n = 3 independent experiments, sample size: shActβ-2: 108, shCtrl: 96, by two-tailed Mann-Whitney test). (C) Axon length of motoneurons are reduced by 12% upon shActγ-2 and by15% upon shActγ-3 transduction (* $p < 0.012$ and ** $p < 0.004$ for n = 3, sample size: shActγ-2: 150, shActγ-3: 184 and shCtrl: 144, by one way ANOVA with Dunn's posttest).

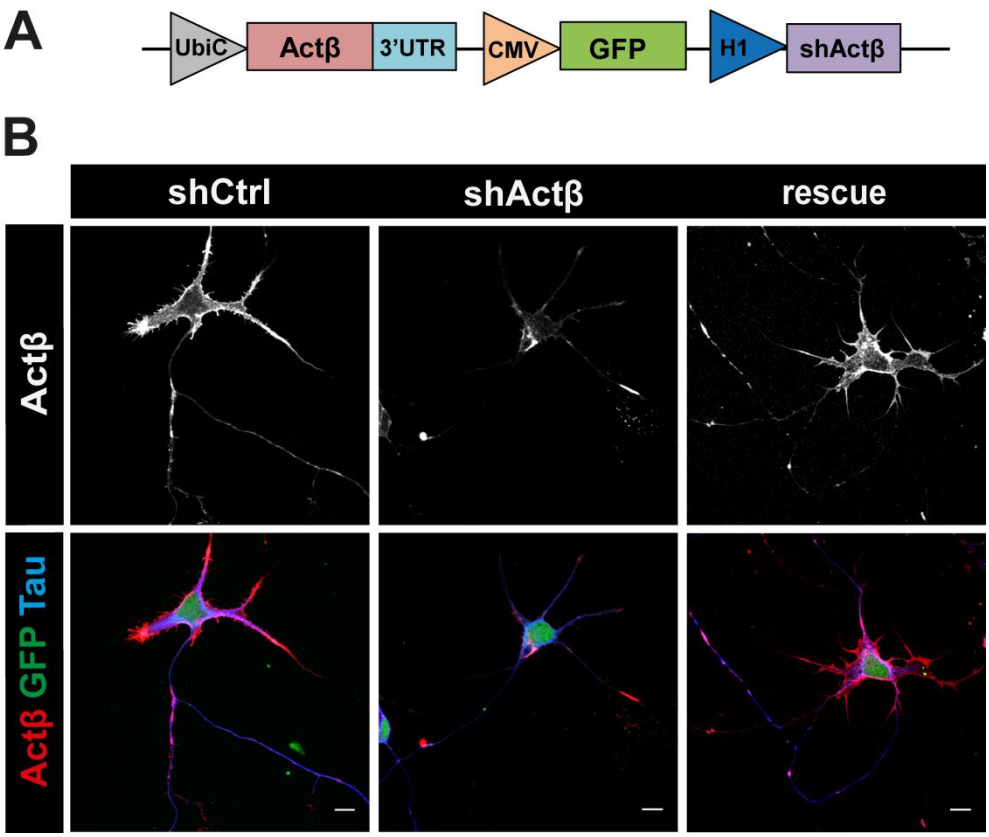

Figure 5.6.9 β-actin rescue construct is expressed in cultured motoneurons. (A) Scheme of the β-actin-rescue construct. In a lentiviral vector, an ubiquitin promotor drives the expression of a shRNA resistant β-actin cDNA and the H1 promotor drives the expression of shActβ. CMV promotor drives the expression of GFP which is used for identification of transduced motoneurons. (B) Immunostaining of motoneurons transduced with shCtrl, shActβ and β-actin rescue shows restored levels of β-actin protein in motoneurons expressing the shRNA resistant β-actin rescue construct. Scale bar: 10 µm.

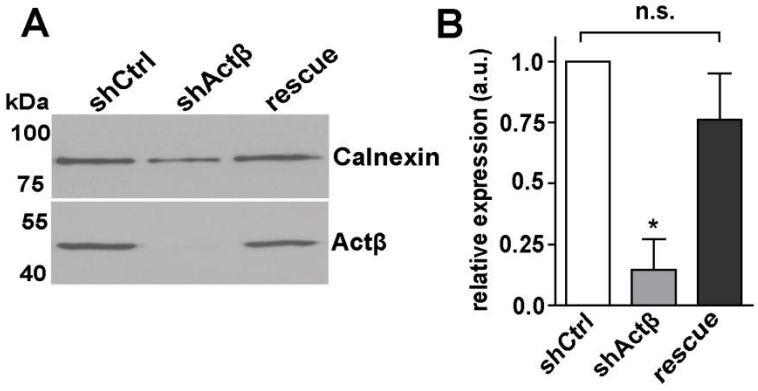

Figure 5.6.10 β-actin protein levels are restored after expression of the β-actin rescue construct. (A) Western blot from lysates of cultured motoneurons transduced with shActβ, shCtrl and the β-actin rescue construct. (B) Quantification of density of immunoreactive bands in the blot in A shows a 60% increase in β-

actin protein levels in lysate of β-actin rescue transduced motoneurons (* $p < 0.016$ for $n = 3$ by one-tailed Mann-Whitney test). Data are shown as mean ± SEM.

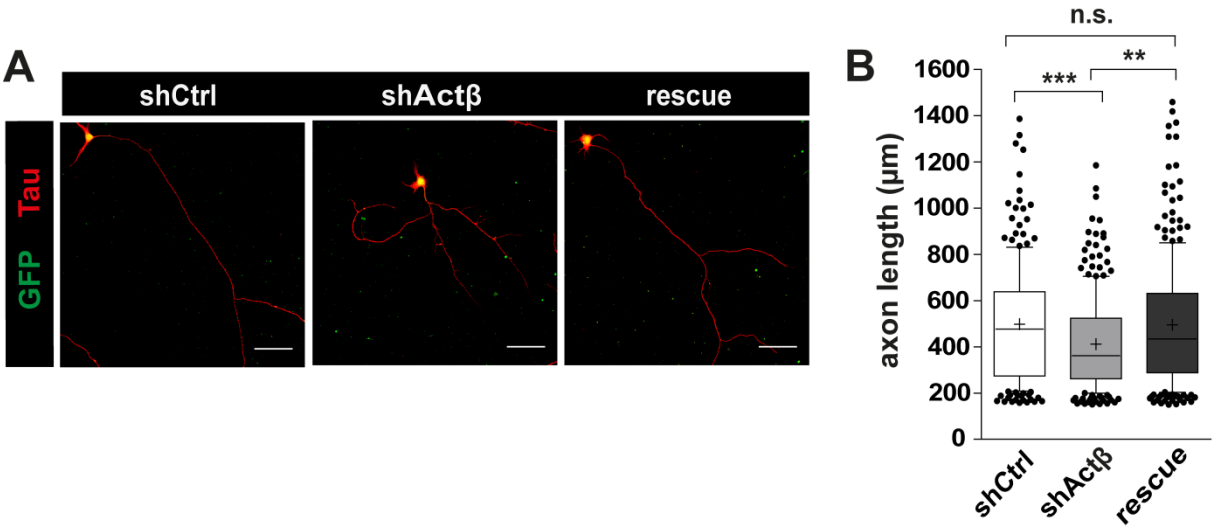

Figure 5.6.11 Axon length defects are rescued after re-expression of the β-actin rescue construct in cultured motoneurons. (A) Motoneurons were transduced with shCtrl, shActβ or β-actin rescue constructs and cultured for 7 days. Axons are labeled against Tau. Scale bar: 50 µm. (B) Re-expression of the β-actin rescue construct rescues axon length and observed defects in axonal growth (** $p < 0.002$ and *** $p < 0.0002$ for $n = 3$, sample size: shActβ: 240, rescue: 266 and shCtrl: 217 by one way ANOVA with Dunn's posttest).

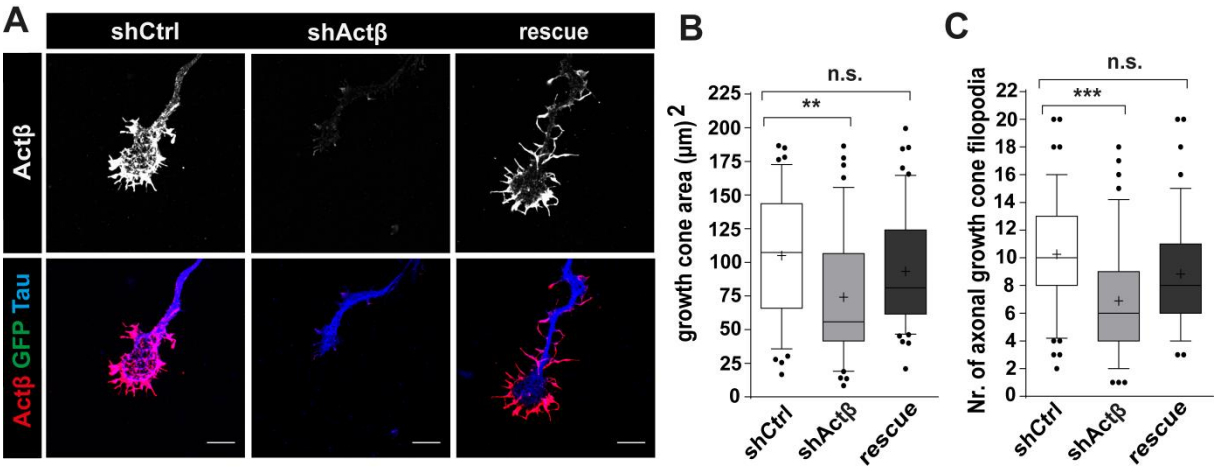

Figure 5.6.12 Defects in axonal growth cone maturation are rescued after re-expression of the β-actin rescue construct in cultured motoneurons. (A) Motoneurons expressing shActβ, shCtrl or β-actin were stained with β-actin and Tau antibodies. Scale bar: 10 µm. (B and C) Re-expression of β-actin with the rescue construct increases axonal growth cone size (B: ** $p < 0.005$) and the number of axonal growth cone filopodia (C: *** $p < 0.0003$). For $n = 3$ independent experiments, sample size: shActβ: 43, rescue: 56 and shCtrl: 48. Statistical analysis: one way ANOVA with Dunn's posttest.

5.7 Actin dynamics is differentially regulated by α-, β- and γ-actin isoforms in axonal filopodia and axonal growth cone filopodia

Axon growth and differentiation occurs in three main steps: (i) axon specification, (ii) axon elongation and path finding, and (iii) collateral branch formation and presynaptic differentiation. All these steps rely on the dynamics of coordinated actin and microtubule polymerization. Collateral branch formation starts with actin polymerization in so-called "actin patches" along the main axon shaft, which gives rise to formation of nascent filopodia (Spillane et al., 2011). These filopodia are enriched in actin filaments and therefore are highly dynamic. *In vitro*, these filopodia undergo many cycles of growth and retraction until they become stabilized by microtubule invasion (Gallo, 2011). Our data have shown that α-actin mRNA and protein localize to axonal branch points and knockdown of this isoform disturbs formation of collateral branches. Hence, we asked whether this isoform exerts this function via regulating actin dynamics at axonal filopodia. To examine such possibility, we performed live cell imaging with motoneurons transduced with α-, β- and γ-actin knockdown lentiviruses and analyzed the dynamics of axonal filopodia (Fig. 5.7.1 A). Quantification of filopodia dynamics in the axon shaft indicated that depletion of α-actin or γ-actin correlates with a 60% decrease in filopodia initiation rate, but depletion of β-actin decreases filopodia initiation rate only by 25% in this region (Fig. 5.7.2, A and B). Interestingly, knockdown of α-actin decreased filopodia life time, whereas knockdown of β-actin increased filopodia life time (Fig. 5.7.2 C). Similarly, knockdown of both α- and γ-actin reduced the rate of filopodia dynamic movements by 50% (Fig. 5.7.2 D). The rate of filopodia dynamic movement was not altered after specific knockdown of β-actin (Fig. 5.7.2 D).

Measuring the total change in filopodia length revealed that knockdown of α- or γ-actin reduces the total filopodia length change by 57%; 10 µm total length change was measured for α-actin depleted filopodia and 11 µm was measured for γ-actin depleted filopodia (Fig. 5.7.2 E). Control filopodia underwent a total length change of 23 µm and β-actin knockdown

filopodia underwent a total length change of 17 µm during the total 40 min imaging period (Fig. 5.7.2 E). We counted also the number of axonal filopodia in phalloidin-labeled motoneurons and observed a decrease of axonal filopodia in α-actin depleted neurons (Fig. 5.7.2 F). These data indicate that α- and γ-actin isoforms control actin dynamics during axonal branching, and not β-actin.

Abundant expression of β-actin protein and mRNA in the axonal growth cone and decreased growth cone filopodia upon specific knockdown of this isoform prompted us to assess the possible function of β-actin in regulating growth cone filopodia dynamics. We examined this by analyzing dynamics of axonal growth cone filopodia (Fig. 5.7.3 A). Time lapse imaging of axonal growth cones revealed that the velocity of filopodia movements is reduced by 50% after β-actin knockdown, but is not affected upon knockdown of α- or γ-actin (Fig. 5.7.3, B-D). Therefore, β-actin specifically modulates actin dynamics in axonal growth cones, a function which is important particularly for the axon pathfinding and growth cone differentiation.

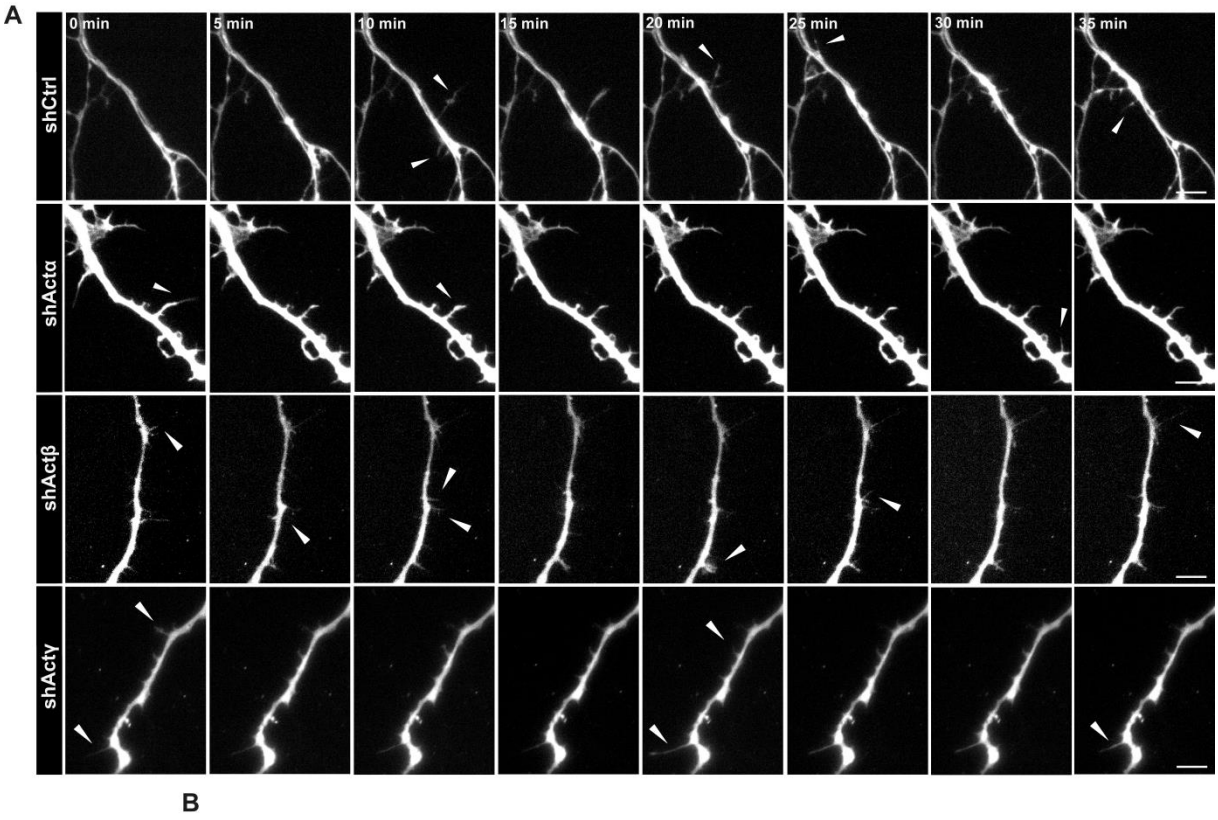

Figure 5.7.1 Axonal filopodia exhibit de novo formation and growth/retraction dynamics in culture. (A) Time lapse images of axonal filopodia dynamics in axons of control and actin isoform-specific depleted motoneurons. Arrows indicate de novo formation of new filopodia along the main axon shaft.

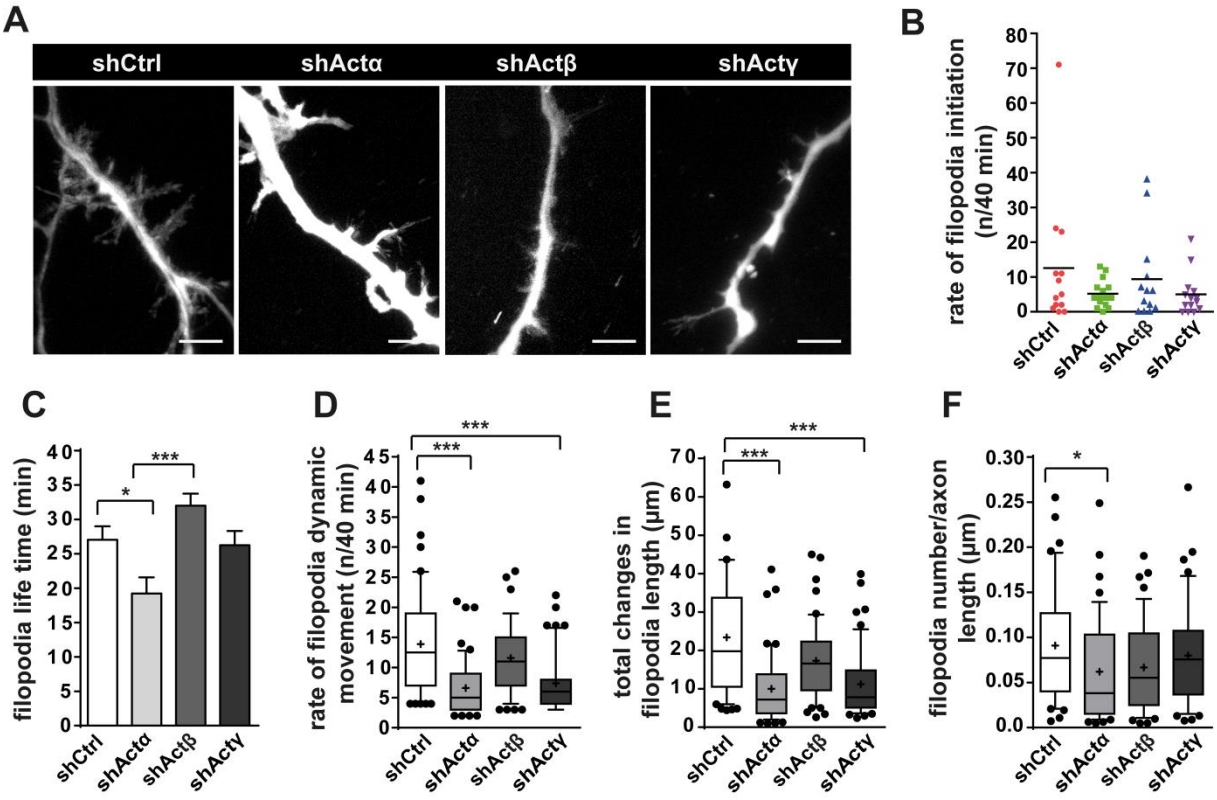

Figure 5.7.2 Knockdown of α- or γ-actin isoforms affects dynamics of axonal filopodia. (A) Maximum projection of 120 time lapse sequences represents filopodia de novo formation and growth dynamics over time. (B) shRNA-mediated depletion of α- or γ-actin, but not β-actin decreases the rate of filopodia initiation by 60%. (C) Graph shows the life time of axonal filopodia. In α-actin depleted motoneurons, axonal filopodia exhibit shorter life time compared to control (* $p < 0.010$) and β-actin depleted motoneurons (*** $p < 0.0008$). Data are shown are mean ± SEM. (D) Depletion of α- or γ-actin decreases the average rate of filopodia dynamic movements. (E) Knockdown of α- or γ-actin significantly reduces total changes in filopodia length extension (D and E: *** $p < 0.0001$, shActα: n = 4, shActβ: n = 5, shActγ: n = 3, shCtrl: n = 6 for 50 filopodia per group). (F) ShActα, shActβ, shActγ and shCtrl transduced motoneurons were fixed and stained with phalloidin. Analysis of axonal filopodia revealed a reduction in the number of axonal filopodia (per µm axon length) in shActα transduced motoneurons (* $p < 0.043$). Statistical analysis: one way ANOVA with Dunn's posttest.

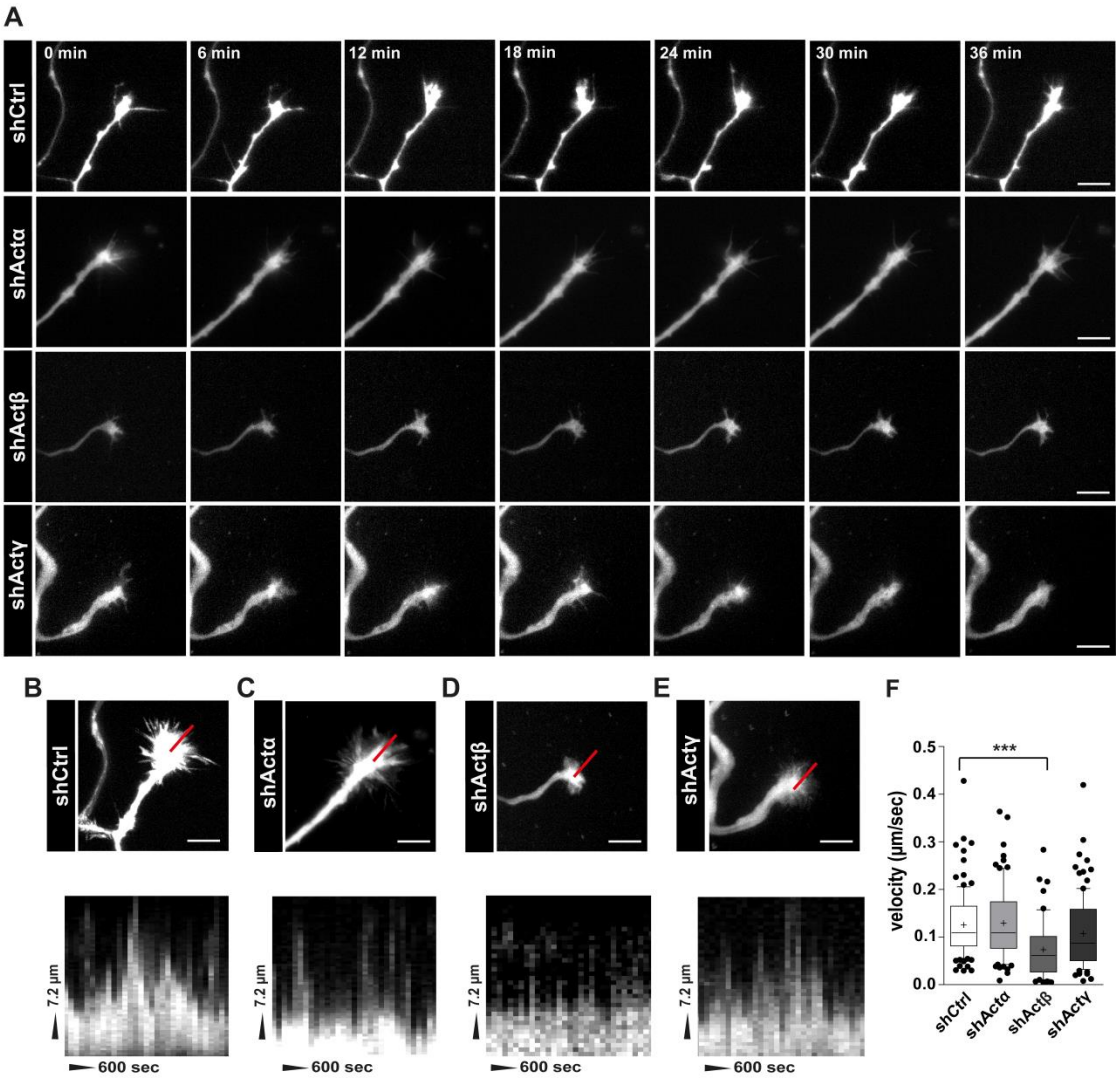

Figure 5.7.3 Dynamics of axonal growth cone filopodia is impaired in β-actin knockdown motoneurons. (A) Time lapse images of axonal growth cone filopodia movements in motoneurons after knockdown of α-, β- and γ-actin. (B-E) Images show maximum projection of 120 frames representing total changes in filopodia length. Multiple kymographs were created for quantification of filopodia movement velocity. X-axis represent filopodia length in µm and Y-axis represents time in sec. (F) Depletion of β-actin significantly decreases the velocity of growth cone filopodia movements, whereas depletion of α- or γ-actin does not affect this parameter (*** $p < 0.0001$ for n = 3, sample size: shActα: n = 17, shActβ: n = 16, shActγ: n = 13, shCtrl: n = 15 by one way ANOVA with Dunn's posttest).

5.8 Depletion of one actin isoform induces a compensatory response which leads to upregulation of other actin isoforms

Motoneuron conditional knockout mice for β-actin are viable and show normal NMJ morphology and function (Cheever et al., 2011). Knockout of this isoform in the central nervous system causes only restricted morphological and behavioral deficits (Cheever et al., 2012). In β-actin depleted mouse fibroblasts, elevated protein levels of α- and γ-actin have been reported (Bunnell et al., 2011; Tondeleir et al., 2012). This compensatory upregulation of these two isoforms can rescue the migratory defects caused by β-actin ablation, indicating that these isoforms could act redundantly and compensate for each other's lost. We investigated this compensatory response in cultured motoneurons after specific shRNA-mediated ablation of α-, β- or γ-actin. We examined first whether these isoforms have redundant functions regarding F-actin polymerization in soma and axons. We stained shActα, shActβ and shActγ treated motoneurons with phalloidin and quantified F-actin levels in soma and axons of these neurons. Quantification of the phalloidin signal intensity showed that the F-actin levels were not altered in the soma of α-, β- or γ-actin depleted motoneurons, thus indicating that these isoforms act redundantly for F-actin polymerization in this compartment (Fig. 5.8.1, A and B). Nevertheless, we observed a significant reduction in F-actin levels in the axon after specific depletion of α- or β-actin indicating a specific function for these two isoforms in F-actin polymerization dynamics in this compartment (Fig. 5.8.1, A and C).

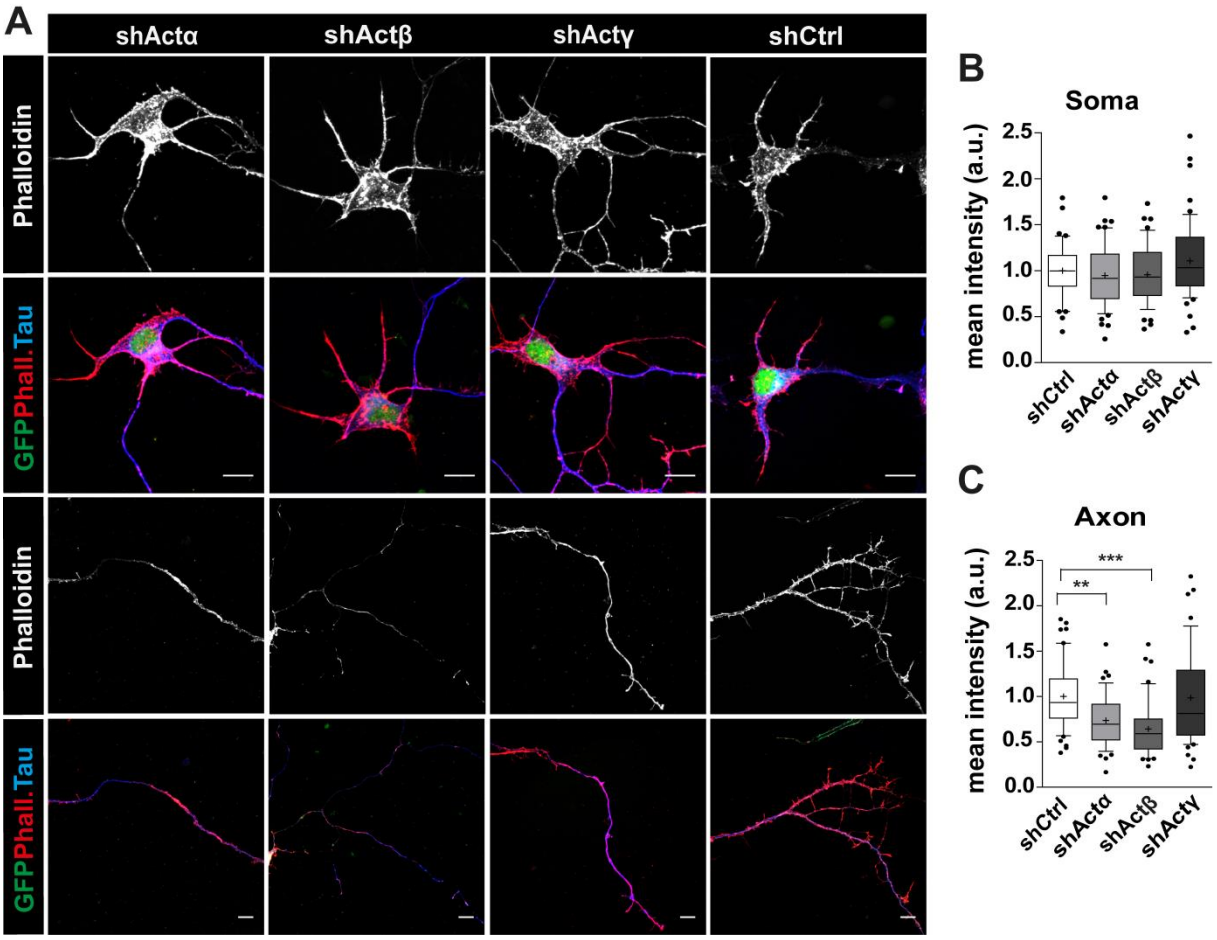

Figure 5.8.1 α- and β-actin isoforms are essential for F-actin polymerization in axons. (A) Motoneurons were transduced with shActα, shActβ, shActγ and shCtrl. On DIV7, cells were fixed and immunostained using Tau antibody and phalloidin. (B and C) Phalloidin signal intensity was measured in soma and axons of shRNA treated motoneurons and normalized to phalloidin intensity of control group. (B) Phalloidin intensity is not reduced in the soma of α-, β- or γ-actin depleted motoneurons ($p < 0.208$ for $n = 3$, sample size: shActα: $n = 55$, shActβ: $n = 47$, shActγ: $n = 53$, shCtrl: $n = 44$). (C) Phalloidin intensity is markedly reduced in axons of α-, and β-actin knockdown motoneurons (** $p < 0.0018$ for shActα and *** $p < 0.0001$ for shActβ for $n = 3$, sample size: shActα: $n = 48$, shActβ: $n = 46$, shActγ: $n = 53$, shCtrl: $n = 54$). Statistical analysis: one way ANOVA with Dunn's posttest. Scale bar: 10 µm.

Next, we examined the total actin levels in lysates of α-, β- or γ-actin depleted motoneurons by Western blot analysis. Intriguingly, the total actin levels did not alter and remained constant after depletion of these individual isoforms (Fig. 5.8.2, A and B). Depletion of β-actin in fibroblast causes a shift in G- to F-actin ratio and decreases the availability of G-actin

(Bunnell et al., 2011). We examined the G/F ratio in lysates of α-, β and γ-actin knockdown motoneurons. G- and F-actin pools were separated by an ultracentrifugation step and probed with a pan-actin antibody (Fig. 5.8.3 A). Quantification of blots revealed that the G/F ratio does not alter after respective knockdown of α-, β- or γ-actin, which is another piece of evidence for a redundant function of these isoforms in motoneurons (Fig. 5.8.3 B). Next, we probed the G- and F-actin pools with a β-actin specific antibody and observed a shift in β-actin from the G-actin to F-actin pool upon knockdown of α- or γ-actin, as the levels of β-actin increased in the G-actin pool and decreased in the F-actin pool (Fig. 5.8.3, C and D). These data indicate that α- and γ-actin control the polymerization rate or stabilization of filaments containing β-actin.

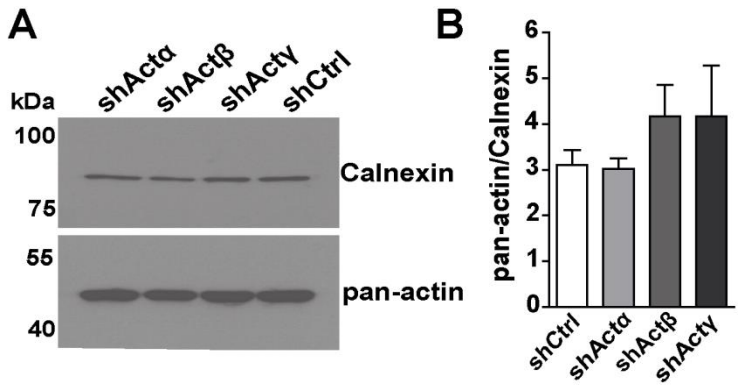

Figure 5.8.2 Pan-actin levels remain constant in α-, β- or γ-actin knockdown motoneurons. (A) Protein lysates of cultured motoneurons transduced with shActα, shActβ, shActγ and shCtrl were analyzed by Western blot using a pan-actin antibody. (B) Quantification of band intensities in the blot shown in A indicates that total actin levels remain unaltered after depletion of α-, β-, or γ-actin (by two-tailed Mann-Whitney test for n = 4). Data are shown are mean ± SEM.

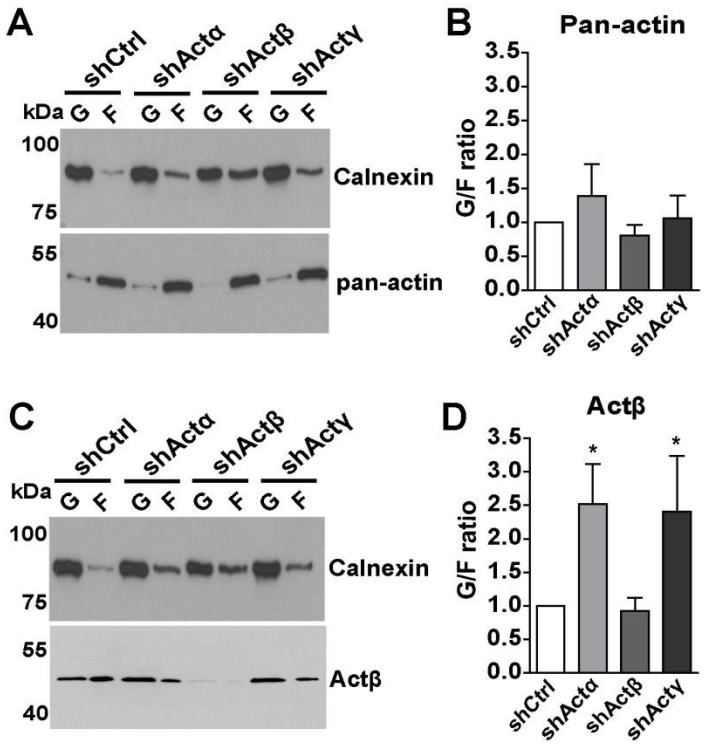

Figure 5.8.3 G/F actin ratio is preserved after knockdown of individual actin isoforms. (A and C) Motoneurons were transduced with shActα, shActβ, shActγ and shCtrl. Lysates were ultra-centrifuged and supernatant (G-actin) and pellet fractions (F-actin) were labeled with pan-actin (A) or β-actin antibodies (C). (B) Quantification of band intensities in the blot shown in A revealed that the G/F-actin ratio is preserved in actin isoform-specific knockdown motoneurons. (C) G- and F-actin pools were probed with β-actin antibody. (D) Quantification of band intensities in the blot shown in C revealed a shift for β-actin protein from G- to F-actin pool after depletion of α-actin and γ-actin (* $p < 0.016$ by one-tailed Mann-Whitney test for $n = 5$). Data are shown are mean ± SEM.

Maintenance of the total actin levels and preserved G/F-actin ratio suggest a compensatory response for actin isoforms. To examine this compensatory response, we analyzed mRNA as well as protein levels of each actin isoform after knockdown of other two isoforms. qRT-PCR showed that depletion of α-actin, does not alter total mRNA expression levels of β- or γ-actin (Fig. 5.8.4 A). Analysis of mRNA levels of β-actin in somatodendritic and axonal compartments of α-actin depleted motoneurons revealed that the mRNAs for β-actin decrease in the somatodendritic compartment and increase in the axonal compartment (Fig. 5.8.4 B).

Depletion of α-actin also associated with increased mRNA levels of γ-actin in the axonal compartment (Fig. 5.8.4 B). Thus, reduced F-actin polymerization capacity in the axon upon α-actin depletion refers to a specific function in axons. This could explain the axon specific compensatory response by β- and γ-actin.

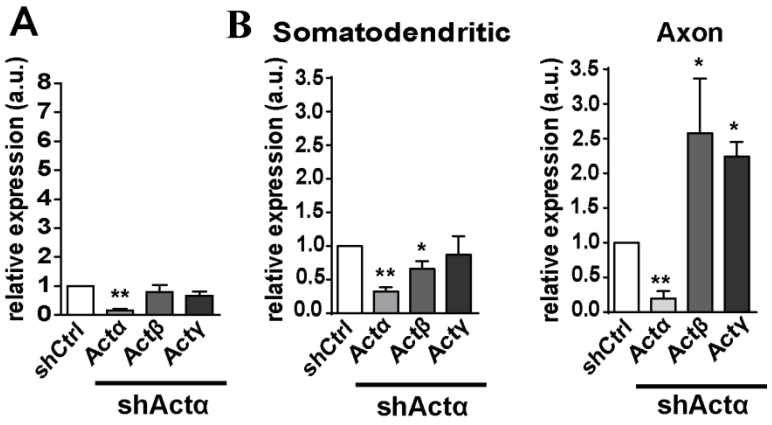

Figure 5.8.4 Compensatory upregulation of β- and γ-actin mRNAs in axons of α-actin depleted motoneurons. qRT-PCR analysis of total RNA (A) as well as somatodendritic/axonal compartments (B) extracted from α-, β- and γ-actin knockdown and control cultured motoneurons. (A) ShActα transduction decreases total mRNA levels of α-actin by 90%, but does not alter expression of β- and γ-actin (** $p < 0.0037$ for $n = 5$). (B) As a compensatory response to α-actin depletion, mRNA levels of β-actin decrease in the somatodendritic compartment (* $p < 0.047$), but mRNA levels of both β- and γ-actin increase in the axonal compartment (* $p < 0.011$ for $n = 5$). Statistical analysis: one-tailed Mann-Whitney test. Data are shown as mean ± SEM.

Analysis of mRNA levels of α- and γ-actin in β-actin knockdown motoneurons revealed a 5.5-fold increase in total mRNA levels for α-actin and a 2.6-fold increase in total mRNA levels of γ-actin (Fig. 5.8.5 A). Similarly, mRNA levels of α- and γ-actin were elevated in axonal and somatodendritic compartments of β-actin knockdown motoneurons (Fig. 5.8.5 B). In γ-actin knockdown motoneurons, α-actin total mRNA levels were increased by 1.6-fold and β-actin total mRNA levels were increased by 2.6-fold (Fig. 5.8.6 A). In the axonal compartment of γ-actin knockdown motoneurons, mRNA levels of α-actin were increased by 2.5-fold, but

mRNA levels of β-actin were not altered (Fig. 5.8.6 B). These results indicate a compensatory upregulation of α- and γ-actin in response to β-actin depletion and a compensatory upregulation of α- and β-actin actin in response to γ-actin depletion.

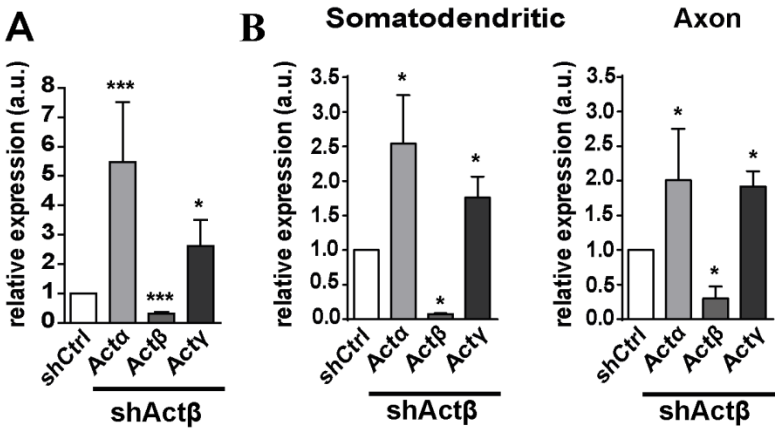

Figure 5.8.5 α- and γ-actin mRNA levels increase in soma and axons of motoneurons as a compensatory response to β-actin knockdown. qRT-PCR analysis of total RNA (A) and somatodendritic/axonal RNA fractions (B) of actin isoform-specific knockdown motoneurons. (A) ShActβ transduction decreases β-actin mRNA levels by 70% (*** $p < 0.0005$), but leads to a 5.5-fold upregulation of α-actin (*** $p < 0.0005$) and 2.6-fold upregulation of γ-actin total mRNA levels (* $p < 0.018$ for $n = 7$). (B) Transcript levels of α- and γ-actin increase in both somatodendritic (* $p < 0.028$) and axonal compartments after knockdown of β-actin (* $p < 0.014$ for $n = 4$). Statistical analysis: one-tailed Mann-Whitney test. Data are shown as mean ± SEM.

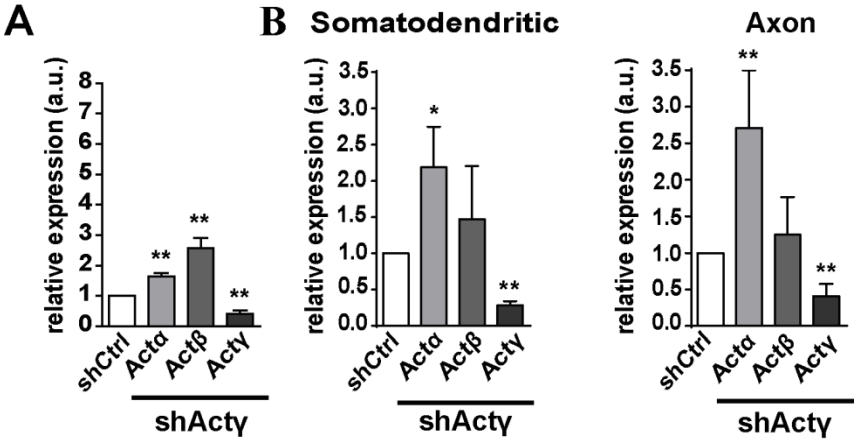

Figure 5.8.6 α- and β-actin mRNAs increase in soma and axons of γ-actin knockdown motoneurons. qRT-PCR analysis of total RNA (A) and somatodendritic/axonal RNA fractions (B) of cultured motoneurons after α-, β- or γ-actin depletion. (A) ShActγ application leads to 80% decrease in γ-actin mRNA levels (** $p < 0.001$), but

a 1.6-fold increase in α-actin and a 2.6-fold increase in β-actin mRNA levels (** $p < 0.0054$ for $n = 5$). (B) α-actin is upregulated in both somatodendritic (* $p < 0.046$) and axonal compartments (** $p < 0.002$ for $n = 5$) of γ-actin depleted motoneurons. Statistical analysis: one-tailed Mann-Whitney test. Data are shown as mean ± SEM.

At last, we assessed protein levels of α-, β- and γ-actin in lysates of cultured motoneurons after knockdown of these individual isoforms using isoform-specific antibodies (Fig. 5.8.7, A-C). Quantification of band intensities in blots showed a 2.5-fold increase in α-actin protein levels in lysates of β-actin knockdown motoneurons (Fig. 5.8.7 D). We also observed a significant increase in β-actin protein levels in lysates of γ-actin knockdown motoneurons (Fig. 5.8.7 E) as well as an increase in γ-actin protein levels in lysates obtained from β-actin depleted motoneurons (Fig. 5.8.7 F). Thus, these data confirm a compensatory upregulation of both mRNA and proteins of α-, β- and γ-actin in response to depletion of the other two isoforms in motoneurons.

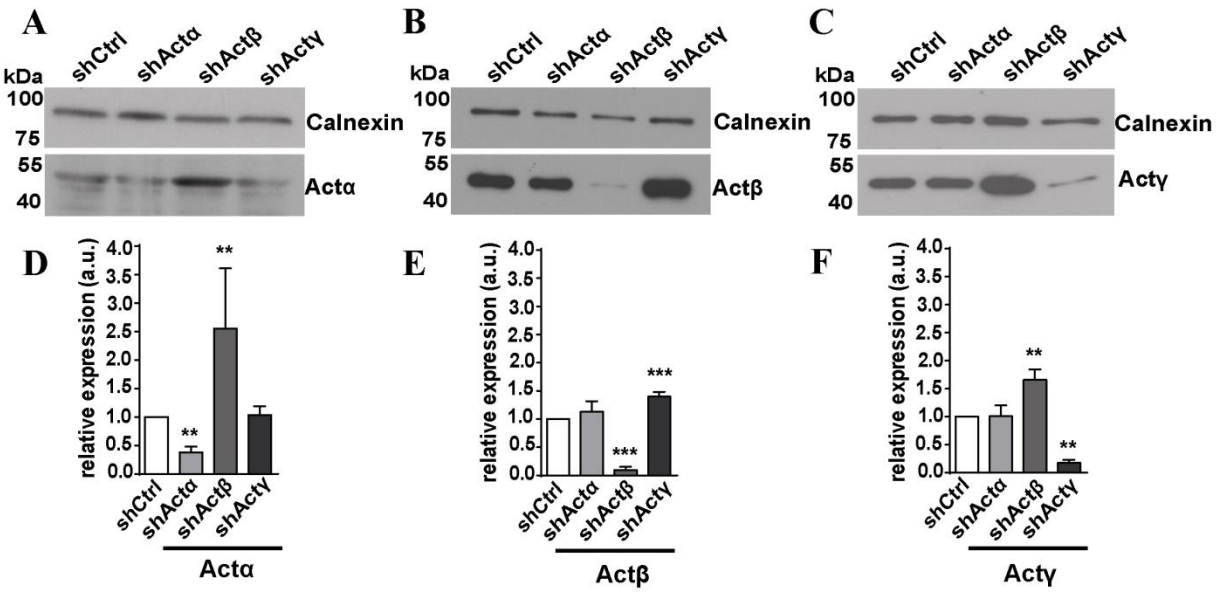

Figure 5.8.7 Compensatory upregulation of α- and γ-actin proteins as a response to β-actin depletion. Motoneurons were transduced with shActα, shActβ or shActγ. Lysates were probed with actin isoform-specific antibodies for Western blot analysis. (A-C) Representative blots labeled with α-actin (A), β-actin (B) and γ-actin (C) specific antibodies. (D) Quantification of blots labeled with α-actin antibody revealed a 2.5-fold upregulation

in α-actin in lysates of β-actin knockdown motoneurons (** $p < 0.004$ for $n = 4$). (E) Quantification of blots labeled with β-actin antibody showed a 1.5-fold upregulation of β-actin in protein lysates of γ-actin depleted motoneurons (*** $p < 0.0003$ for $n = 8$). (F) Quantification of blots labeled with γ-actin antibody showed a1.7-fold upregulation of γ-actin protein in lysates of β-actin knockdown motoneurons (** $p < 0.002$ for $n = 6$). Statistical analysis: one-tailed Mann-Whitney test. Data are shown as mean ± SEM.

5.9 Smn is involved in the regulation of axonal mRNA trafficking and translation of actin isoforms in motoneurons

Several previous studies have reported that, in motoneurons isolated from a severe SMA mouse model, β-actin mRNA and protein levels decrease in the distal axon and axonal growth cones which correlates with reduced axonal growth and spontaneous Ca^{+2} influx in these neurons (Jablonka et al., 2007; Rossoll et al., 2003). Furthermore, it has been reported that local translation of β-actin is disturbed in Smn-deficient motoneurons (Rathod et al., 2012) indicating that Smn plays a major role in mRNA trafficking and local translation of this isoform. Nevertheless, the potential role of Smn in axonal translocation and local translation of α- and γ-actin mRNAs has not been investigated yet. To address this question, we analyzed mRNA levels of these three actin isoforms in the somatodendritic and axonal compartment of Smn knockdown motoneurons (Fig. 5.9.1 A). qRT-PCR analysis showed that, upon Smn knockdown mRNA levels of α-, β- and γ-actin decrease in the axonal compartment (Fig. 5.9.1 C), but do not alter in the somatodendritic compartment (Fig. 5.9.1 B). Thus, Smn is required for the axonal trafficking of α-, β- and γ-actin mRNAs. Next, we asked whether Smn is involved in regulation of the local translation of these isoforms. We performed FRAP with motoneurons from embryonic SMA mice and found that the fluorescence recovery for α- and β-actin reporters is decreased in axonal growth cones of Smn-deficient motoneurons, indicating a role for Smn in local translation of these two isoforms (Fig. 5.9.2, A and B). We also observed a delayed recovery for γ-actin reporter but first at 48 min post bleach (Fig. 5.9.2

C). These findings suggest that impaired axonal growth observed in SMA motoneurons could be due to the depletion of α- and β-actin mRNAs from axons.

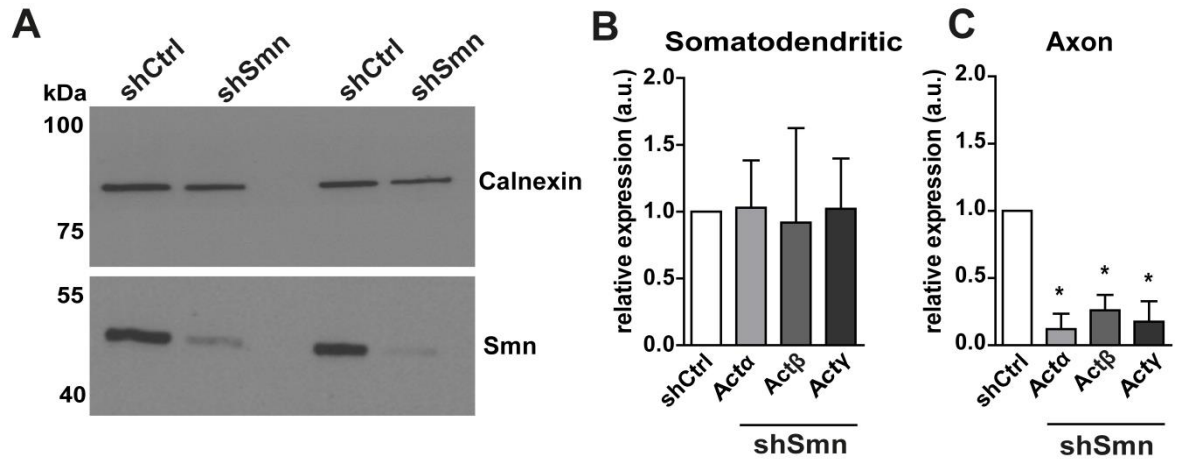

Figure 5.9.1 Smn is required for axonal translocation of α-, β- and γ-actin transcripts in motoneurons. (A) Smn was knocked down by lentiviral shRNA transduction. Western blot analysis showed a major reduction in Smn protein levels in lysates of Smn knockdown motoneurons (representative for n = 3 independent experiments). (B and C) qRT-PCR analysis of RNA fractions from somatodendritic (B) and axonal compartment (C) of Smn depleted motoneurons. mRNA levels of α-, β- and γ-actin are not altered in the somatodendritic compartment (B), but are significantly decreased in the axonal compartment of Smn knockdown motoneurons (* $p < 0.021$ for α-actin, * $p < 0.013$ for β- and γ-actin for $n = 4$). Statistical analysis: one-tailed Mann-Whitney test. Data are shown as mean ± SEM.

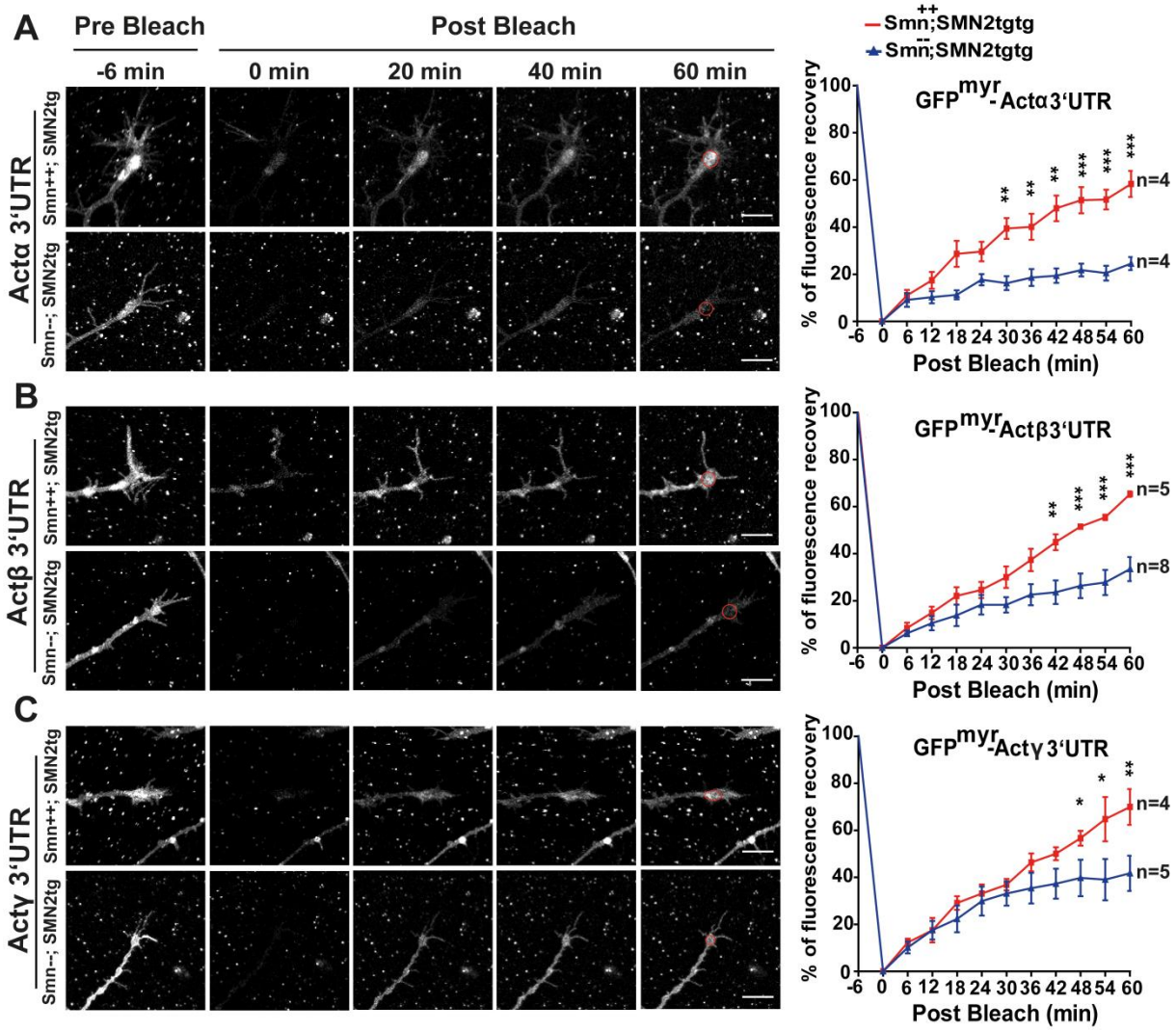

Figure 5.9.2 Smn is required for local translation of α-, β- and γ-actin reporters in axonal growth cones of motoneurons. (A-C) Left: representative pre- and post-bleach time lapse sequences of axonal growth cones of SMA and wild type motoneurons expressing α- (A), β- (B) and γ-actin reporters (C). (A) Right: Quantification of fluorescence recovery revealed a reduction in recovery of the α-actin reporter in *Smn*$^{-}$; *SMN2tgtg* motoneurons already at 30 min post bleach (** $p < 0.01$ and *** $p < 0.001$). (B) Right: The graph shows a significant reduction in fluorescence recovery of the β-actin reporter in *Smn*$^{-}$; *SMN2tgtg* motoneurons at 42 min post bleach (** $p < 0.01$ and *** $p < 0.001$). (C) Right: Fluorescence recovery of the γ-actin reporter is slightly reduced in *Smn*$^{-}$; *SMN2tgtg* motoneurons at 48 min post bleach (* $p < 0.05$ and ** $p < 0.01$). Statistical analysis: two way ANOVA with Bonferroni posthoc test. Shown are mean ± SEM. Scale bar: 10 µm.

6. Discussion

6.1 Protein and mRNAs for α-, β- and γ-actin isoforms are differentially distributed in axons of cultured motoneurons

In this study, we investigated the axonal mRNA translocation and local translation of the three actin isoforms; α-, β- and γ-actin in primary cultured motoneurons. High resolution *in situ* hybridization and qRT-PCR with compartmentalized cultures have revealed that the mRNAs for all three actin isoforms are sorted into axons. FRAP assays using isoform-specific $eGFP^{myr}$ reporters showed that transcripts for α-, β- and γ-actin become translated in specific regions within the axonal growth cones and axonal branch points. This indicates that intra-axonal synthesis of these isoforms plays an important role in axon growth and differentiation in developing motoneurons. These data also show that 3'UTRs of these isoforms harbor elements which are sufficient for RNA binding proteins to regulate their axonal translocation and local translation. mRNAs for α-, β- and γ-actin differ completely in their 3'UTR regions, but show about 90% homology in their coding regions. Due to these different 3'UTRs, subcellular transport and translation of these isoactin mRNAs are differentially regulated. Interestingly, we observed specific and different localization of α-, β- and γ-actin mRNAs within the axon of motoneurons. β-actin transcripts are highly abundant in the axonal growth cone. Conversely, mRNAs for α-actin are found at relatively low levels in the axonal growth cone, but they appear highly enriched in the axon and mRNAs for γ-actin are distributed uniformly in axons and axonal growth cones. Consistent with this, the rate of local translation of α-, β- and γ-actin mRNAs differs in the axonal growth cone and axonal branch points. α-actin transcripts have a higher translational rate in axonal branch points compared to β- and γ-actin mRNAs.

mRNA transport and localization of actin isoforms seem to be tissue specific and highly regulated. Studies in differentiating myoblasts have shown that α- and β-actin transcripts

become sorted into different cellular regions. β-actin mRNAs are sorted to the leading edge, while α-actin mRNAs are found predominantly in a perinuclear compartment (Kislauskis et al., 1993; Taneja and Singer, 1990). Previous studies with cultured cortical neurons have shown that β- and γ-actin transcripts differently localize in the soma and axons; β-actin mRNAs become translocated into axons and axonal growth cones, while γ-actin mRNAs are restricted to the soma (Bassell et al., 1998). However, using high sensitive methods, we were able to detect mRNAs for γ-actin in axons of cultured cortical neurons. In cultured sensory neurons, overexpression of a GFP construct containing the 3'UTR of β- or γ-actin results in axonal localization of GFP mRNA with β-actin 3'UTR, but not with γ-actin 3'UTR indicating that intra-axonal translation of only β-actin is involved in axon regeneration and plasticity in these neurons (Donnelly et al., 2011; Willis et al., 2007; Willis et al., 2011). However, in hippocampal neurons, in contrast to sensory neurons, γ-actin mRNAs become sorted into dendritic synapses, and mRNAs for both α-actin and γ-actin localize to neuropil layers of the hippocampus CA1 area (Cajigas et al., 2012; Schreiber et al., 2015). Thus, axonal mRNA localization of α- and γ-actin isoforms seems to be unique and special for spinal motoneurons. Likewise, proteins for α-, β- and γ-actin are highly similar and differ only at few amino acid residues within the N-terminus. Our immunocytochemistry data showed that despite these small sequence differences these proteins are sorted into different compartments within the motor axon. α-actin protein localizes predominately to axons and axonal branch points. β-actin protein is abundant in axonal growth cones and growth cone filopodia, and γ-actin protein is present both in the axonal filopodia and axonal growth cone filopodia. These differences in mRNA and protein distributions are indicative of specific cellular functions of these isoforms. Of note, α-actin transcript and protein are present only at low levels in the soma, but highly enriched in the axon suggesting a specific axonal function for this isoform in motoneurons.

This differential distribution of isoactin proteins has also been reported in other cell types. In fibroblast and endothelial cells, β-actin protein is found at the leading edge and in lamellae (Hoock et al., 1991). in cultured cerebrocortical neurons, β-actin protein localizes mainly at the growth cone and other highly motile structures, while γ-actin protein is distributed uniformly throughout the cell (Micheva et al., 1998).

6.2 α-, β- and γ-actin exert specific and overlapping functions in motoneurons

There are accumulative evidences about specific cellular functions of α-, β- and γ-actin isoforms. This hypothesis is based on four different observations:

1) Specific distribution of protein as well as mRNAs for these different isoforms refers to their unique cellular functions as discussed above.

2) Discriminative binding of actin regulatory proteins to some specific isoforms could also explain why different actin isoforms accomplish unique cellular functions. Actin binding proteins regulate the polymerization dynamics and stability of actin filaments. Several actin binding proteins have been reported to bind preferentially to a specific actin isoform. Cofilin/ADF is an actin severing protein which depolymerizes actin filaments. The cooperative binding of cofilin to β/γ-actin filaments is higher than to α-actin filaments (De La Cruz, 2005). Profilin is another actin regulating protein which binds to monomeric actin and promotes actin polymerization at the barbed end of filaments. Also profilin shows higher binding affinity to β/γ-actin monomers than to α-actin (Larsson and Lindberg, 1988). Similarly, Ezerin binds selectively to β-actin isoform and only poorly to α-actin (Yao et al., 1996).

3) Specific functions of actin isoforms might be due to differences in their chemical and physical properties which in turn influence their polymerization and depolymerization kinetics. For instance, phalloidin binding affinity is higher for β-actin than for α-actin (Nyman et al., 2002) and also viscoelasticity properties of these two isoforms differ completely. Based

on studies carried out by Bergeron et al, α-, β- and γ-actin isoforms show different polymerization kinetics (Bergeron et al., 2010). In the presence of Ca^{2+}, the nucleotide exchange rate of γ-actin monomers is slower than in β-actin monomers and their nucleation phase is prolonged. Moreover, the polymerization rate of γ-actin containing filaments is very slow. Likewise, α-actin monomers exhibit slow polymerization rate and generate highly stable filament. Conversely, the polymerization rate of β-actin containing filaments is very fast, but these filaments have a high turnover rate and thus, depolymerize rapidly. This indicates that β-actin makes highly dynamic filaments, whereas α- and γ-actin make more stable filaments.

Profilin and cofilin are two actin binding proteins that regulate polymerization dynamics and stability of F-actin filaments. Due to lower binding affinity of these two regulatory proteins to α-actin monomer/filaments compared to β-actin, filaments composed of α-actin show lower turnover rate and are hence more stable (De La Cruz, 2005; Larsson and Lindberg, 1988). Since, these three actin isoforms can copolymerize readily, the incorporation of α-actin or γ-actin into β-actin filaments stabilizes them and decreased the high turnover rate of such filaments (Bergeron et al., 2010). Our data provide supporting evidence for such different polymerization properties of these actin isoforms and thus, confirm previously reported observations; (i) First; we observed that after depletion of α- or γ-actin, the levels of β-actin protein increase in the G-actin pool and decrease in the F-actin pool. This altered G/F-actin ratio of β-actin upon α- or γ-actin depletions indicates that the polymerization rate and/or stability of filaments composed of β-actin depend on α- and γ-actin. In line with this, we showed that β-actin knockdown motoneurons grow shorter axon than α- or γ-actin knockdown motoneurons. This can be explained by the fact that α- and γ-actin slow down the turnover rate of β-actin filaments and hence stabilize the actin cytoskeleton. Therefore, increased protein levels of α- and γ-actin upon β-actin knockdown could disturb the balance between the dynamics and stability of the actin cytoskeleton in the motor axon and consequently decrease the axonal growth cone movement and in turn axonal elongation.

Disturbing the balance of actin cytoskeleton in hippocampal neurons has been reported to influence synaptic transmission and learning and memory. Upon depletion of E3 ubiquitin ligase TRIM3 in hippocampal neurons, the protein levels of γ-actin elevate in the dendrites. This in turn causes increased spine density and long-term potentiation, thereby enhancing short-term contextual fear memory acquisition (Schreiber et al., 2015). γ-actin mRNA co-localizes with TRIM3 protein in hippocampal dendrites, where TRIM3 regulates the synaptic protein levels of γ-actin via ubiquitin degradation. The increased spine size and consequently increased short-term memory observed in TRIM3 null mice can be explained by elevated levels of γ-actin in hippocampal synapses which in turn increases F-actin stability and thus alters the spine morphology.

(ii) Different studies have reported that the protrusion activity differs in the axonal growth cone and axon shaft. Compared to axonal growth cone filopodia which are highly dynamic, the filopodia along the axon shaft exhibit relatively low dynamics indicating that the F-actin polymerization rate differs in these two regions (Letourneau, 2009). Differences in actin polymerization rate in axonal growth cone filopodia and axonal filopodia have also been observed in sensory neurons. In these cells, treatment with NGF results in increased numbers of growth cone filopodia already after 5 min. In contrast, the number of axonal filopodia increases only after 30 min NGF treatment (Spillane et al., 2012). These differences can be mediated by actin isoforms which differently influence the polymerization dynamic of actin filaments in filopodia in these two compartments. Our data obtained from live cell imaging confirm this hypothesis. We observed that similar as in sensory neurons, the dynamics of axonal filopodia differ from axonal growth cone filopodia in motoneurons. In the axonal growth cone of motoneurons, filopodia dynamic movement is very high, but in the axon shaft we observed less dynamic movements of filopodia. Interestingly, we found that knockdown of α-, β- or γ-actin differentially affects filopodia dynamics in the axonal growth cone and axonal filopodia. Knockdown of α- or γ-actin completely diminished the dynamics of axonal

filopodia extension/retraction, while knockdown of β-actin only affected the dynamics of axonal growth cone filopodia. α-actin protein is highly abundant in the axonal branch points and the rate of its local translation is relatively high in this region. This could explain the mechanism by which α-actin modulates axonal filopodia dynamics; i.e. in actin patches, locally synthetized α-actin triggers actin nucleation leading to filament polymerization and thereby emerging of nascent filopodia from the axon shaft. Similarly, knockdown of γ-actin affects dynamics of axonal filopodia. Interestingly, we found a specific localization of this protein in the axonal filopodia suggesting that γ-actin regulates the stability and turnover rate of newly polymerized filaments inside the filopodia. Finally, knockdown of β-actin abolishes dynamic movements of axonal growth cones. Since β-actin protein is highly abundant in the axonal growth cone filopodia, it seems that this isoform contributes to polymerization of a highly dynamic actin cytoskeleton in the axonal growth cone.

Consistent with this differential regulation of F-actin dynamics/stability by α-, β- and γ-actin, knockdown of these individual isoforms differently influences the axon growth and development in primary motoneurons. Knockdown of α-actin diminishes formation of axonal filopodia and collateral branches, knockdown of β-actin impairs axonal growth and disturbs differentiation of axonal growth cones and knockdown of γ-actin also affects axon elongation. Thus, these three actin isoforms carry out different functions in axon growth and differentiation by spatial regulation of F-actin dynamic/stability in motoneurons. These findings are in line with previous studies that have reported a role for locally synthetized β-actin in growth cone turning in response to guidance cues in *Xenopus* retinal neurons (Leung et al., 2006). Also, in mature neurons, β-actin is required for synaptic plasticity and maintenance and its intra-axonal synthesis contributes to axon regeneration upon nerve injury (Micheva et al., 1998; Zheng et al., 2001).

Nevertheless, in primary sensory neurons, β-actin mRNA becomes translated at site of axonal branches together with other cytoskeletal proteins; i.e. subunits of Arp2/3 complex, WAVE1,

and the complex stabilizer cortactin (Spillane et al., 2012; Spillane et al., 2013) and furthermore siRNA-mediated knockdown of this isoform reduces the number of axonal collateral branches (Donnelly et al., 2013). These findings demonstrate a role for this isoform in axon arborization in sensory neurons. Thus, β-actin accomplishes specific functions in different neuronal cell types. In addition, a specific function of dendritically synthetized γ-actin has been proposed in hippocampal neurons in the context of synaptic plasticity, learning and memory (Schreiber et al., 2015). In these cells γ-actin regulates F-actin dynamics in the spines, thereby controlling synapse density and synaptic plasticity. There is no report about the potential function of α-actin in neuronal cells and this is the first study reporting a role for this isoform in axon growth and differentiation in neurons.

However, studies with adult rats after spinal cord lesion have provided primary indications for a potential role of α-actin in axon arborization and sprouting. Treatment of lesioned spinal cord with antibodies against myelin-associated growth inhibitory protein Nogo-A enhances the sprouting rate in the corticospinal tract (Bareyre et al., 2002; Blochlinger et al., 2001; Chen et al., 2000; Schwab, 2004; Z'Graggen et al., 1998). This sprouting seems to be a compensatory mechanism for axon regeneration because it correlates with upregulation of essential growth factors such as BDNF, GAP-43 and myosin, but interestingly also leads to an enormous increase in α-actin mRNA levels (Bareyre et al., 2002). Since, local protein synthesis is crucial for axon sprouting *in vivo* and *in vitro* (Buckmaster and Wen, 2011; McWhorter et al., 2003; Qiu et al., 2009), increased mRNA expression and enhanced local translation of α-actin might promote polymerization of highly stable actin filaments which in turn stabilize transiently formed sprouts and thus contribute to axon regeneration. These effects could add to the effects of Nogo-A on the local regulation of cofilin and Rho-GTPases for regulation of the actin cytoskeleton during branching in intact neuronal tissues (Montani et al., 2009; Zhou et al., 2003).

4) α-, β- and γ-actin knockout mouse models exhibit distinct phenotypes which are only partially rescued by the overexpression of the other two isoforms confirming non-redundant functions of these isoforms.

β-actin null knockout mice are not viable and die at E7 embryonal stages. In fibroblasts isolated from these mice, the G/F-actin ratio is altered and these cells display perturbations in growth, cell cycle and migration (Bunnell et al., 2011; Dugina et al., 2009). CNS conditional β-actin knockout mice are viable and show only restricted morphological and behavioral defects. These mice are hyperactive and exhibit impaired maternal behavior, poor cognitive performance and altered cerebellum and hippocampus morphology (Cheever et al., 2012). Motoneuron conditional β-actin knockout mice are also viable and exhibit intact NMJ morphology and synaptic as well as motor functions (Cheever et al., 2011).

Ablation of skeletal α-actin in the mouse also causes lethality at early postnatal stages. These α-actin knockout mice show defects in growth and heart function and display pronounced muscle weakness (Crawford et al., 2002; Schildmeyer et al., 2000). In humans, point mutations in skeletal α-actin gene are the cause of congenital nemaline myopathy which is characterized by muscle weakness and hypotonia (Nowak et al., 1999; Ohlsson et al., 2004; Wallgren-Pettersson et al., 2004). In contrast to α- and β-actin null mice, γ-actin null mice are viable but display reduced adult survival. These knockout mice do not show any morphological perturbations, but exhibit progressive hearing loss, growth delay during embryonic and postnatal periods, muscle necrosis and myopathy (Belyantseva et al., 2009; Sonnemann et al., 2006). Moreover, cell survival is reduced in fibroblasts isolated from these knockout mice and cell growth and migration are disturbed (Bunnell and Ervasti, 2010; Dugina et al., 2009). Hippocampus-specific knockout of γ-actin leads to enhanced short-term contextual fear memory consolidation suggesting a role for this isoform in synaptic plasticity and learning and memory (Schreiber et al., 2015). These unique phenotypes caused by depletion of a particular actin isoform provide strong evidence for specific cellular functions

and indicate that some of these isoforms cannot functionally substitute other isoforms. Our data also demonstrate that depletion of α-, β- or γ-actin causes distinct phenotypes in cultured motoneurons which cannot be fully compensated by other two isoforms *in vitro*.

6.3 Compensatory response triggered by α-, β- or γ-actin ablation

Interestingly, in all these knockout mouse models a compensatory upregulation of the remaining actin isoforms has been reported suggesting that these isoforms could also have redundant functions. In β-actin depleted fibroblasts the observed migration defects can be rescued by inhibiting the ROCK signaling pathway which leads to a compensatory upregulation of α- and γ-actin isoforms (Tondeleir et al., 2012). In β-actin null knockout mice both α-actin and γ-actin isoforms become upregulated (Bunnell et al., 2011; Cheever et al., 2012; Tondeleir et al., 2012). Also, in CNS-specific β-actin knockout mice, a compensatory upregulation of α- and γ-actin has been demonstrated in the brain (Cheever et al., 2012).

Similarly, in fibroblasts isolated from γ-actin null mice, increased expression of both α- and β-actin have been reported. In hippocampus-specific γ-actin knockout mice increased expression of β-actin has been shown (Belyantseva et al., 2009; Bunnell and Ervasti, 2010; Dugina et al., 2009; Schreiber et al., 2015).

This compensatory response has also been reported for the depletion of different α-actin isoforms. Knockout mouse models of cardiac α-actin show increased levels of skeletal muscle α-actin (Kumar et al., 2004). In knockout mouse models of skeletal muscle α-actin, the protein levels of both vascular and cardiac α-actin isoforms increase (Crawford et al., 2002). In knockout mouse models of smooth muscle α-actin the expression of skeletal muscle α-actin increases as a compensatory response (Schildmeyer et al., 2000). Of note, the overexpression of cardiac α-actin rescues the lethality in skeletal muscle α-actin null mice and improves the heart defects and muscle performance (Nowak et al., 2009). However, in cardiac α-actin null mice, the overexpression of smooth muscle γ-actin only partially rescues the defective heart

phenotype (Kumar et al., 1997). Likewise, transgenic mice overexpressing γ-actin in skeletal muscle α-actin null mice die during early postnatal stages indicating that γ-actin cannot rescue the lethality caused by ablation of skeletal muscle α-actin (Jaeger et al., 2009). However, it was not clear whether ablation of one actin isoform could also induce such compensatory response in spinal motoneurons. We investigated this in cultured spinal motoneurons by applying isoform-specific shRNAs to suppress respective mRNAs for α-, β- or γ-actin. Intriguingly, we found that both protein and mRNA levels of α-actin and γ-actin remarkably increase after knockdown of β-actin from cultured motoneurons. Similarly, we observed a compensatory upregulation in protein and mRNA levels of β-actin after depletion of γ-actin, but only an upregulation in mRNA but not protein levels of α-actin in these motoneurons. In contrast, depletion of α-actin did not lead to an increment in total protein or mRNA levels of β- or γ-actin. However, surprisingly, we observed an axon specific compensatory response, as mRNA levels for both β- and γ-actin significantly increased in the axonal compartment of α-actin depleted motoneurons. Thus, these data put emphasis for an axon specific function of locally synthesized α-actin.

Investigation of the total actin levels and G/F-actin ratio revealed that the total actin levels remain maintained in motoneurons upon specific knockdown of α-, β- or γ-actin. Depletion of these individual isoforms also did not alter G/F-actin ratio. Consistent with this, the total F-actin levels in the soma remained unaltered indicating that actin isoforms could act redundantly in the soma and preserve the F-actin polymerization capacity in this compartment. Nevertheless, F-actin levels were remarkably decreased in the axon after knockdown of either α-actin or γ-actin indicating a specific function for these two isoforms in F-actin polymerization in this compartment. Thus, these data could explain why motoneuron specific β-actin knockout mice described previously are viable and do not show any abnormalities (Cheever et al., 2011). A complex compensatory response provided by α- and γ-actin accounts for preserved synaptic transmission and motor functions *in vivo*.

6.4 Mechanisms of the compensatory response

It remains open how neurons sense axonal cytoskeletal alterations to signal to the nucleus in order to upregulate expression of other genes in a compensatory manner. Such functions have been shown in the context of regulation of the microtubule cytoskeleton which can be modulated both by local actions of STAT3 (Selvaraj et al., 2012) but also by local synthesis of STAT3 after nerve lesion, which leads to a retrograde response in the nucleus for upregulation of transcripts necessary for nerve regeneration (Ben-Yaakov et al., 2012; Rishal and Fainzilber, 2014). It is also possible that such effects are mediated by a nuclear function of actin in regulation of transcription (Olson and Nordheim, 2010; Visa and Percipalle, 2010; Zheng et al., 2009). In the nucleus, β-actin is part of a transcriptional pre-initiation complex which contains RNA polymerase II and is involved in transcriptional regulation of genes implicated in cell growth, differentiation and signal transduction (Xu et al. 2010; Hofmann et al. 2004). Moreover, co-immunoprecipitation assays have provided evidence for a direct interaction of actin with RNA polymerases I and III (Fomproix and Percipalle 2004; Hofmann et al. 2004; Hu et al. 2004) and chromatin remodeling and histone acetyltransferase (HAT) complexes (Obrdlik et al. 2008; Farrants 2008; Blessing et al. 2004). In a complex with ribonucleoproteins, actin associates to nascent transcripts and facilitates transcription elongation through recruiting transcriptional coactivators (Kukalev et al. 2005; Percipalle et al. 2003; Sjolinder et al. 2005; Obrdlik et al. 2008). Yet, it remains speculative how depletion of a single actin isoform elicits a signaling pathway giving cells feedback how to about reprogram the expression of other actin genes. The transcriptional cofactors myocardin and MAL act downstream of the transcription factor serum response factor (SRF) that is involved in transcription regulation of actin isoforms and actin regulators (Wang et al. 2001; Miano et al. 2007; Wang et al. 2003). Several lines of evidence have demonstrated that monomeric α-, β- and γ-actin directly bind to MAL or myocardin and hence suppress their transcriptional activity (Olson and Nordheim 2010; Posern and Treisman 2006; Miralles et al. 2003;

Kuwahara et al. 2005). Reduced total actin levels releases G-actin from SRF cofactors and favor their nuclear translocation. Myocardin and MAL in turn activate SRF which results in transcription of its target genes including different isoforms of α-actin (Posern and Treisman 2006; Takano et al. 1998; Wei et al. 1998).

6.5 Mislocalization of α-, β- and γ-actin mRNAs in neurodegenerative diseases

SMA and ALS are two forms of degenerative motoneuron diseases that are both associated with disturbed RNA metabolism and processing. Though SMN is ubiquitously expressed in all cell types, only spinal motoneurons undergo cell death in SMA patients. Two hypotheses are proposed to explain the mechanism of motoneuron cell death in SMA:

(i) Since SMN plays a role in snRNP assembly involved in pre-mRNA splicing, reduced levels of this protein might disrupt the splicing of important genes involved in motoneuron function and survival (Burghes and Beattie, 2009).

(ii) Alternatively, SMN is required for the assembly of mRNP complexes and thus plays a role in axonal transport, stability and local translation of certain transcripts (Fallini et al., 2012b). Smn interaction with hnRNP R/Q is required for β-actin mRNA transport in motor axons (Rossoll et al., 2003). Smn interaction with HuD is implicated in mRNA transport of cpg15 into axons (Akten et al., 2011), and its interaction with FMRP is essential for dendritic transport of target mRNAs implicated in synaptic function and maintenance (Piazzon et al., 2008).

Studies in mouse models of the severe form of SMA have provided evidence for a second hypothesis. In cultured motoneurons from type I SMA mice, aberrant axon elongation and defective clustering of voltage-gated Ca^{2+} channels in the growth cone are observed (Ning et al., 2010; Rossoll et al., 2003). Also, in zebrafish and *Xenopus* knockdown of Smn impairs axonal branching and path finding (McWhorter et al., 2003; Winkler et al., 2005). *In vivo* studies with *Smn* knockout mice have shown that, NMJs are morphologically altered,

neurotransmitter release is disturbed and severe neuromuscular denervation is observed (Jablonka et al., 2007; Kariya et al., 2008; Kong et al., 2009; Ling et al., 2012). Therefore, SMN ablation might affect NMJ maturation more than motoneuron survival.

In contrast to type I SMA mice, mouse models of mild SMA (type III SMA) show an enhanced axonal branching (Cifuentes-Diaz et al., 2002; Murray et al., 2008; Simon et al., 2010). Interestingly, this enhanced sprouting has also been reported in mild SMA patients, but not in severe SMA patients (Crawford and Pardo, 1996; Simon et al., 2010). This compensatory sprouting allows the remaining intact motor axons to reinnervate the denervated muscles, thereby providing a mechanism to improve the synaptic transmission and rescue the muscle weakness in type III SMA mice and in SMA patients. Thus, inducing axonal sprouting would be an important therapeutic strategy for retrieval of the synaptic innervation and motor function in severe SMA patients (Bosch-Marce et al., 2011). Interestingly, our data show that the localization of α-, β- and γ-actin mRNAs is disturbed in axons of Smn knockdown motoneurons. Moreover, local translation of these mRNAs is delayed in motoneurons isolated from type I SMA mice. We have provided evidence about specific function of α-actin in axonal branching and specific function of β-actin in axon elongation and axonal growth cone differentiation. Therefore, lack of sprouting and impaired synaptic transmission observed in SMA mouse models and patients might correlate with mislocalization of α- and β-actin mRNAs in the axon and thus could explain motoneuron vulnerability in SMA patients.

Altered mRNA translocation and local translation have been also reported in iPS cell-derived motoneurons from ALS patients and in primary cortical neurons after introducing ALS *TDP-43* mutations. The axonal transport of TDP-43 granules containing Nefl mRNAs is disturbed in these cells (Alami et al., 2014).

New studies have shown that γ-actin becomes upregulated in peripheral blood lymphocytes of sporadic ALS patients (Baciu et al., 2012). γ-actin filaments are more stable than β-actin

filaments and have a lower turnover rate (Bergeron et al., 2010). Therefore, upregulation of γ-actin in motoneurons of ALS patients might contribute to a more stable actin cytoskeleton in the axon which in turn could attenuate the axon degeneration and support the axon maintenance.

Taken together, our data provide evidence for specific functions of different actin isoforms in motoneuron growth and differentiation. We demonstrate that α-actin regulates formation of axonal collateral branches in developing motoneurons. β-actin contributes to maturation of the axonal growth cone as well as axon elongation, and γ-actin modulates axonal growth.

The mechanism of such specific cellular functions could be explained by different polymerization kinetics of these isoforms. The differential distribution of the transcripts and proteins for α-, β- and γ-actin isoforms in particular regions within motor axons contributes to spatial regulation of the actin filament dynamic and stability in these regions. Incorporation of α- and γ-actin into F-actin stabilizes these filaments in the axonal filopodia, thereby promoting collateral branching. Incorporation of β-actin into F-actin on the contrary contributes to a highly dynamic cytoskeleton in the axon and axonal growth cones thereby promoting axon elongation and guidance. Our data also suggest that mechanism of SMA pathogenesis might involve disturbed axonal translocation and local translation of α-, β- and γ-actin isoforms in motoneurons and thus provide new targets for potential therapeutic strategies for treatment of SMA patients.

7. References

Adeli, K. 2011. Translational control mechanisms in metabolic regulation: critical role of RNA binding proteins, microRNAs, and cytoplasmic RNA granules. *American journal of physiology. Endocrinology and metabolism*. 301:E1051-1064.

Ainger, K., D. Avossa, F. Morgan, S.J. Hill, C. Barry, E. Barbarese, and J.H. Carson. 1993. Transport and localization of exogenous myelin basic protein mRNA microinjected into oligodendrocytes. *The Journal of cell biology*. 123:431-441.

Akten, B., M.J. Kye, T. Hao le, M.H. Wertz, S. Singh, D. Nie, J. Huang, T.T. Merianda, J.L. Twiss, C.E. Beattie, J.A. Steen, and M. Sahin. 2011. Interaction of survival of motor neuron (SMN) and HuD proteins with mRNA cpg15 rescues motor neuron axonal deficits. *Proc Natl Acad Sci U S A*. 108:10337-10342.

Alami, N.H., R.B. Smith, M.A. Carrasco, L.A. Williams, C.S. Winborn, S.S. Han, E. Kiskinis, B. Winborn, B.D. Freibaum, A. Kanagaraj, A.J. Clare, N.M. Badders, B. Bilican, E. Chaum, S. Chandran, C.E. Shaw, K.C. Eggan, T. Maniatis, and J.P. Taylor. 2014. Axonal transport of TDP-43 mRNA granules is impaired by ALS-causing mutations. *Neuron*. 81:536-543.

Andersen, P.M., and A. Al-Chalabi. 2011. Clinical genetics of amyotrophic lateral sclerosis: what do we really know? *Nature reviews. Neurology*. 7:603-615.

Anderson, P., and N. Kedersha. 2006. RNA granules. *The Journal of cell biology*. 172:803-808.

Anjum, R., and J. Blenis. 2008. The RSK family of kinases: emerging roles in cellular signalling. *Nature reviews. Molecular cell biology*. 9:747-758.

Aschrafi, A., A.D. Schwechter, M.G. Mameza, O. Natera-Naranjo, A.E. Gioio, and B.B. Kaplan. 2008. MicroRNA-338 regulates local cytochrome c oxidase IV mRNA levels and oxidative phosphorylation in the axons of sympathetic neurons. *The Journal of neuroscience : the official journal of the Society for Neuroscience*. 28:12581-12590.

Auinger, S., and J.V. Small. 2008. Correlated light and electron microscopy of the cytoskeleton. *Methods in cell biology*. 88:257-272.

Baciu, C., K.J. Thompson, J.L. Mougeot, B.R. Brooks, and J.W. Weller. 2012. The LO-BaFL method and ALS microarray expression analysis. *BMC bioinformatics*. 13:244.

Bareyre, F.M., B. Haudenschild, and M.E. Schwab. 2002. Long-lasting sprouting and gene expression changes induced by the monoclonal antibody IN-1 in the adult spinal cord. *The Journal of neuroscience : the official journal of the Society for Neuroscience*. 22:7097-7110.

Bassell, G.J., and S. Kelic. 2004. Binding proteins for mRNA localization and local translation, and their dysfunction in genetic neurological disease. *Current opinion in neurobiology*. 14:574-581.

Bassell, G.J., H. Zhang, A.L. Byrd, A.M. Femino, R.H. Singer, K.L. Taneja, L.M. Lifshitz, I.M. Herman, and K.S. Kosik. 1998. Sorting of beta-actin mRNA and protein to neurites and growth cones in culture. *The Journal of neuroscience : the official journal of the Society for Neuroscience*. 18:251-265.

Beal, M.F. 2000. Mitochondria and the pathogenesis of ALS. *Brain : a journal of neurology*. 123 (Pt 7):1291-1292.

Belyantseva, I.A., B.J. Perrin, K.J. Sonnemann, M. Zhu, R. Stepanyan, J. McGee, G.I. Frolenkov, E.J. Walsh, K.H. Friderici, T.B. Friedman, and J.M. Ervasti. 2009. Gamma-actin is required for cytoskeletal maintenance but not development. *Proceedings of the National Academy of Sciences of the United States of America*. 106:9703-9708.

Ben-Yaakov, K., S.Y. Dagan, Y. Segal-Ruder, O. Shalem, D. Vuppalanchi, D.E. Willis, D. Yudin, I. Rishal, F. Rother, M. Bader, A. Blesch, Y. Pilpel, J.L. Twiss, and M. Fainzilber. 2012. Axonal transcription factors signal retrogradely in lesioned peripheral nerve. *The EMBO journal*. 31:1350-1363.

Bergeron, S.E., M. Zhu, S.M. Thiem, K.H. Friderici, and P.A. Rubenstein. 2010. Ion-dependent polymerization differences between mammalian beta- and gamma-nonmuscle actin isoforms. *J Biol Chem*. 285:16087-16095.

Blochlinger, S., O. Weinmann, M.E. Schwab, and M. Thallmair. 2001. Neuronal plasticity and formation of new synaptic contacts follow pyramidal lesions and neutralization of Nogo-A: a light and electron microscopic study in the pontine nuclei of adult rats. *The Journal of comparative neurology*. 433:426-436.

Bosch-Marce, M., C.D. Wee, T.L. Martinez, C.E. Lipkes, D.W. Choe, L. Kong, J.P. Van Meerbeke, A. Musaro, and C.J. Sumner. 2011. Increased IGF-1 in muscle modulates the phenotype of severe SMA mice. *Human molecular genetics*. 20:1844-1853.

Bradke, F., and C.G. Dotti. 1997. Neuronal polarity: vectorial cytoplasmic flow precedes axon formation. *Neuron*. 19:1175-1186.

Buckmaster, P.S., and X. Wen. 2011. Rapamycin suppresses axon sprouting by somatostatin interneurons in a mouse model of temporal lobe epilepsy. *Epilepsia*. 52:2057-2064.

Bunnell, T.M., B.J. Burbach, Y. Shimizu, and J.M. Ervasti. 2011. beta-Actin specifically controls cell growth, migration, and the G-actin pool. *Molecular biology of the cell*. 22:4047-4058.

Bunnell, T.M., and J.M. Ervasti. 2010. Delayed embryonic development and impaired cell growth and survival in Actg1 null mice. *Cytoskeleton (Hoboken)*. 67:564-572.

Burghes, A.H., and C.E. Beattie. 2009. Spinal muscular atrophy: why do low levels of survival motor neuron protein make motor neurons sick? *Nature reviews. Neuroscience*. 10:597-609.

Buxbaum, A.R., G. Haimovich, and R.H. Singer. 2015. In the right place at the right time: visualizing and understanding mRNA localization. *Nature reviews. Molecular cell biology*. 16:95-109.

Cajigas, I.J., G. Tushev, T.J. Will, S. tom Dieck, N. Fuerst, and E.M. Schuman. 2012. The local transcriptome in the synaptic neuropil revealed by deep sequencing and high-resolution imaging. *Neuron*. 74:453-466.

Campbell, D.S., and C.E. Holt. 2001. Chemotropic responses of retinal growth cones mediated by rapid local protein synthesis and degradation. *Neuron*. 32:1013-1026.

Cartegni, L., S.L. Chew, and A.R. Krainer. 2002. Listening to silence and understanding nonsense: exonic mutations that affect splicing. *Nat Rev Genet*. 3:285-298.

Cheever, T.R., B. Li, and J.M. Ervasti. 2012. Restricted morphological and behavioral abnormalities following ablation of beta-actin in the brain. *PloS one*. 7:e32970.

Cheever, T.R., E.A. Olson, and J.M. Ervasti. 2011. Axonal regeneration and neuronal function are preserved in motor neurons lacking ss-actin in vivo. *PloS one*. 6:e17768.

Chen, M.S., A.B. Huber, M.E. van der Haar, M. Frank, L. Schnell, A.A. Spillmann, F. Christ, and M.E. Schwab. 2000. Nogo-A is a myelin-associated neurite outgrowth inhibitor and an antigen for monoclonal antibody IN-1. *Nature*. 403:434-439.

Chia, P.H., B. Chen, P. Li, M.K. Rosen, and K. Shen. 2014. Local F-actin network links synapse formation and axon branching. *Cell*. 156:208-220.

Chia, P.H., M.R. Patel, and K. Shen. 2012. NAB-1 instructs synapse assembly by linking adhesion molecules and F-actin to active zone proteins. *Nature neuroscience*. 15:234-242.

Cifuentes-Diaz, C., S. Nicole, M.E. Velasco, C. Borra-Cebrian, C. Panozzo, T. Frugier, G. Millet, N. Roblot, V. Joshi, and J. Melki. 2002. Neurofilament accumulation at the motor endplate and lack of axonal sprouting in a spinal muscular atrophy mouse model. *Human molecular genetics*. 11:1439-1447.

Cox, L.J., U. Hengst, N.G. Gurskaya, K.A. Lukyanov, and S.R. Jaffrey. 2008. Intra-axonal translation and retrograde trafficking of CREB promotes neuronal survival. *Nature cell biology*. 10:149-159.

Crawford, K., R. Flick, L. Close, D. Shelly, R. Paul, K. Bove, A. Kumar, and J. Lessard. 2002. Mice lacking skeletal muscle actin show reduced muscle strength and growth deficits and die during the neonatal period. *Molecular and cellular biology*. 22:5887-5896.

Crawford, T.O., and C.A. Pardo. 1996. The neurobiology of childhood spinal muscular atrophy. *Neurobiology of disease*. 3:97-110.

De La Cruz, E.M. 2005. Cofilin binding to muscle and non-muscle actin filaments: isoform-dependent cooperative interactions. *J Mol Biol*. 346:557-564.

DeJesus-Hernandez, M., I.R. Mackenzie, B.F. Boeve, A.L. Boxer, M. Baker, N.J. Rutherford, A.M. Nicholson, N.A. Finch, H. Flynn, J. Adamson, N. Kouri, A. Wojtas, P. Sengdy, G.Y. Hsiung, A.

Karydas, W.W. Seeley, K.A. Josephs, G. Coppola, D.H. Geschwind, Z.K. Wszolek, H. Feldman, D.S. Knopman, R.C. Petersen, B.L. Miller, D.W. Dickson, K.B. Boylan, N.R. Graff-Radford, and R. Rademakers. 2011. Expanded GGGGCC hexanucleotide repeat in noncoding region of C9ORF72 causes chromosome 9p-linked FTD and ALS. *Neuron*. 72:245-256.

Dent, E.W., S.L. Gupton, and F.B. Gertler. 2011. The growth cone cytoskeleton in axon outgrowth and guidance. *Cold Spring Harb Perspect Biol*. 3.

Dent, E.W., and K. Kalil. 2001. Axon branching requires interactions between dynamic microtubules and actin filaments. *The Journal of neuroscience : the official journal of the Society for Neuroscience*. 21:9757-9769.

Donnelly, C.J., M. Park, M. Spillane, S. Yoo, A. Pacheco, C. Gomes, D. Vuppalanchi, M. McDonald, H.H. Kim, T.T. Merianda, G. Gallo, and J.L. Twiss. 2013. Axonally synthesized beta-actin and GAP-43 proteins support distinct modes of axonal growth. *J Neurosci*. 33:3311-3322.

Donnelly, C.J., D.E. Willis, M. Xu, C. Tep, C. Jiang, S. Yoo, N.C. Schanen, C.B. Kirn-Safran, J. van Minnen, A. English, S.O. Yoon, G.J. Bassell, and J.L. Twiss. 2011. Limited availability of ZBP1 restricts axonal mRNA localization and nerve regeneration capacity. *The EMBO journal*. 30:4665-4677.

Dugina, V., I. Zwaenepoel, G. Gabbiani, S. Clement, and C. Chaponnier. 2009. Beta and gamma-cytoplasmic actins display distinct distribution and functional diversity. *Journal of cell science*. 122:2980-2988.

Dull, T., R. Zufferey, M. Kelly, R.J. Mandel, M. Nguyen, D. Trono, and L. Naldini. 1998. A third-generation lentivirus vector with a conditional packaging system. *Journal of virology*. 72:8463-8471.

Durand, G.M., N. Marandi, S.D. Herberger, R. Blum, and A. Konnerth. 2006. Quantitative single-cell RT-PCR and Ca2+ imaging in brain slices. *Pflugers Archiv : European journal of physiology*. 451:716-726.

Eom, T., L.N. Antar, R.H. Singer, and G.J. Bassell. 2003. Localization of a beta-actin messenger ribonucleoprotein complex with zipcode-binding protein modulates the density of dendritic filopodia and filopodial synapses. *The Journal of neuroscience : the official journal of the Society for Neuroscience*. 23:10433-10444.

Fallini, C., G.J. Bassell, and W. Rossoll. 2012a. The ALS disease protein TDP-43 is actively transported in motor neuron axons and regulates axon outgrowth. *Human molecular genetics*. 21:3703-3718.

Fallini, C., G.J. Bassell, and W. Rossoll. 2012b. Spinal muscular atrophy: the role of SMN in axonal mRNA regulation. *Brain research*. 1462:81-92.

Fallini, C., H. Zhang, Y. Su, V. Silani, R.H. Singer, W. Rossoll, and G.J. Bassell. 2011. The survival of motor neuron (SMN) protein interacts with the mRNA-binding protein HuD and regulates localization of poly(A) mRNA in primary motor neuron axons. *J Neurosci*. 31:3914-3925.

Fan, J., S.G. Mansfield, T. Redmond, P.R. Gordon-Weeks, and J.A. Raper. 1993. The organization of F-actin and microtubules in growth cones exposed to a brain-derived collapsing factor. *The Journal of cell biology*. 121:867-878.

Gallo, G. 2011. The cytoskeletal and signaling mechanisms of axon collateral branching. *Dev Neurobiol*. 71:201-220.

Geraldo, S., and P.R. Gordon-Weeks. 2009. Cytoskeletal dynamics in growth-cone steering. *J Cell Sci*. 122:3595-3604.

Gioio, A.E., M. Eyman, H. Zhang, Z.S. Lavina, A. Giuditta, and B.B. Kaplan. 2001. Local synthesis of nuclear-encoded mitochondrial proteins in the presynaptic nerve terminal. *Journal of neuroscience research*. 64:447-453.

Glinka, M., T. Herrmann, N. Funk, S. Havlicek, W. Rossoll, C. Winkler, and M. Sendtner. 2010. The heterogeneous nuclear ribonucleoprotein-R is necessary for axonal beta-actin mRNA translocation in spinal motor neurons. *Human molecular genetics*. 19:1951-1966.

Groen, E.J., K. Fumoto, A.M. Blokhuis, J. Engelen-Lee, Y. Zhou, D.M. van den Heuvel, M. Koppers, F. van Diggelen, J. van Heest, J.A. Demmers, J. Kirby, P.J. Shaw, E. Aronica, W.G. Spliet, J.H.

Veldink, L.H. van den Berg, and R.J. Pasterkamp. 2013. ALS-associated mutations in FUS disrupt the axonal distribution and function of SMN. *Human molecular genetics*. 22:3690-3704.

Gumy, L.F., C.L. Tan, and J.W. Fawcett. 2010. The role of local protein synthesis and degradation in axon regeneration. *Experimental neurology*. 223:28-37.

Harris, W.A., C.E. Holt, and F. Bonhoeffer. 1987. Retinal axons with and without their somata, growing to and arborizing in the tectum of Xenopus embryos: a time-lapse video study of single fibres in vivo. *Development*. 101:123-133.

Hay, N., and N. Sonenberg. 2004. Upstream and downstream of mTOR. *Genes & development*. 18:1926-1945.

Hengst, U., A. Deglincerti, H.J. Kim, N.L. Jeon, and S.R. Jaffrey. 2009. Axonal elongation triggered by stimulus-induced local translation of a polarity complex protein. *Nature cell biology*. 11:1024-1030.

Hillefors, M., A.E. Gioio, M.G. Mameza, and B.B. Kaplan. 2007. Axon viability and mitochondrial function are dependent on local protein synthesis in sympathetic neurons. *Cellular and molecular neurobiology*. 27:701-716.

Honda, D., S. Ishigaki, Y. Iguchi, Y. Fujioka, T. Udagawa, A. Masuda, K. Ohno, M. Katsuno, and G. Sobue. 2013. The ALS/FTLD-related RNA-binding proteins TDP-43 and FUS have common downstream RNA targets in cortical neurons. *FEBS open bio*. 4:1-10.

Hoock, T.C., P.M. Newcomb, and I.M. Herman. 1991. Beta actin and its mRNA are localized at the plasma membrane and the regions of moving cytoplasm during the cellular response to injury. *The Journal of cell biology*. 112:653-664.

Hsieh-Li, H.M., J.G. Chang, Y.J. Jong, M.H. Wu, N.M. Wang, C.H. Tsai, and H. Li. 2000. A mouse model for spinal muscular atrophy. *Nat Genet*. 24:66-70.

Hubers, L., H. Valderrama-Carvajal, J. Laframboise, J. Timbers, G. Sanchez, and J. Cote. 2011. HuD interacts with survival motor neuron protein and can rescue spinal muscular atrophy-like neuronal defects. *Hum Mol Genet*. 20:553-579.

Jablonka, S., M. Beck, B.D. Lechner, C. Mayer, and M. Sendtner. 2007. Defective Ca2+ channel clustering in axon terminals disturbs excitability in motoneurons in spinal muscular atrophy. *J Cell Biol*. 179:139-149.

Jablonka, S., S. Wiese, and M. Sendtner. 2004. Axonal defects in mouse models of motoneuron disease. *Journal of neurobiology*. 58:272-286.

Jaeger, M.A., K.J. Sonnemann, D.P. Fitzsimons, K.W. Prins, and J.M. Ervasti. 2009. Context-dependent functional substitution of alpha-skeletal actin by gamma-cytoplasmic actin. *FASEB journal : official publication of the Federation of American Societies for Experimental Biology*. 23:2205-2214.

Kalil, K., and E.W. Dent. 2014. Branch management: mechanisms of axon branching in the developing vertebrate CNS. *Nature reviews. Neuroscience*. 15:7-18.

Kariya, S., G.H. Park, Y. Maeno-Hikichi, O. Leykekhman, C. Lutz, M.S. Arkovitz, L.T. Landmesser, and U.R. Monani. 2008. Reduced SMN protein impairs maturation of the neuromuscular junctions in mouse models of spinal muscular atrophy. *Human molecular genetics*. 17:2552-2569.

Ketschek, A., and G. Gallo. 2010. Nerve growth factor induces axonal filopodia through localized microdomains of phosphoinositide 3-kinase activity that drive the formation of cytoskeletal precursors to filopodia. *The Journal of neuroscience : the official journal of the Society for Neuroscience*. 30:12185-12197.

Kiebler, M.A., and G.J. Bassell. 2006. Neuronal RNA granules: movers and makers. *Neuron*. 51:685-690.

Kim, S., and K.C. Martin. 2015. Neuron-wide RNA transport combines with netrin-mediated local translation to spatially regulate the synaptic proteome. *eLife*. 4.

Kislauskis, E.H., Z. Li, R.H. Singer, and K.L. Taneja. 1993. Isoform-specific 3'-untranslated sequences sort alpha-cardiac and beta-cytoplasmic actin messenger RNAs to different cytoplasmic compartments. *The Journal of cell biology*. 123:165-172.

Kong, L., X. Wang, D.W. Choe, M. Polley, B.G. Burnett, M. Bosch-Marce, J.W. Griffin, M.M. Rich, and C.J. Sumner. 2009. Impaired synaptic vesicle release and immaturity of neuromuscular junctions in spinal muscular atrophy mice. *The Journal of neuroscience : the official journal of the Society for Neuroscience*. 29:842-851.

Korobova, F., and T. Svitkina. 2008. Arp2/3 complex is important for filopodia formation, growth cone motility, and neuritogenesis in neuronal cells. *Molecular biology of the cell*. 19:1561-1574.

Kumar, A., K. Crawford, L. Close, M. Madison, J. Lorenz, T. Doetschman, S. Pawlowski, J. Duffy, J. Neumann, J. Robbins, G.P. Boivin, B.A. O'Toole, and J.L. Lessard. 1997. Rescue of cardiac alpha-actin-deficient mice by enteric smooth muscle gamma-actin. *Proceedings of the National Academy of Sciences of the United States of America*. 94:4406-4411.

Kumar, A., K. Crawford, R. Flick, R. Klevitsky, J.N. Lorenz, K.E. Bove, J. Robbins, and J.L. Lessard. 2004. Transgenic overexpression of cardiac actin in the mouse heart suggests coregulation of cardiac, skeletal and vascular actin expression. *Transgenic research*. 13:531-540.

Larsson, H., and U. Lindberg. 1988. The effect of divalent cations on the interaction between calf spleen profilin and different actins. *Biochimica et biophysica acta*. 953:95-105.

Lee, C.W., E.A. Vitriol, S. Shim, A.L. Wise, R.P. Velayutham, and J.Q. Zheng. 2013. Dynamic localization of G-actin during membrane protrusion in neuronal motility. *Current biology : CB*. 23:1046-1056.

Lefebvre, S., L. Burglen, S. Reboullet, O. Clermont, P. Burlet, L. Viollet, B. Benichou, C. Cruaud, P. Millasseau, M. Zeviani, and et al. 1995. Identification and characterization of a spinal muscular atrophy-determining gene. *Cell*. 80:155-165.

Letourneau, P.C. 2009. Actin in axons: stable scaffolds and dynamic filaments. *Results and problems in cell differentiation*. 48:65-90.

Letourneau, P.C., T.A. Shattuck, and A.H. Ressler. 1987. "Pull" and "push" in neurite elongation: observations on the effects of different concentrations of cytochalasin B and taxol. *Cell Motil Cytoskeleton*. 8:193-209.

Leung, K.M., F.P. van Horck, A.C. Lin, R. Allison, N. Standart, and C.E. Holt. 2006. Asymmetrical beta-actin mRNA translation in growth cones mediates attractive turning to netrin-1. *Nature neuroscience*. 9:1247-1256.

Li, C., G.J. Bassell, and Y. Sasaki. 2009. Fragile X Mental Retardation Protein is Involved in Protein Synthesis-Dependent Collapse of Growth Cones Induced by Semaphorin-3A. *Frontiers in neural circuits*. 3:11.

Ling, K.K., R.M. Gibbs, Z. Feng, and C.P. Ko. 2012. Severe neuromuscular denervation of clinically relevant muscles in a mouse model of spinal muscular atrophy. *Human molecular genetics*. 21:185-195.

Little, D., C.F. Valori, C.A. Mutsaers, E.J. Bennett, M. Wyles, B. Sharrack, P.J. Shaw, T.H. Gillingwater, M. Azzouz, and K. Ning. 2015. PTEN depletion decreases disease severity and modestly prolongs survival in a mouse model of spinal muscular atrophy. *Mol Ther*. 23:270-277.

Liu, Q., and G. Dreyfuss. 1996. A novel nuclear structure containing the survival of motor neurons protein. *The EMBO journal*. 15:3555-3565.

Luo, L. 2002. Actin cytoskeleton regulation in neuronal morphogenesis and structural plasticity. *Annu Rev Cell Dev Biol*. 18:601-635.

Mackenzie, I.R., R. Rademakers, and M. Neumann. 2010. TDP-43 and FUS in amyotrophic lateral sclerosis and frontotemporal dementia. *The Lancet. Neurology*. 9:995-1007.

Martin, K.C., and A. Ephrussi. 2009. mRNA localization: gene expression in the spatial dimension. *Cell*. 136:719-730.

McWhorter, M.L., U.R. Monani, A.H. Burghes, and C.E. Beattie. 2003. Knockdown of the survival motor neuron (Smn) protein in zebrafish causes defects in motor axon outgrowth and pathfinding. *The Journal of cell biology*. 162:919-931.

Meister, G., D. Buhler, R. Pillai, F. Lottspeich, and U. Fischer. 2001. A multiprotein complex mediates the ATP-dependent assembly of spliceosomal U snRNPs. *Nature cell biology*. 3:945-949.

Merianda, T.T., C. Gomes, S. Yoo, D. Vuppalanchi, and J.L. Twiss. 2013a. Axonal localization of neuritin/CPG15 mRNA in neuronal populations through distinct 5' and 3' UTR elements. *The Journal of neuroscience : the official journal of the Society for Neuroscience*. 33:13735-13742.

Merianda, T.T., D. Vuppalanchi, S. Yoo, A. Blesch, and J.L. Twiss. 2013b. Axonal transport of neural membrane protein 35 mRNA increases axon growth. *Journal of cell science*. 126:90-102.

Messaoudi, E., T. Kanhema, J. Soule, A. Tiron, G. Dagyte, B. da Silva, and C.R. Bramham. 2007. Sustained Arc/Arg3.1 synthesis controls long-term potentiation consolidation through regulation of local actin polymerization in the dentate gyrus in vivo. *The Journal of neuroscience : the official journal of the Society for Neuroscience*. 27:10445-10455.

Micheva, K.D., A. Vallee, C. Beaulieu, I.M. Herman, and N. Leclerc. 1998. beta-Actin is confined to structures having high capacity of remodelling in developing and adult rat cerebellum. *Eur J Neurosci*. 10:3785-3798.

Miller, S., M. Yasuda, J.K. Coats, Y. Jones, M.E. Martone, and M. Mayford. 2002. Disruption of dendritic translation of CaMKIIalpha impairs stabilization of synaptic plasticity and memory consolidation. *Neuron*. 36:507-519.

Ming, G.L., S.T. Wong, J. Henley, X.B. Yuan, H.J. Song, N.C. Spitzer, and M.M. Poo. 2002. Adaptation in the chemotactic guidance of nerve growth cones. *Nature*. 417:411-418.

Mingorance-Le Meur, A., and T.P. O'Connor. 2009. Neurite consolidation is an active process requiring constant repression of protrusive activity. *The EMBO journal*. 28:248-260.

Monani, U.R., C.L. Lorson, D.W. Parsons, T.W. Prior, E.J. Androphy, A.H. Burghes, and J.D. McPherson. 1999. A single nucleotide difference that alters splicing patterns distinguishes the SMA gene SMN1 from the copy gene SMN2. *Hum Mol Genet*. 8:1177-1183.

Monani, U.R., M. Sendtner, D.D. Coovert, D.W. Parsons, C. Andreassi, T.T. Le, S. Jablonka, B. Schrank, W. Rossoll, T.W. Prior, G.E. Morris, and A.H. Burghes. 2000. The human centromeric survival motor neuron gene (SMN2) rescues embryonic lethality in Smn(-/-) mice and results in a mouse with spinal muscular atrophy. *Human molecular genetics*. 9:333-339.

Montani, L., B. Gerrits, P. Gehrig, A. Kempf, L. Dimou, B. Wollscheid, and M.E. Schwab. 2009. Neuronal Nogo-A modulates growth cone motility via Rho-GTP/LIMK1/cofilin in the unlesioned adult nervous system. *The Journal of biological chemistry*. 284:10793-10807.

Murray, L.M., L.H. Comley, D. Thomson, N. Parkinson, K. Talbot, and T.H. Gillingwater. 2008. Selective vulnerability of motor neurons and dissociation of pre- and post-synaptic pathology at the neuromuscular junction in mouse models of spinal muscular atrophy. *Human molecular genetics*. 17:949-962.

Napoli, I., V. Mercaldo, P.P. Boyl, B. Eleuteri, F. Zalfa, S. De Rubeis, D. Di Marino, E. Mohr, M. Massimi, M. Falconi, W. Witke, M. Costa-Mattioli, N. Sonenberg, T. Achsel, and C. Bagni. 2008. The fragile X syndrome protein represses activity-dependent translation through CYFIP1, a new 4E-BP. *Cell*. 134:1042-1054.

Ning, K., C. Drepper, C.F. Valori, M. Ahsan, M. Wyles, A. Higginbottom, T. Herrmann, P. Shaw, M. Azzouz, and M. Sendtner. 2010. PTEN depletion rescues axonal growth defect and improves survival in SMN-deficient motor neurons. *Human molecular genetics*. 19:3159-3168.

Nowak, K.J., G. Ravenscroft, C. Jackaman, A. Filipovska, S.M. Davies, E.M. Lim, S.E. Squire, A.C. Potter, E. Baker, S. Clement, C.A. Sewry, V. Fabian, K. Crawford, J.L. Lessard, L.M. Griffiths, J.M. Papadimitriou, Y. Shen, G. Morahan, A.J. Bakker, K.E. Davies, and N.G. Laing. 2009. Rescue of skeletal muscle alpha-actin-null mice by cardiac (fetal) alpha-actin. *The Journal of cell biology*. 185:903-915.

Nowak, K.J., D. Wattanasirichaigoon, H.H. Goebel, M. Wilce, K. Pelin, K. Donner, R.L. Jacob, C. Hubner, K. Oexle, J.R. Anderson, C.M. Verity, K.N. North, S.T. Iannaccone, C.R. Muller, P.

Nurnberg, F. Muntoni, C. Sewry, I. Hughes, R. Sutphen, A.G. Lacson, K.J. Swoboda, J. Vigneron, C. Wallgren-Pettersson, A.H. Beggs, and N.G. Laing. 1999. Mutations in the skeletal muscle alpha-actin gene in patients with actin myopathy and nemaline myopathy. *Nature genetics*. 23:208-212.

Nyman, T., H. Schuler, E. Korenbaum, C.E. Schutt, R. Karlsson, and U. Lindberg. 2002. The role of MeH73 in actin polymerization and ATP hydrolysis. *J Mol Biol*. 317:577-589.

Ogawa, C., K. Usui, F. Ito, M. Itoh, Y. Hayashizaki, and H. Suzuki. 2009. Role of survival motor neuron complex components in small nuclear ribonucleoprotein assembly. *The Journal of biological chemistry*. 284:14609-14617.

Ohlsson, M., H. Tajsharghi, N. Darin, M. Kyllerman, and A. Oldfors. 2004. Follow-up of nemaline myopathy in two patients with novel mutations in the skeletal muscle alpha-actin gene (ACTA1). *Neuromuscular disorders : NMD*. 14:471-475.

Ohnami, S., M. Endo, S. Hirai, N. Uesaka, Y. Hatanaka, T. Yamashita, and N. Yamamoto. 2008. Role of RhoA in activity-dependent cortical axon branching. *The Journal of neuroscience : the official journal of the Society for Neuroscience*. 28:9117-9121.

Olson, E.N., and A. Nordheim. 2010. Linking actin dynamics and gene transcription to drive cellular motile functions. *Nature reviews. Molecular cell biology*. 11:353-365.

Otey, C.A., M.H. Kalnoski, J.L. Lessard, and J.C. Bulinski. 1986. Immunolocalization of the gamma isoform of nonmuscle actin in cultured cells. *The Journal of cell biology*. 102:1726-1737.

Pan, L., E. Woodruff, 3rd, P. Liang, and K. Broadie. 2008. Mechanistic relationships between Drosophila fragile X mental retardation protein and metabotropic glutamate receptor A signaling. *Molecular and cellular neurosciences*. 37:747-760.

Papponen, H., T. Kaisto, S. Leinonen, M. Kaakinen, and K. Metsikko. 2009. Evidence for gamma-actin as a Z disc component in skeletal myofibers. *Experimental cell research*. 315:218-225.

Paquin, N., and P. Chartrand. 2008. Local regulation of mRNA translation: new insights from the bud. *Trends in cell biology*. 18:105-111.

Perrone-Bizzozero, N., and F. Bolognani. 2002. Role of HuD and other RNA-binding proteins in neural development and plasticity. *Journal of neuroscience research*. 68:121-126.

Pfaffl, M.W. 2001. A new mathematical model for relative quantification in real-time RT-PCR. *Nucleic acids research*. 29:e45.

Piazzon, N., F. Rage, F. Schlotter, H. Moine, C. Branlant, and S. Massenet. 2008. In vitro and in cellulo evidences for association of the survival of motor neuron complex with the fragile X mental retardation protein. *The Journal of biological chemistry*. 283:5598-5610.

Piper, M., R. Anderson, A. Dwivedy, C. Weinl, F. van Horck, K.M. Leung, E. Cogill, and C. Holt. 2006. Signaling mechanisms underlying Slit2-induced collapse of Xenopus retinal growth cones. *Neuron*. 49:215-228.

Plath, N., O. Ohana, B. Dammermann, M.L. Errington, D. Schmitz, C. Gross, X. Mao, A. Engelsberg, C. Mahlke, H. Welzl, U. Kobalz, A. Stawrakakis, E. Fernandez, R. Waltereit, A. Bick-Sander, E. Therstappen, S.F. Cooke, V. Blanquet, W. Wurst, B. Salmen, M.R. Bosl, H.P. Lipp, S.G. Grant, T.V. Bliss, D.P. Wolfer, and D. Kuhl. 2006. Arc/Arg3.1 is essential for the consolidation of synaptic plasticity and memories. *Neuron*. 52:437-444.

Porter, B.E., J. Weis, and J.R. Sanes. 1995. A motoneuron-selective stop signal in the synaptic protein S-laminin. *Neuron*. 14:549-559.

Qiu, L.F., T.J. Lu, X.L. Hu, Y.H. Yi, W.P. Liao, and Z.Q. Xiong. 2009. Limbic epileptogenesis in a mouse model of fragile X syndrome. *Cerebral cortex*. 19:1504-1514.

Raker, V.A., K. Hartmuth, B. Kastner, and R. Luhrmann. 1999. Spliceosomal U snRNP core assembly: Sm proteins assemble onto an Sm site RNA nonanucleotide in a specific and thermodynamically stable manner. *Molecular and cellular biology*. 19:6554-6565.

Rathod, R., S. Havlicek, N. Frank, R. Blum, and M. Sendtner. 2012. Laminin induced local axonal translation of beta-actin mRNA is impaired in SMN-deficient motoneurons. *Histochemistry and cell biology*. 138:737-748.

Rehberg, M., A. Lepier, B. Solchenberger, P. Osten, and R. Blum. 2008. A new non-disruptive strategy to target calcium indicator dyes to the endoplasmic reticulum. *Cell calcium*. 44:386-399.

Renton, A.E., A. Chio, and B.J. Traynor. 2014. State of play in amyotrophic lateral sclerosis genetics. *Nature neuroscience*. 17:17-23.

Renton, A.E., E. Majounie, A. Waite, J. Simon-Sanchez, S. Rollinson, J.R. Gibbs, J.C. Schymick, H. Laaksovirta, J.C. van Swieten, L. Myllykangas, H. Kalimo, A. Paetau, Y. Abramzon, A.M. Remes, A. Kaganovich, S.W. Scholz, J. Duckworth, J. Ding, D.W. Harmer, D.G. Hernandez, J.O. Johnson, K. Mok, M. Ryten, D. Trabzuni, R.J. Guerreiro, R.W. Orrell, J. Neal, A. Murray, J. Pearson, I.E. Jansen, D. Sondervan, H. Seelaar, D. Blake, K. Young, N. Halliwell, J.B. Callister, G. Toulson, A. Richardson, A. Gerhard, J. Snowden, D. Mann, D. Neary, M.A. Nalls, T. Peuralinna, L. Jansson, V.M. Isoviita, A.L. Kaivorinne, M. Holtta-Vuori, E. Ikonen, R. Sulkava, M. Benatar, J. Wuu, A. Chio, G. Restagno, G. Borghero, M. Sabatelli, I. Consortium, D. Heckerman, E. Rogaeva, L. Zinman, J.D. Rothstein, M. Sendtner, C. Drepper, E.E. Eichler, C. Alkan, Z. Abdullaev, S.D. Pack, A. Dutra, E. Pak, J. Hardy, A. Singleton, N.M. Williams, P. Heutink, S. Pickering-Brown, H.R. Morris, P.J. Tienari, and B.J. Traynor. 2011. A hexanucleotide repeat expansion in C9ORF72 is the cause of chromosome 9p21-linked ALS-FTD. *Neuron*. 72:257-268.

Rishal, I., and M. Fainzilber. 2014. Axon-soma communication in neuronal injury. *Nature reviews. Neuroscience*. 15:32-42.

Robberecht, W. 2000. Oxidative stress in amyotrophic lateral sclerosis. *Journal of neurology*. 247 Suppl 1:I1-6.

Rook, M.S., M. Lu, and K.S. Kosik. 2000. CaMKIIalpha 3' untranslated region-directed mRNA translocation in living neurons: visualization by GFP linkage. *The Journal of neuroscience : the official journal of the Society for Neuroscience*. 20:6385-6393.

Rossoll, W., S. Jablonka, C. Andreassi, A.K. Kroning, K. Karle, U.R. Monani, and M. Sendtner. 2003. Smn, the spinal muscular atrophy-determining gene product, modulates axon growth and localization of beta-actin mRNA in growth cones of motoneurons. *J Cell Biol*. 163:801-812.

Rossoll, W., A.K. Kroning, U.M. Ohndorf, C. Steegborn, S. Jablonka, and M. Sendtner. 2002. Specific interaction of Smn, the spinal muscular atrophy determining gene product, with hnRNP-R and gry-rbp/hnRNP-Q: a role for Smn in RNA processing in motor axons? *Human molecular genetics*. 11:93-105.

Rubenstein, P.A. 1990. The functional importance of multiple actin isoforms. *Bioessays*. 12:309-315.

Rybakova, I.N., J.R. Patel, and J.M. Ervasti. 2000. The dystrophin complex forms a mechanically strong link between the sarcolemma and costameric actin. *The Journal of cell biology*. 150:1209-1214.

Saal, L., M. Briese, S. Kneitz, M. Glinka, and M. Sendtner. 2014. Subcellular transcriptome alterations in a cell culture model of spinal muscular atrophy point to widespread defects in axonal growth and presynaptic differentiation. *RNA*. 20:1789-1802.

Sachdeva, R., C.C. Theisen, V. Ninan, J.L. Twiss, and J.D. Houle. 2016. Exercise dependent increase in axon regeneration into peripheral nerve grafts by propriospinal but not sensory neurons after spinal cord injury is associated with modulation of regeneration-associated genes. *Experimental neurology*. 276:72-82.

Sasaki, S., T. Komori, and M. Iwata. 2000. Excitatory amino acid transporter 1 and 2 immunoreactivity in the spinal cord in amyotrophic lateral sclerosis. *Acta neuropathologica*. 100:138-144.

Schildmeyer, L.A., R. Braun, G. Taffet, M. Debiasi, A.E. Burns, A. Bradley, and R.J. Schwartz. 2000. Impaired vascular contractility and blood pressure homeostasis in the smooth muscle alpha-actin null mouse. *FASEB journal : official publication of the Federation of American Societies for Experimental Biology*. 14:2213-2220.

Schneider, C.A., W.S. Rasband, and K.W. Eliceiri. 2012. NIH Image to ImageJ: 25 years of image analysis. *Nature methods*. 9:671-675.

Schoch, S., and E.D. Gundelfinger. 2006. Molecular organization of the presynaptic active zone. *Cell and tissue research*. 326:379-391.

Schrank, B., R. Gotz, J.M. Gunnersen, J.M. Ure, K.V. Toyka, A.G. Smith, and M. Sendtner. 1997. Inactivation of the survival motor neuron gene, a candidate gene for human spinal muscular atrophy, leads to massive cell death in early mouse embryos. *Proceedings of the National Academy of Sciences of the United States of America*. 94:9920-9925.

Schratt, G.M., F. Tuebing, E.A. Nigh, C.G. Kane, M.E. Sabatini, M. Kiebler, and M.E. Greenberg. 2006. A brain-specific microRNA regulates dendritic spine development. *Nature*. 439:283-289.

Schreiber, J., M.J. Vegh, J. Dawitz, T. Kroon, M. Loos, D. Labonte, K.W. Li, P. Van Nierop, M.T. Van Diepen, C.I. De Zeeuw, M. Kneussel, R.M. Meredith, A.B. Smit, and R.E. Van Kesteren. 2015. Ubiquitin ligase TRIM3 controls hippocampal plasticity and learning by regulating synaptic gamma-actin levels. *The Journal of cell biology*. 211:569-586.

Schwab, M.E. 2004. Nogo and axon regeneration. *Current opinion in neurobiology*. 14:118-124.

Selvaraj, B.T., N. Frank, F.L. Bender, E. Asan, and M. Sendtner. 2012. Local axonal function of STAT3 rescues axon degeneration in the pmn model of motoneuron disease. *The Journal of cell biology*. 199:437-451.

Shahbazian, D., P.P. Roux, V. Mieulet, M.S. Cohen, B. Raught, J. Taunton, J.W. Hershey, J. Blenis, M. Pende, and N. Sonenberg. 2006. The mTOR/PI3K and MAPK pathways converge on eIF4B to control its phosphorylation and activity. *The EMBO journal*. 25:2781-2791.

Shelly, M., L. Cancedda, S. Heilshorn, G. Sumbre, and M.M. Poo. 2007. LKB1/STRAD promotes axon initiation during neuronal polarization. *Cell*. 129:565-577.

Shelly, M., L. Cancedda, B.K. Lim, A.T. Popescu, P.L. Cheng, H. Gao, and M.M. Poo. 2011. Semaphorin3A regulates neuronal polarization by suppressing axon formation and promoting dendrite growth. *Neuron*. 71:433-446.

Shiina, N., K. Shinkura, and M. Tokunaga. 2005. A novel RNA-binding protein in neuronal RNA granules: regulatory machinery for local translation. *The Journal of neuroscience : the official journal of the Society for Neuroscience*. 25:4420-4434.

Simon, C.M., S. Jablonka, R. Ruiz, L. Tabares, and M. Sendtner. 2010. Ciliary neurotrophic factor-induced sprouting preserves motor function in a mouse model of mild spinal muscular atrophy. *Hum Mol Genet*. 19:973-986.

Sivadasan, R., D. Hornburg, C. Drepper, N. Frank, S. Jablonka, A. Hansel, X. Lojewski, J. Sterneckert, A. Hermann, P.J. Shaw, P.G. Ince, M. Mann, F. Meissner, and M. Sendtner. 2016. C9ORF72 interaction with cofilin modulates actin dynamics in motor neurons. *Nature neuroscience*.

Song, A.H., D. Wang, G. Chen, Y. Li, J. Luo, S. Duan, and M.M. Poo. 2009. A selective filter for cytoplasmic transport at the axon initial segment. *Cell*. 136:1148-1160.

Sonnemann, K.J., D.P. Fitzsimons, J.R. Patel, Y. Liu, M.F. Schneider, R.L. Moss, and J.M. Ervasti. 2006. Cytoplasmic gamma-actin is not required for skeletal muscle development but its absence leads to a progressive myopathy. *Developmental cell*. 11:387-397.

Spillane, M., A. Ketschek, C.J. Donnelly, A. Pacheco, J.L. Twiss, and G. Gallo. 2012. Nerve growth factor-induced formation of axonal filopodia and collateral branches involves the intra-axonal synthesis of regulators of the actin-nucleating Arp2/3 complex. *The Journal of neuroscience : the official journal of the Society for Neuroscience*. 32:17671-17689.

Spillane, M., A. Ketschek, S.L. Jones, F. Korobova, B. Marsick, L. Lanier, T. Svitkina, and G. Gallo. 2011. The actin nucleating Arp2/3 complex contributes to the formation of axonal filopodia and branches through the regulation of actin patch precursors to filopodia. *Dev Neurobiol*. 71:747-758.

Spillane, M., A. Ketschek, T.T. Merianda, J.L. Twiss, and G. Gallo. 2013. Mitochondria coordinate sites of axon branching through localized intra-axonal protein synthesis. *Cell reports*. 5:1564-1575.

St Johnston, D. 2005. Moving messages: the intracellular localization of mRNAs. *Nature reviews. Molecular cell biology*. 6:363-375.

Suter, D.M., and K.E. Miller. 2011. The emerging role of forces in axonal elongation. *Prog Neurobiol*. 94:91-101.

Takei, N., M. Kawamura, K. Hara, K. Yonezawa, and H. Nawa. 2001. Brain-derived neurotrophic factor enhances neuronal translation by activating multiple initiation processes: comparison with the effects of insulin. *The Journal of biological chemistry*. 276:42818-42825.

Taneja, K.L., and R.H. Singer. 1990. Detection and localization of actin mRNA isoforms in chicken muscle cells by in situ hybridization using biotinated oligonucleotide probes. *J Cell Biochem*. 44:241-252.

Tapia, R. 2014. Cellular and molecular mechanisms of motor neuron death in amyotrophic lateral sclerosis: a perspective. *Frontiers in cellular neuroscience*. 8:241.

Tessier, C.R., and K. Broadie. 2008. Drosophila fragile X mental retardation protein developmentally regulates activity-dependent axon pruning. *Development*. 135:1547-1557.

Tondeleir, D., A. Lambrechts, M. Muller, V. Jonckheere, T. Doll, D. Vandamme, K. Bakkali, D. Waterschoot, M. Lemaistre, O. Debeir, C. Decaestecker, B. Hinz, A. Staes, E. Timmerman, N. Colaert, K. Gevaert, J. Vandekerckhove, and C. Ampe. 2012. Cells lacking beta-actin are genetically reprogrammed and maintain conditional migratory capacity. *Molecular & cellular proteomics : MCP*. 11:255-271.

Uesaka, N., Y. Hayano, A. Yamada, and N. Yamamoto. 2007. Interplay between laminar specificity and activity-dependent mechanisms of thalamocortical axon branching. *The Journal of neuroscience : the official journal of the Society for Neuroscience*. 27:5215-5223.

Van Baelen, H., R. Bouillon, and P. De Moor. 1980. Vitamin D-binding protein (Gc-globulin) binds actin. *The Journal of biological chemistry*. 255:2270-2272.

van Kesteren, R.E., C. Carter, H.M. Dissel, J. van Minnen, Y. Gouwenberg, N.I. Syed, G.E. Spencer, and A.B. Smit. 2006. Local synthesis of actin-binding protein beta-thymosin regulates neurite outgrowth. *The Journal of neuroscience : the official journal of the Society for Neuroscience*. 26:152-157.

Vandekerckhove, J., and K. Weber. 1978. At least six different actins are expressed in a higher mammal: an analysis based on the amino acid sequence of the amino-terminal tryptic peptide. *J Mol Biol*. 126:783-802.

Verma, P., S. Chierzi, A.M. Codd, D.S. Campbell, R.L. Meyer, C.E. Holt, and J.W. Fawcett. 2005. Axonal protein synthesis and degradation are necessary for efficient growth cone regeneration. *The Journal of neuroscience : the official journal of the Society for Neuroscience*. 25:331-342.

Visa, N., and P. Percipalle. 2010. Nuclear functions of actin. *Cold Spring Harbor perspectives in biology*. 2:a000620.

Volkening, K., C. Leystra-Lantz, W. Yang, H. Jaffee, and M.J. Strong. 2009. Tar DNA binding protein of 43 kDa (TDP-43), 14-3-3 proteins and copper/zinc superoxide dismutase (SOD1) interact to modulate NFL mRNA stability. Implications for altered RNA processing in amyotrophic lateral sclerosis (ALS). *Brain research*. 1305:168-182.

Wallgren-Pettersson, C., K. Pelin, K.J. Nowak, F. Muntoni, N.B. Romero, H.H. Goebel, K.N. North, A.H. Beggs, N.G. Laing, and E.I.C.O.N. Myopathy. 2004. Genotype-phenotype correlations in nemaline myopathy caused by mutations in the genes for nebulin and skeletal muscle alpha-actin. *Neuromuscular disorders : NMD*. 14:461-470.

Wang, W., E. van Niekerk, D.E. Willis, and J.L. Twiss. 2007. RNA transport and localized protein synthesis in neurological disorders and neural repair. *Developmental neurobiology*. 67:1166-1182.

Weeks, D.L., and D.A. Melton. 1987. A maternal mRNA localized to the vegetal hemisphere in Xenopus eggs codes for a growth factor related to TGF-beta. *Cell*. 51:861-867.

Welshhans, K., and G.J. Bassell. 2011. Netrin-1-induced local beta-actin synthesis and growth cone guidance requires zipcode binding protein 1. *The Journal of neuroscience : the official journal of the Society for Neuroscience*. 31:9800-9813.

Wiese, S., T. Herrmann, C. Drepper, S. Jablonka, N. Funk, A. Klausmeyer, M.L. Rogers, R. Rush, and M. Sendtner. 2010. Isolation and enrichment of embryonic mouse motoneurons from the lumbar spinal cord of individual mouse embryos. *Nat Protoc*. 5:31-38.

Wiese, S., F. Metzger, B. Holtmann, and M. Sendtner. 1999. The role of p75NTR in modulating neurotrophin survival effects in developing motoneurons. *Eur J Neurosci*. 11:1668-1676.

Willis, D., K.W. Li, J.Q. Zheng, J.H. Chang, A.B. Smit, T. Kelly, T.T. Merianda, J. Sylvester, J. van Minnen, and J.L. Twiss. 2005. Differential transport and local translation of cytoskeletal, injury-response, and neurodegeneration protein mRNAs in axons. *The Journal of neuroscience : the official journal of the Society for Neuroscience*. 25:778-791.

Willis, D.E., E.A. van Niekerk, Y. Sasaki, M. Mesngon, T.T. Merianda, G.G. Williams, M. Kendall, D.S. Smith, G.J. Bassell, and J.L. Twiss. 2007. Extracellular stimuli specifically regulate localized levels of individual neuronal mRNAs. *The Journal of cell biology*. 178:965-980.

Willis, D.E., M. Xu, C.J. Donnelly, C. Tep, M. Kendall, M. Erenstheyn, A.W. English, N.C. Schanen, C.B. Kirn-Safran, S.O. Yoon, G.J. Bassell, and J.L. Twiss. 2011. Axonal Localization of transgene mRNA in mature PNS and CNS neurons. *J Neurosci*. 31:14481-14487.

Winkler, C., C. Eggert, D. Gradl, G. Meister, M. Giegerich, D. Wedlich, B. Laggerbauer, and U. Fischer. 2005. Reduced U snRNP assembly causes motor axon degeneration in an animal model for spinal muscular atrophy. *Genes Dev*. 19:2320-2330.

Wu, K.Y., U. Hengst, L.J. Cox, E.Z. Macosko, A. Jeromin, E.R. Urquhart, and S.R. Jaffrey. 2005. Local translation of RhoA regulates growth cone collapse. *Nature*. 436:1020-1024.

Xu, K., G. Zhong, and X. Zhuang. 2013. Actin, spectrin, and associated proteins form a periodic cytoskeletal structure in axons. *Science*. 339:452-456.

Yan, D., Z. Wu, A.D. Chisholm, and Y. Jin. 2009. The DLK-1 kinase promotes mRNA stability and local translation in C. elegans synapses and axon regeneration. *Cell*. 138:1005-1018.

Yao, J., Y. Sasaki, Z. Wen, G.J. Bassell, and J.Q. Zheng. 2006. An essential role for beta-actin mRNA localization and translation in Ca2+-dependent growth cone guidance. *Nat Neurosci*. 9:1265-1273.

Yao, X., L. Cheng, and J.G. Forte. 1996. Biochemical characterization of ezrin-actin interaction. *The Journal of biological chemistry*. 271:7224-7229.

Z'Graggen, W.J., G.A. Metz, G.L. Kartje, M. Thallmair, and M.E. Schwab. 1998. Functional recovery and enhanced corticofugal plasticity after unilateral pyramidal tract lesion and blockade of myelin-associated neurite growth inhibitors in adult rats. *The Journal of neuroscience : the official journal of the Society for Neuroscience*. 18:4744-4757.

Zhang, H.L., T. Eom, Y. Oleynikov, S.M. Shenoy, D.A. Liebelt, J.B. Dictenberg, R.H. Singer, and G.J. Bassell. 2001a. Neurotrophin-induced transport of a beta-actin mRNP complex increases beta-actin levels and stimulates growth cone motility. *Neuron*. 31:261-275.

Zhang, W., and D.L. Benson. 2001. Stages of synapse development defined by dependence on F-actin. *The Journal of neuroscience : the official journal of the Society for Neuroscience*. 21:5169-5181.

Zhang, Y.J., K. Jansen-West, Y.F. Xu, T.F. Gendron, K.F. Bieniek, W.L. Lin, H. Sasaguri, T. Caulfield, J. Hubbard, L. Daughrity, J. Chew, V.V. Belzil, M. Prudencio, J.N. Stankowski, M. Castanedes-Casey, E. Whitelaw, P.E. Ash, M. DeTure, R. Rademakers, K.B. Boylan, D.W. Dickson, and L. Petrucelli. 2014. Aggregation-prone c9FTD/ALS poly(GA) RAN-translated proteins cause neurotoxicity by inducing ER stress. *Acta neuropathologica*. 128:505-524.

Zhang, Y.Q., A.M. Bailey, H.J. Matthies, R.B. Renden, M.A. Smith, S.D. Speese, G.M. Rubin, and K. Broadie. 2001b. Drosophila fragile X-related gene regulates the MAP1B homolog Futsch to control synaptic structure and function. *Cell*. 107:591-603.

Zheng, B., M. Han, M. Bernier, and J.K. Wen. 2009. Nuclear actin and actin-binding proteins in the regulation of transcription and gene expression. *The FEBS journal*. 276:2669-2685.

Zheng, J.Q., T.K. Kelly, B. Chang, S. Ryazantsev, A.K. Rajasekaran, K.C. Martin, and J.L. Twiss. 2001. A functional role for intra-axonal protein synthesis during axonal regeneration from adult sensory neurons. *The Journal of neuroscience : the official journal of the Society for Neuroscience*. 21:9291-9303.

Zhong, G., J. He, R. Zhou, D. Lorenzo, H.P. Babcock, V. Bennett, and X. Zhuang. 2014. Developmental mechanism of the periodic membrane skeleton in axons. *Elife*. 3.

Zhou, C., Y. Li, A. Nanda, and J.H. Zhang. 2003. HBO suppresses Nogo-A, Ng-R, or RhoA expression in the cerebral cortex after global ischemia. *Biochemical and biophysical research communications*. 309:368-376.

Zufferey, R., T. Dull, R.J. Mandel, A. Bukovsky, D. Quiroz, L. Naldini, and D. Trono. 1998. Self-inactivating lentivirus vector for safe and efficient in vivo gene delivery. *Journal of virology*. 72:9873-9880.

8. Appendix

8.1 List of figures

Figure 3.3.4.1	Formation of collateral branches	Page 14
Figure 3.4.1	RNA granule formation for axonal transport	Page 17
Figure 3.4.1.1	Role of SMN in splicing and mRNP assembly	Page 19
Figure 5.1.1	External calibration curves for α-, β- and γ-actin	Page 72
Figure 5.1.2	α-, β- and γ-actin transcripts are expressed in motoneurons *in vivo*	Page 72
Figure 5.2.1	α-, β- and γ-actin transcripts are transported into axons in motoneurons	Page 74
Figure 5.2.2	mRNAs for α-actin are enriched in axons of motoneurons	Page 75
Figure 5.2.3	Subcellular localization of endogenous α-, β- and γ-actin mRNAs in cultured motoneurons	Page 76
Figure 5.2.4	α-, β- and γ-actin mRNAs are present in different RNA transport granules	Page 77
Figure 5.2.5	Gapdh mRNA and 18srRNA, but not DapB are detected in motoneurons	Page 78
Figure 5.2.6	Signals for α-, β- and γ-actin mRNAs are decreased after shRNA repression of these isoforms	Page 79
Figure 5.3.1	α-actin isoforms expression in mouse primary cortical neurons	Page 80
Figure 5.3.2	Localization of β-actin mRNA in mouse primary cortical neurons	Page 80
Figure 5.3.3	Localization of γ-actin mRNAs in mouse primary cortical neurons	Page 81
Figure 5.3.4	qRT-PCR detection of α-, β- and γ-actin transcripts in axons of cultured cortical neurons	Page 81
Figure 5.4.1	Validation of actin isoform-specific antibodies by Western blot	Page 83
Figure 5.4.2	Validation of actin isoform-specific antibodies by immunocytochemistry experiments	Page 84
Figure 5.4.3	Specificity of α-actin antibody is validated by Western blot using α-, β- and γ-actin expression plasmids	Page 84
Figure 5.4.4	Differential localization of isoactin proteins in cultured motoneurons	Page 86
Figure 5.4.5	Actin isoforms incorporate into F-actin in different regions within the axon	Page 87
Figure 5.4.6	G-actin and other globular proteins are washed out after Triton X-100 treatment	Page 88
Figure 5.5.1	Studying local translation of α-, β- and γ-actin using $eGFP^{myr}$ reporters	Page 90

Figure 5.5.2	Reporters of α-, β- and γ-actin are locally translated in axonal growth cones of motoneurons	Page 91
Figure 5.5.3	α-actin reporter shows a faster recovery rate in axonal branch points compared to β- and γ-actin reporters	Page 92
Figure 5.6.1	mRNA levels of α-, β- and γ-actin isoforms are significantly reduced after respective shRNA mediated knockdown of these isoforms	Page 93
Figure 5.6.2	Depletion of α-, β- or γ-actin does not affect cell survival in motoneurons	Page 94
Figure 5.6.3	Depletion of α-, β- or γ-actin isoforms does not affect dendrite growth	Page 95
Figure 5.6.4	Depletion of α-actin isoform impairs axonal branching in motoneurons	Page 96
Figure 5.6.5	Depletion of α-, β- or γ-actin impairs axon elongation in cultured motoneurons	Page 97
Figure 5.6.6	β-actin knockdown motoneurons show deficit growth cones maturation	Page 98
Figure 5.6.7	ShActα-2 lentiviral transduction impairs axonal growth and collateral branch formation in cultured motoneurons	Page 100
Figure 5.6.8	ShActβ-2 and ShActγ-2 and -3 cause similar phenotypes in axonal elongation and axonal growth cone maturation as shActβ-1 and shActγ-1	Page 100
Figure 5.6.9	β-actin rescue construct is expressed in cultured motoneurons	Page 101
Figure 5.6.10	β-actin protein levels are restored after expression of β-actin rescue construct	Page 101
Figure 5.6.11	Axon length defects are recuse after re-expression of β-actin rescue construct in cultured motoneurons	Page 102
Figure 5.6.12	Defects in axonal growth cone maturation are recused after re-expression of β-actin rescue construct in cultured motoneurons	Page 102
Figure 5.7.1	Axonal filopodia exhibit de novo formation and growth/retraction dynamics in culture	Page 105
Figure 5.7.2	Knockdown of α- or γ-actin isoforms affects dynamics of axonal filopodia	Page 105
Figure 5.7.3	Dynamics of axonal growth cone filopodia are impaired in β-actin knockdown motoneurons	Page 106
Figure 5.8.1	α- and β-actin isoforms are essential for F-actin polymerization in axons	Page 108
Figure 5.8.2	Pan-actin levels remain constant in α-, β- or γ-actin knockdown motoneurons	Page 109
Figure 5.8.3	G/F actin ratio is preserved after knockdown of individual actin isoforms	Page 110
Figure 5.8.4	Compensatory upregulation of β- and γ-actin mRNAs in axons of α-actin depleted motoneurons	Page 111
Figure 5.8.5	α- and γ-actin mRNA levels increase in soma and axons of motoneurons as a compensatory response to β-actin knockdown	Page 112

Figure 5.8.6	α- and β-actin mRNAs increase in soma and axons of γ-actin knockdown motoneurons	Page 112
Figure 5.8.7	Compensatory upregulation of α- and γ-actin proteins as a response to β-actin depletion	Page 113
Figure 5.9.1	Smn is required for axonal translocation of α-, β- and γ-actin transcripts in motoneurons	Page 115
Figure 5.9.2	Smn is required for local translation of α-, β- and γ-actin reporters in axonal growth cones of motoneurons	Page 116

8.2 List of tables

Table 4.1.1	list of primary antibodies used for immunofluorescence
Table 4.1.2	list of secondary antibodies used for immunofluorescence
Table 4.1.3	list of primary antibodies used for Western blot
Table 4.1.4	list of secondary antibodies used for Western blot
Table 4.1.5	list of used primers for genotyping
Table 4.1.6	list of used primers for qRT-PCR
Table 4.1.7	list of used oligos for shRNA cloning
Table 4.1.8	list of used primers for HA-tag expression cloning
Table 4.1.9	list of used primers for Myr-GFP-3'UTR expression cloning
Table 4.1.10	list of used primers for β-actin rescue cloning
Table 4.1.11	list of used plasmids for cloning
Table 4.2.1	PCR program for Smn wt and Smn knockout
Table 4.2.2	PCR program for SMN2tg
Table 4.2.3	qRT-PCR program using FastStart SYBR Green I master mix
Table 4.2.4	qRT-PCR program using Luminaris Color HiGreen master mix
Table 4.2.5	PCR program for amplification of α-actin, β-actin and γ-actin qRT-PCR products

Table 4.2.6	4.2.6 PCR program for cloning LCK-Myr-eGFP-3'UTR report for γ-actin
Table 4.2.7	PCR program for cloning HA-tag-expression constructs of α-, β- and γ-actin and rescue construct for β-actin

8.3 List of abbreviations

4EBP1	4E-binding protein-1
ACSF	Artificial cerebrospinal fluid
ADF	Actin depolymerizing factor
AIS	Axon initial segment
Akt/PKB	Akt kinase / protein kinase B
ALS	Amyotrophic lateral sclerosis
ATP	Adenosine triphosphate
BCA	Bicinchoninic acid
BDNF	Brain-derived neurotrophic factor
bps	Base pairs
BSA	Bovine serum albumin
°C	Celsius grad
CaMIIKα	Calcium/calmodulin-dependent protein kinase II α
cAMP	Cyclic adenosine monophosphate
CB buffer	Cytoskeleton buffer
cDNA	Copy deoxyribonucleic acid
CEBP-1	CAAT/enhancer binding protein1
CNS	Central nervous system
CNTF	Ciliary neurotrophic factor
cpg15	Candidate plasticity-related gene
CREB	cAMP-responsive element (CRE)-binding protein
Da	Dalton
DAG	Diacylglycerol
DAPI	4', 6-diamidino-2-phenylindole
DEPC	Diethyl pyrocarbonate
DIV	Day of invitro
DMEM	Dulbecco's modified essential medium
DMSO	Dimethyl sulfoxide
DNA	Deoxyribonucleic acid

dNTP	Deoxyribonucleotide
DRG	Dorsal root ganglia
DTT	Dithiothreitol
E	Embryonic
E	PCR efficiency
E. coli	Escherichia coli
ECL	Enhanced chemiluminescence
EDTA	Ethylenediaminetetraacetic acid
eF1α	Eukaryotic translation elongation factor 1 alpha 1
eGFP	Enhanced green fluorescent protein
eIF4B	Eukaryotic translation initiation factor-4B
For	Forward
FCS	Fetal calf serum
FISH	Fluorescence in situ hybridization
FMRP	Fragile X mental retardation protein
g	Gram
g	G-force
FRAP	Fluorescence recovery after photobleaching
GAP-43	Growth associated protein 43
GAPDH	Glyceraldehyde 3-phosphate dehydrogenase
GFP	Green fluorescent protein
h	Hours
HBSS	Hanks' balanced salt solution
HEK	Human embryonic kidney
hnRNP R/Q	Heterogeneous nuclear ribonucleoprotein R/Q
HRP	Horseradish peroxidase
IF	Immunofluorescence
IMP1	Insulin-like growth factor 2 mRNA-binding protein 1
JIR	Jackson ImmunoResearch
kb	Kilo base pair
KSRP	Far upstream element-binding protein 2
KO	Knockout
L	Liter
LMD	Laser capture microdissection

LTP	Long term potentiation
Max	Maximum
$MgCl_2$	Magnesium chloride 2
min	Minute
miRNAs	Micro interference RNA
ml	Milliliter
mRNA	Messenger RNA
mTOR	Mammalian target of rapamycin
mV	Millivolt
NA	Numerical aperture
Nefl	Neurofilament light chain
NGF	Nerve growth factor
NMJ	Neuromuscular junction
NP-40	Nonidet P-40
Nr.	Number
NSC-34	Mouse motor neuron like cells-34
ORF	Open reading frame
P	Postnatal
PAGE	Polyacrylamid gel electrophoresis
PAR3	proteinase-activated receptor 3
PBS	Phosphate buffered saline
PCR	Polymerase chain reaction
P/S	Penicillin-Streptomycin
PFA	Paraformaldehyde
PI3K	Phosphatidylinositol 3-kinase
PIPES	2-ethanesulfonic acid
PLP	Paraformaldehyde lysine phosphate buffer
PORN	Poly-DL-ornithine hydrobromide
PTEN	Phosphatase and tensin homolog
PVDF	Polyvinylidene difluoride
qRT-PCR	Quantitative reverse transcriptase-polymerase chain reaction
RE	Restriction enzyme
Rev	Reverse

RIMs	Rab3-interacting molecules
RNA	Ribonucleic acid
RNP	Ribonucleoprotein
ROCK	Rho-associated protein kinase
ROI	Region of interest
rpm	Revolutions per minute
RSK	P90 ribosomal S6 Kinase
RT	Room temperature
S6K	P60 ribosomal S6 Kinase
SDS	Sodium dodecyl sulfate
shRNA	Short hairpin RNA
siRNA	Small interference RNA
SMA	Spinal muscular atrophy
SMN	Survival motor neuron
snRNA	Small nuclear ribonucleic acid
snRNPs	Small nuclear ribonucleoprotein particles
SRF	Serum response factor
STAT3	Activator of transcription 3
TAE	Tris acetate EDTA
TBE	Tris borate EDTA
TBS	Tris buffered saline
TDP43	TAR DNA-binding protein 43
tg	Transgene
TGFβ	Transforming growth factor β
TRIM	Tripartite motif
TRIS	Tris hydroxymethyl aminomethane
Trk	Tropomyosin receptor kinase
TSC1/2	Tumor-suppressor tuberous sclerosis complex-1/2
UTR	Untranslated region
VSVG	Glycoproteins of vesicular stomatitis virus
WB	Western blot
wt	Wild type
ZBP1	Zipcode binding protein

9. Affidavit

I hereby confirm that my thesis entitled “Differential roles of α-, β- and γ-actin isoforms in regulation of cytoskeletal dynamics and stability during axon elongation and collateral branch formation in primary mouse motoneurons” is the result of my own work. I did not receive any help or support from commercial consultants. All sources and / or materials applied are listed and specified in the thesis.

Furthermore, I confirm that this thesis has not yet been submitted as part of another examination process neither in identical nor in similar form.

Place, Date Signature

Eidesstattliche Erklärung

Hiermit erkläre ich an Eides statt, die Dissertation „Rolle der α-, β- und γ-Aktin Isoformen bei Regulation von Dynamik und Stabilität des Zytoskeletts während des Axonwachstums und beim Ausbilden von axonalen Verzweigungen in Motoneuronen“ eigenständig, d.h. insbesondere selbstständig und ohne Hilfe eines kommerziellen Promotionsberaters, angefertigt und keine anderen als die von mir angegebenen Quellen und Hilfsmittel verwendet zu haben.

Ich erkläre außerdem, dass die Dissertation weder in gleicher noch in ähnlicher Form bereits in einem anderen Prüfungsverfahren vorgelegen hat.

Ort, Datum Unterschrift

10. Acknowledgments

Dear Prof. Sendtner, I would like to express my sincere gratitude for giving me excellent projects and for supervising my through my PhD. This work would not be what it is now without your valuable scientific and technical guidance and your immense knowledge. You continuously encouraged and motivated me in our morning meetings and showed me the career path in research. Thank you again and again for your patience and personal support.

I would like to thank the members of my thesis committee: Prof. Utz Fischer and Prof. Erich Buchner for monitoring my PhD and for their helpful suggestions and feedbacks in our annual meetings.

Robert thank you very much especially for the advices with qRT-PCR data analysis and great suggestions for cloning. I never stopped learning from you in all these years, many thanks for sharing your lab expertise with me.

Sibylle you were always there for me when I needed your help. Thank you for the useful scientific dissections we had in our office and for motivating me during the hard times.

Anna-Maria I sincerely appreciate your valuable scientific inputs and especially your constructive advices and suggestions during manuscript preparation.

Patrick, Benjamin, Rajeeve, Lena, Reena thank you guys for helping with conducting experiments and especially during the tough time of the revision. Preeti, thank you for teaching me the LMD technique and for the great time we had together in the lab and outside. Hanaa, thank you for providing me with motoneuron cultures during the revision of my paper. My special thanks to Michaela for assisting me with culturing primary cortical neuron. Many thanks also go to Elke and Hildegard for their great work in virus production, Regine and the entire animal facility for mouse breeding and Nicole for taking care of the genotyping of Smn transgenic line.

And my gratitude to my fellow lab mates: Stefanie, Thomas, Michael Skoruppa, Annalena, Verena, Christian, Urveen and Judita and also to my previous colleagues, Manuela, Dominique, Bhuvaneish, Daria and Sabina. Thank you guys for the great working atmosphere and for your cooperation and personal support and for all the fun we had together.

I sincerely thank the excellent funding from SFB and Hermann and Lilli Schilling foundation that made this challenging research work possible. I would also like to thank Graduate School of Life Science Würzburg for the administrative assistance and for giving me support during the period of my PhD.

I am very thankful to my family and friends. First, I would like to thank my husband Ahmad for his patience and continuous support throughout my PhD. Without your love and support this work would have remained a dream. Mom, dad, my sisters and brothers, you were always with me and shared the big burden of the hard work with me. Thank you my loves. And Oana many thanks for correcting the first draft of this thesis. It was a big help.

11. Curriculum Vitae

Conferences and summer schools

16-17 Oct 2012; 7th International Symposium organized by the Doctoral Researchers of the Graduate School of Life Sciences "EPOS", Würzburg, Germany. Contribution: Poster "Axonal mRNA trafficking and local translation in motor neuron disease"

24-28 Sep 2013; ISN summer school organized by FENS "Local protein synthesis in axons and dendrites", Kolymbari, Crete, Greece. Contribution: Oral presentation and poster "Axonal mRNA trafficking and local translation in in Spinal Muscular Atrophy"

9-10 Oct 2013; 8th International Symposium organized by the Doctoral Researchers of the Graduate School of Life Sciences "SCI", Würzburg, Germany. Contribution: Poster "Axonal mRNA trafficking and local translation in Spinal Muscular Atrophy"

14-15 Oct 2013; 10th International Symposium organized by the Doctoral Researchers of the Graduate School of Life Sciences "Eureka", Würzburg, Germany. Contribution: Poster "Axonal transport and translation of α- and γ-actin mRNAs are altered in Smn-deficient motoneurons"

15-19 Nov 2014; 44th Annual meeting of the society for neuroscience organized by "SfN", Washington D.C. USA. Contribution: Poster "Axonal transport and translation of α- and γ-actin mRNAs are altered in Smn-deficient motoneurons"

18-19 Sep 2015; International Symposium organized by the Graduate School of Life Sciences "Subcellular Signaling and Mechanisms of neurodegeneration", Würzburg, Germany. Contribution: Poster "Axonal mRNA trafficking and local translation in motor neuron disease"

Publication list

Differential roles of α, β and γ-actin in axon growth and collateral branch formation in motoneurons. *Moradi M, Sivadasan R, Saal L, Lüningschrör P, Dombert B, Rathod R, Dieterich D.C, Blum R, Sendtner S. J Cell Biol. 2017 Mar 6;216(3):793-814. doi: 10.1083/jcb.201604117. Epub 2017 Feb 28.*

Neurofilament depletion improves microtubule dynamics via modulation of tat3/stathmin signaling. *Yadav P, Selvaraj BT, Bender FL, Behringer M, Moradi M, Sivadasan R, Dombert B, Blum R, Asan E, Sauer M, Julien JP, Sendtner M. Acta Neuropathol. 2016 Jul; 132(1):93-110. doi: 10.1007/s00401-016-1564-y. Epub 2016 Mar 28.*

Whole transcriptome profiling reveals the RNA content of motor axons. *Briese M, Saal L, Appenzeller S, Moradi M, Baluapuri A, Sendtner M. Nucleic Acids Res. 2016 Feb 29;44(4):e33. doi: 10.1093/nar/gkv1027. Epub 2015 Oct 12.*